Discovery of Synthetic Lethal Interactions with *CDH1* in Medulloblastoma

Tom Brew

Submitted to the University of Otago
in partial fulfilment of the
requirements for the degree of
Master of Science
Genetics Major

Abstract

Medulloblastoma is the most frequently occurring malignant brain tumour in children, affecting just under two individuals per million annually. Medulloblastomas have an aggressive, invasive growth pattern, with a high risk of metastasis to structures of both the brain and spine. The five-year survival rate for medulloblastoma is currently 70-75%, however, due to the high rate of recurrence observed in this cancer, the 20-year survival rate drops to approximately 50%. Therapeutic options for medulloblastoma involve neurosurgery, cranial radiation therapy and chemotherapy. This highly aggressive therapy leaves surviving patients with long-term debilitating side effects, such as deficits in neurocognitive and endocrine function.

CDH1 is a tumour suppressor gene involved in cell-cell adhesion, differentiation and proliferation which is commonly lost across various cancer types, including medulloblastoma. Tumour suppressor gene inactivation results in a lack of expressed protein, and therefore cannot be exploited by conventional drugs as there is no protein to target. The concept of synthetic lethality has important implications in this context, as it allows for the exploitation of inactivated tumour suppressor genes in cancerous cells. Any two genes are said to be in a synthetic lethal relationship if mutation of either gene maintains cell viability, but simultaneous mutation of both genes causes cell death. This allows for the development of novel treatment strategies which target the synthetic lethal partner of a silenced tumour suppressor gene, selectively killing tumour cells and leaving healthy tissue relatively unharmed. This is particularly significant in medulloblastoma where the toxicity of current treatment regimens is high, and provides a large margin for improvement.

The aim of this study was to make use of publicly available microarray expression data to first identify a *CDH1*-low subgroup of medulloblastomas. This group of tumours was then used to identify potential synthetic lethal interactions with *CDH1*, using a novel bioinformatic strategy. Following this, experimental validation of the putative synthetic lethal candidates, *RARB* and *PDGFD*, involved short hairpin RNA (shRNA) knockdown of identified candidate genes within a cell line pair representing a model of E-cadherin loss. This was accompanied by quantitative real-time PCR (qPCR) to confirm gene knockdown. Both of the investigated putative synthetic lethal candidate genes were validated as synthetic lethal partners of *CDH1*, as knockdown induced selective killing of E-cadherin deficient cells. To further characterise these synthetic lethal partnerships, drug inhibition of candidate genes within the same model of E-cadherin loss was performed. For *RARB*, drug inhibition was successful in inducing a synthetic lethal phenotype, and to a greater degree than observed through shRNA knockdown. For *PDGFD*, drug inhibition was unsuccessful in producing a synthetic lethal phenotype. However, the drug used was not specific to the synthetic lethal candidate, and inhibition of other biological pathways was likely deleterious to E-cadherin expressing cells as well as E-cadherin deficient cells.

In summary, this study has demonstrated the effectiveness of a novel bioinformatic strategy for the identification of synthetic lethal partnerships. Two synthetic lethal partners of *CDH1* in a medulloblastoma context have been identified and validated by this study, adding further support to the development of novel therapeutic techniques utilising the concept of synthetic lethality.

Table of contents

List of figures

List of tables

List of abbreviations

% w/v = Weight per volume %

°C = Degrees Celsius

µg = Microgram(s)

µL = Microlitre(s)

µm = Micrometre(s)

µM = Micromole(s) per litre

ALL = Acute lymphoblastic leukaemia

APS = Ammonium persulfate

ATCC = American Type Culture Collection

cDNA = Complementary DNA

CO = Cell only

CO_2 = Carbon dioxide

CpG = C-phosphate-G

Ct = Cycle threshold

D/N = Desmoplastic nodular

DMEM = Dulbecco's modified Eagle's medium

DMEM-F12 = Dulbecco's modified Eagle's medium and F12 medium

DMSO = Dimethyl sulfoxide

DNA = Deoxyribonucleic acid

ECL = Enchanced chemiluminescence

EGF = Epidermal growth factor

EMT = Epithelial-mesenchymal transition

FBS = Fetal bovine serum

FDR = False discovery rate

GEO = Gene Expression Omnibus

GSK3B = Glycogen synthase kinase 3 beta

hr = Hour(s)

IN = Internodular

L = Litre(s)

LCA = Large cell and anaplastic

LOH = Loss of heterozygosity

LRLP = Lower rhombic lip progenitor

MAPRE3 = Microtubule-associated protein RP/EB family member 3

MBEN = Medulloblastoma with extensive nodularity

MET = Mesenchymal-epithelial transition

min = Minute(s)

mL = Millilitre(s)

mM = Millimole(s) per litre

MM = Mismatch

MMP = Matrix metalloproteinase

MOI = Multiplicity of infection

mQH2O = Milli-Q H_2O

mRNA = Messenger RNA

N = Nodules

ng = Nanogram(s)

NS = Non-silencing

optiMEM = Reduced serum media

PARP1 = Poly [ADP-ribose] polymerase 1

PBS = Phosphate buffered saline

PFA = Paraformaldehyde

PGN = Pontine grey nucleus

PI = Propidium iodide

PM = Perfect match

qPCR = Quantitative real-time PCR

RA = Retinoic acid

RAR = Retinoic acid receptor

RARE = Retinoic acid response element

RMA = Robust multi-array average

RNA = Ribonucleic acid

rpm = Revolutions per minute

RPMI-1640 = Eagle's minimum essential medium

RT = Reverse transcriptase

RXR = Retinoic X receptor

sec = seconds

SDS = Sodium dodecyl sulfate

SHH = Sonic hedgehog

shRNA = Short hairpin RNA

siRNA = Small interfering RNA

TBST = Tris-buffered saline and tween-20

TCF = T-cell factor

TEMED = Tetramethylethylenediamine

V = Volt(s)

WT = Wild-type

ZFN = Zinc finger nuclease

1. Introduction

There is a strong need for the development of new drugs which target defined molecular mechanisms, particularly in paediatric cancer types where patient prognosis is poor, or treatment toxicity is high. Paediatric cancer is the greatest cause of mortality in children up to the age of 14 in the United States, with only accidents surpassing this number. Advancements in genomic and proteomic techniques have enabled the molecular characterisation of many tumour types, including paediatric cancers, and such studies reveal weaknesses that are acquired during tumour development. These tumour-specific weaknesses could potentially be targeted using novel molecular therapies, providing hope for those afflicted with these debilitating diseases. Drugs which are able to go beyond the direct targeting of oncogenes, and instead exploit the silencing of tumour suppressor genes, have recently shown promise in this area.

1.1. Synthetic lethality

The concept of synthetic lethality was first hinted at by Dobzhansky in 1945, in *Drosophila pseudoobscura*. It was noted that particular chromosomal regions contained genes, or groups of genes, which led to *Drosophila* viability when inherited separately, but lethal when combined [1]. From this observation came the concept of synthetic lethality. Any two genes are said to be in a synthetic lethal relationship if mutation of either gene maintains cell viability, but simultaneous mutation of both genes causes cell death (Figure 1.1.) [2]. Synthetic lethal interactions are very common in the budding yeast, *Saccharomyces cerevisiae*, with around 80% of genes having synthetic lethal interactions with at least one other gene. It is estimated that these genes have, on average, ten synthetic lethal interactions per gene [3].

At the biological level, synthetic lethality represents one gene buffering the loss of function in the other, but this effect is lost when both are simultaneously mutated. Alternatively, it can be viewed from the idea that mutation in one gene causes genetic vulnerabilities in the cell, with additional mutation of synthetic lethal partners resulting in cell death. There are many possibilities for the biological reasoning behind these synthetic lethal interactions. For example, two genes may function together in an essential pathway, make up separate subunits of an essential protein complex, or provide some redundancy for the other as they both provide a similar, essential, biological function [2].

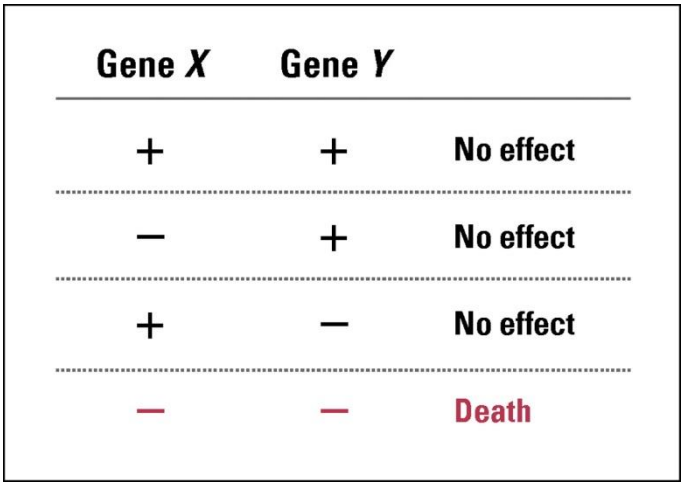

Figure 1.1. Summary of synthetic lethality and the differing effects on cell viability. Therapies which utilise this concept and inhibit synthetic lethal partners of tumour suppressor genes may lead to novel drugs for cancer treatment. Excerpt from Ashworth [4].

Synthetic lethality has important therapeutic implications for anticancer drug treatment. If a particular cancer is known to commonly silence or mutate specific tumour suppressor genes, these can be exploited via their synthetic lethal partners. This is particularly true if the synthetic lethal partner is an enzyme, receptor, or otherwise suitable drug target. This approach to anticancer treatment is important for two primary reasons. Firstly, because many cancers have characteristic mutations resulting in a loss of function, these mutations can be especially difficult to target. For example, a mutation may result in either reduced levels, or

even complete absence, of protein. As a result, these proteins cannot be targeted with anticancer drugs, and so the concept of synthetic lethality provides a method of exploitation in such cases, where the synthetic lethal partners of the mutant gene become the drug targets [2].

Secondly, a major problem with current anticancer treatment is the cytotoxicity of drugs, which results in the death of healthy cells as well as the intended cancer cells. Utilising synthetic lethality can effectively differentiate between healthy cells and cancer cells, as only the cancerous cells contain the targeted mutation, providing selective killing. In a perfect situation, healthy cells would be completely unaffected, while cancer cells would be killed by even partial inhibition [2]. One successful example of synthetic lethal drug development can be seen in Poly [ADP-ribose] polymerase 1 (PARP1) inhibitors, which have been developed to selectively kill cancerous cells harboring *BRCA1*/*BRCA2* mutations, based on their association in DNA repair pathways [4, 5]. The success of these PARP1 inhibitors provides strong support for the development of drugs harnessing the concept of synthetic lethality.

1.2. Microarrays and publicly available data

One potential method for identifying genes which interact in a synthetic lethal manner is via an *in silico* analysis using publicly available gene expression data, such as that generated by microarray and RNA-seq technologies. Microarrays, while a relatively old technology, remain an important tool for generating genome-wide information and have a wide variety of uses, particularly in large-scale studies. They can be used to examine and discover gene function, classify tissue or disease, and determine relationships between genes at the expression level [6]. Microarrays have been widely used, to the point that there were over 64,000 PubMed citations of the term between 2000 and 2015. Because microarray data can be

easily stored and handled for computational use, several large dataset repositories have been established. One example of this is the Gene Expression Omnibus (GEO) [7]. Such data repositories house tens of thousands of microarray datasets. The microarray data from various studies can be downloaded and analysed statistically using computational environments such as R [8]. The use of public data repositories therefore allows the easy sharing of data, which enables analysis by other groups and the potential for additional findings in a different context [6].

Affymetrix produce oligonucleotide microarrays, and these are the most common microarrays types found in these data repositories. The oligonucleotide probes are produced nucleotide by nucleotide through photolithographic synthesis [9]. This involves the synthesis of probe sequences upon the array itself, using light and light-sensitive masking agents. Other methods can involve the depositing of probe sequences onto the array which have been synthesised previously. The oligonucleotide probes are short sequences designed to bind a target mRNA sequence. There are generally around 11-20 probes present on an Affymetrix array for each gene, and information from this probe set is combined to form a single measure of activity per gene. Biotin-labelled RNA from the sample of interest is added to the array, which is then scanned and quantified, returning an "expression level" in the form of intensity, which is based on the amount of probe hybridisation which occurred between the probes and target transcripts [10].

Each probe on these microarrays comes in a pair. The perfect match (PM) probe is complementary to the mRNA of interest, whereas the paired mismatch probe (MM) is identical to the PM probe except for a single base change at the central position of the sequence. This MM probe acts as an internal control for the specificity of array hybridisation

[11], as it provides a measure of nonspecific signal [12]. These probe pairs are utilised during background correction, which allows for biases introduced into microarray experiments such as variation in sample preparation and variations in hybridisation specificity [13]. There are several methods for background correction, such as Robust Multiarray Average (RMA). This approach also performs quantile normalisation, which effectively standardises each sample to the same distribution of signal intensity, and results in more comparable statistical properties between any two separate microarrays [13]. Although this aids in correcting intra-cohort variation, such as that observed between different microarray chips, different datasets are often combined as part of bioinformatic analyses to increase sample size and statistical power, which requires a different approach. Because variation will inherently exist due to potential differences such as experimental setup and the method of data collection, the separate datasets require normalisation upon merging, before any meaningful results can be extracted from such an analysis. One example of this is the use of COMBAT [14].

COMBAT normalisation first identifies batch-specific effects on gene expression levels through the assumption that batch biases will have a similar effect on many separate genes. For example, a batch-specific effect may result in increased expression or variability across an array of genes. After these batch-specific effects have been identified, this batch-specific parameter is "shrunk" towards the overall mean of the estimated batch effects for all genes [14]. This essentially normalises the separate datasets to reduce the overall impact of batch-specific effects, and results in more comparable data. However, due to the assumptions within the COMBAT normalisation methodology, some biological effects of interest may be obscured by this process. For example, if an entire gene pathway is upregulated due to a biological event, this may be identified as a batch-specific effect which resulted in a widespread increase in gene expression. However, this effect is not a common occurrence, as

this upregulation must be consistent across a substantial proportion of the dataset. This can be observed in breast cancer datasets, where entire datasets comprise ER+ or ER- tumours.

An additional confounding factor in microarray analysis is the effect of cross-hybridisation between probes and unintended mRNA transcripts. Probes are designed to be perfectly complementary to the target mRNA transcripts, but commonly share similarities to other sequences that may be present, and can therefore hybridise to these off-target transcripts. This effect of cross-hybridisation has effects on the estimated expression levels of the intended transcripts for each probe set. Some methods exist to counteract the effects of cross-hybridisation, such as GeneBASE-xhyb, a method described by Kapur *et al*. [15]. GeneBASE-xhyb removes any probe pairs predicted to exhibit significant cross-hybridisation, through either sequence similarity to off-target transcripts, or probe pairs which exhibit a high correlation with an estimate of off-target expression levels [15].

In a cancer setting, microarray data from tumour samples can be used to identify gene interactions which are indicative of synthetic lethality. For example, if gene *A* and gene *B* form a synthetic lethal pair, both genes would not exhibit very low levels of expression simultaneously, as this would result in cell death. If gene *A* was downregulated, gene *B* should be expressed at a relatively normal, if not an increased level. As a result, tumours with low levels of both gene *A* and gene *B* should occur at a reduced frequency in the microarray dataset, thus providing a mechanism by which potential synthetic lethal partnerships can be identified *in silico* (Figure 1.2.).

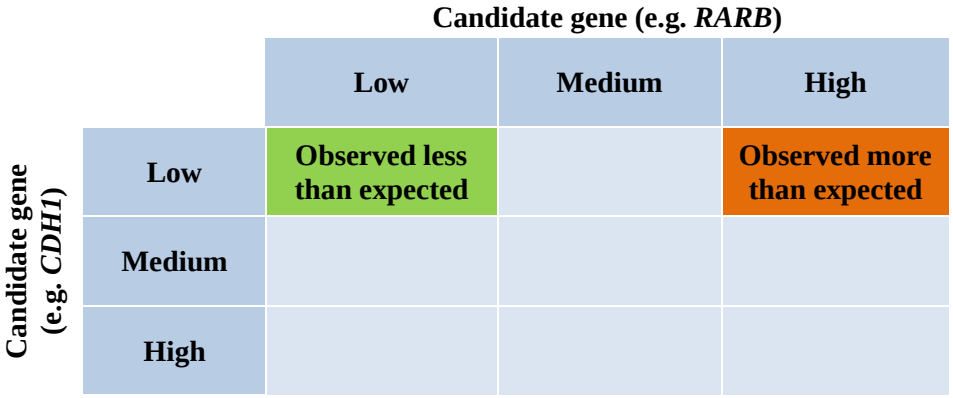

Figure 1.2. A strategy for identifying synthetic lethal interactions from gene expression data. Adapted from Kelly [16].

1.3. E-cadherin

Cadherins are glycoproteins which are found on the cell surface, and are involved in Ca^{2+}-dependent cell-cell adhesion. Adhesion molecules are important for the regular maintenance and organisation of tissue. Cadherins are also important regarding both morphogenesis and histogenesis [17].

E-cadherin, encoded by the *CDH1* gene, falls into the cadherin superfamily and encodes a cell adhesion protein. E-cadherin is a well characterised tumour suppressor gene [18], and *CDH1* dysfunction can result in abnormal cell differentiation, proliferation, tumour invasiveness and metastasis [19-21]. It has been shown that inhibition of *CDH1* prevents the formation of the adherens junction and leads to abnormal cytoskeletal organisation [22]. Decreased *CDH1* levels have been associated with aggressive carcinomas, and a poor clinical outcome. In addition to this, the restoration of *CDH1* expression levels in tumour cells appears to inhibit the invasiveness of epithelial tumour cells [23].

The adherens junction is a cell-cell adhesion structure which is present in a wide variety of cell types. It is comprised of two separate plasma membranes with rod-shaped molecules

making up the intercellular space. The adherens junction is associated with actin filaments within the cytoplasm of each of these two cells [24, 25]. Within epithelial cells, the adherens junction is part of a complex which makes up both the tight junctions and desmosomes, and is therefore also involved in maintaining cell polarity [26]. As well as maintaining polarity, adherens junctions are required to form a physical connection between cells, and adherens junction dysfunction can cause loose cell-cell contacts [27]. This role in maintaining cell-cell contact is the tumour suppressing function of *CDH1*, as this decreases tumour invasiveness by physically preventing cell migration. Another proposed mechanism of tumour suppression is that loss of *CDH1* may result in decreased cell-cell adhesion which then allows escape from growth-control signals, increasing the proliferation rate of E-cadherin deficient cells [23].

E-cadherin binds to β-catenin, encoded by the *CTNNB1* gene, which forms part of the complex that links E-cadherin to the actin cytoskeleton (Figure 1.3.) [27]. As well as a role in cell-cell adhesion, *CTNNB1* also plays a signaling role. β-catenin contains a conserved *armadillo* repeat region, and this is required for interaction with E-cadherin. *CTNNB1* was found to be the mammalian homologue of the *armadillo* gene in *Drosophila*. This gene is involved in the wingless signaling pathway [28], which first suggested that *CTNNB1* itself might have a signaling function.

Since then, *CTNNB1* has been shown to play a signalling role as a component of the Wnt-signalling pathway. E-cadherin can sequester β-catenin at the cellular membrane, and therefore by extension, has a role in the signalling pathway itself by affecting the availability of β-catenin for the nucleus. β-catenin migrates to the nucleus if not isolated by E-cadherin, and forms a transcription factor with the T-cell factor/lymphoid enhancer factor (TCF/LEF).

Following this, the carboxy terminus of β-catenin recruits various protein complexes that remodel chromatin and promote transcription of genes under Wnt control [29].

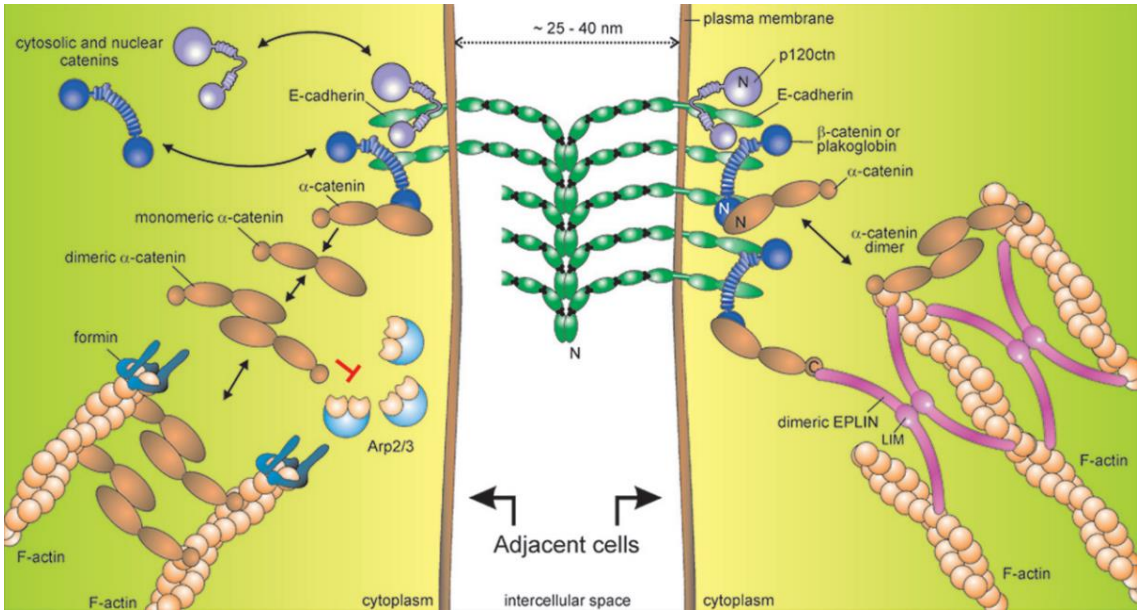

Figure 1.3. A schematic overview of the E-cadherin-catenin complex (CCC) at the adherens junction of two epithelial cells. E-cadherin binds to the *armadillo* repeat region of β-catenin which sequesters β-catenin at the cellular membrane and links E-cadherin to the actin cytoskeleton. As depicted by double-headed arrows, β-catenin has a role in both the cytoplasm and the nucleus. Excerpt from van Roy and Berx [30].

Overexpression of *CTNNB1* has been shown to provide sufficient signal to activate TCF transcriptional activity [31-33], and *CTNNB1* expression levels must be carefully regulated due to this signaling function. As such, it is phosphorylated by Glycogen synthase kinase 3 beta (GSK3B), which marks the protein for degradation. Multiple amino acids are phosphorylated in this way, and these same residues increase β-catenin stability when mutated [34]. By extension, this illustrates that *CDH1* plays an indirect role in the Wnt-signalling pathway, by affecting β-catenin availability, as well as having a cell-cell adhesion role.

1.4. E-cadherin in cancer

CDH1 germline mutations have been found to predispose individuals to familial gastric cancer. This was confirmed in several families, all with dysfunctional *CDH1* genes [23]. Although germline *CDH1* mutations had not previously been reported for familial cancer, somatic mutations had previously been identified in lobular breast cancer [35, 36], diffuse gastric carcinomas [37-39] and carcinomas of both the ovary and endometrium [40]. It is likely that these germline *CDH1* mutations provided susceptibility to a second hit, and this second mutation encourages tumourigenesis. That is, one mutant *CDH1* copy was originally inherited, followed by either somatic mutation, loss of heterozygosity (LOH), or DNA hypermethylation [41] of the second *CDH1* copy, ultimately resulting in tumour formation. It has previously been shown however, that inactivation of both *CDH1* alleles by mutation, as well as LOH is common in non-familial cases [35-37, 39].

1.5. E-cadherin in the epithelial-mesenchymal transition

The epithelial-mesenchymal transition (EMT) is a process which occurs during embryogenesis, as well as the reverse process, mesenchymal-epithelial transition (MET). Both of these processes are required for the embryonic development of various tissues and organs, such as the neural crest and heart valve [42]. This results in a drastic change in cellular phenotype as these two cell types differ in many ways. Epithelial cells are very closely adhered and connected via several junctions, including adherens junctions, have polarisation of the actin cytoskeleton, and are bound to a basal lamina at their basal surface. Conversely, mesenchymal cells lack this polarisation and have reduced intercellular interaction [43]. There have been three primary types of EMT previously characterised: developmental, wound healing and cancerous [44].

In cancer, metastasis involves the migration of tumour cells to a non-adjacent organ or region of the body. Tumours situated at these new disease locations are referred to as metastases [45, 46]. For metastasis to occur, invasion is required, and one such mechanism for this is via EMT. Cell-cell adhesion is lost due to decreased *CDH1* expression, and cells are able to invade the basal membrane. As a result, there is potential for these cells to enter the bloodstream or lymphatic system and spread throughout the body as circulating tumour cells. These can then exit the bloodstream or lymphatics and undergo MET to form a new metastatic site. Both EMT and MET are therefore required to initiate and complete metastasis [47]. *CDH1* loss can be induced through many mechanisms, both transcriptional and epigenetic. For example, the genes *SNAI1* and *SNAI2* both repress *CDH1* expression by binding to the *CDH1* promoter region, and can induce EMT progression [48, 49].

Because *CDH1* loss is implicated in various cancers, and is also a hallmark of EMT progression, this identifies *CDH1* as an attractive target for therapies based on a synthetic lethal concept. If synthetic lethal therapies prove effective in the treatment of cells lacking *CDH1* in a medulloblastoma context, these therapies may have a wide range of uses, such as the treatment of other cancers lacking *CDH1*. Additionally, because *CDH1* expression is commonly lost during EMT, these therapies may also be effective at reducing or even eliminating metastases that have recently been established, or at targeting disseminated tumour cells.

1.6. Paediatric cancer

Paediatric cancer is commonly defined as a cancer occurring in an individual under the age of 20 years. Paediatric cancer is currently the most common cause of disease-associated death in children up until the age of 14 in the United States, with accidents the only cause of death

greater than this. For children aged between 0 and 14 years of age, acute lymphoblastic leukaemia (ALL) is the most common cancer type, responsible for around 25% of all cancer diagnoses in children. Closely following this, cancers of the central nervous system, primarily within the brain, account for around 20% of paediatric cancers [50].

Within 15 to 19-year olds, the forms of cancer diagnoses are significantly different in proportion, with the most common diagnosis for this age range being Hodgkin disease at 16.2%. Central nervous system tumours are still relatively prevalent, as the third most common cancer type, constituting 10% of diagnoses. Interestingly, there are other paediatric cancer types such as Ewing's sarcoma (2.2%) which are incredibly rare in 0 to 14 year-olds compared to this age range [50].

There are significant gender differences within some paediatric cancer types, with males generally more susceptible, with the exception of a select few cancers such as thyroid carcinomas. These gender differences are fairly consistent between the 0 to 14 and 14 to 19 age ranges, however there are exceptions. For example, the increased male susceptibility to Ewing's sarcoma is 1.7-fold in the 15 to 19 age range, compared to 1.4-fold within the 0 to 14 age range [50].

The overall 5-year survival rates for paediatric cancer were as low as 28% in the 1960s. This has improved greatly, and is now estimated to be nearing 80%. However, this increase in survival also varies greatly between the various paediatric cancer types. ALL has had the most significant increase from a practically incurable disease to a 5-year survival rate of 80% [50]. The drastic improvement in survival is likely due to ALL remaining the most prevalent childhood cancer and thus, has attracted the attention of many researchers. However, an

example of relatively poor survival is acute myeloid leukaemia which currently only has a survival rate of around 50%, despite research efforts [50].

These statistics illustrate the overall impact of paediatric cancer in terms of both incidence and mortality, as well as the complexity associated with it. Overall, this stresses the importance of developing improved therapies to better handle these complex and debilitating diseases.

1.7. Medulloblastoma

Medulloblastoma is the most frequently occurring malignant brain tumour in children, affecting just under two people per million each year. These tumours form in the cerebellum, within the external granular layer. Medulloblastomas have an aggressive, invasive growth pattern, with a high risk of metastasis to structures of both the brain and spine. The five-year survival rate for medulloblastoma has risen by approximately 20% since 1979, from 54% [51] to 70-75% today [52]. However, due to the invasive growth and recurrence observed in medulloblastomas, the 20-year survival rate remains around 50% [51], and survivors suffer from long-term debilitating side-effects from current therapies.

Therapeutic techniques for medulloblastoma involve neurosurgery, cranial radiation therapy and chemotherapy. There are several chemotherapy regimens, usually involving the use of lomustine, cisplatin, carboplatin, vincristine or cyclophosphamide. This highly aggressive therapy often results in deficits in neurocognitive and endocrine function, psychological development, hearing, fertility and cardiopulmonary fitness [53-59]. Medulloblastoma patients have also been shown to suffer decreased academic ability. Specifically, decreases in mean IQ for reading, spelling and mathematics following treatment with craniospinal

irradiation and chemotherapy have been observed. Additionally, survivors also experience deficits in processing speed and memory retention [60].

Abberations during neurogenesis are currently believed to constitute the cellular basis for the cognitive impairments which are seen in cancer patients following treatment with cranial radiation therapy and chemotherapy [61, 62]. Patients receiving cranial radiation therapy have particular difficulty with encoding new episodic memories [63]. Disruption of hippocampal neurogenesis results in decreased performance in memory tasks [64-69], and both chemotherapy and cranial radiation therapy have been shown to negatively affect neurogenesis in the hippocampus [69-76]. One particular study used immunohistochemical analysis of post-mortem brain tissue to show that medulloblastoma patients treated with surgery, cranial radiation therapy and chemotherapy presented with near complete dysregulation of hippocampal neurogenesis [77].

Current treatment protocols involve the stratification of patients into risk groups, based on the presence or absence of metastasis at disease presentation and whether residual tumour tissue is present post-resection. These risk groupings allow for reduced treatment exposure for average-risk patients, such as decreased craniospinal radiation doses, and result in increased exposure for high-risk patients. This has effectively reduced mortality in high-risk patients, whilst reducing toxicity of treatments in average-risk patients, where full exposure to treatment is not necessary [58].

Medulloblastoma is a heterogeneous disease histologically, with a classic subtype, and four histological variants: desmoplastic nodular (D/N), medulloblastoma with extensive nodularity (MBEN), anaplastic, and large cell (Figure 1.4.). The histological variants can be paired into

two groups which share morphological properties: desmoplastic tumours containing D/N and MBEN subtypes, and the large cell and anaplastic (LCA) subtype [78]. The identification of these variants can then be utilised in a clinical setting, as prognosis differs depending on histological classification. As a result, current clinical trials are assigning therapy based on histology, as well as clinical risk as described above [79, 80]. This is an important advance in medulloblastoma treatment as it recognises the need for thoroughly characterising individual tumours before assigning therapy [52], and is a step towards personalised medicine.

However, this strategy does not allow for molecular differences within histological subtypes, and illustrates the need for drugs which exploit individual tumour weaknesses at the molecular level. Concordant with this, medulloblastoma survivors continue to suffer from a decreased quality of life due to the many side effects which current treatments induce, despite these advances in treatment regimens.

Medulloblastoma has four molecular subgroupings that have been previously defined by gene expression profiling: the sonic hedgehog (SHH) subgroup, Wnt subgroup, subgroup 3 and subgroup 4 [81]. These subgroups show differences in prevalence, karyotype, histology, driver mutations, and most importantly, prognosis (Table 1.1.) [82]. These subgroupings also exist in mice, and in mouse models of each individual subgroup it was shown that each arises from different cell types, as one might suspect from the differences in gene expression profiling [83-86]. The identification of these distinct subgroups of medulloblastoma has not resulted in a significant change in clinical practice. All subgroups currently receive the same combination of neurosurgery, irradiation and chemotherapy [60, 82].

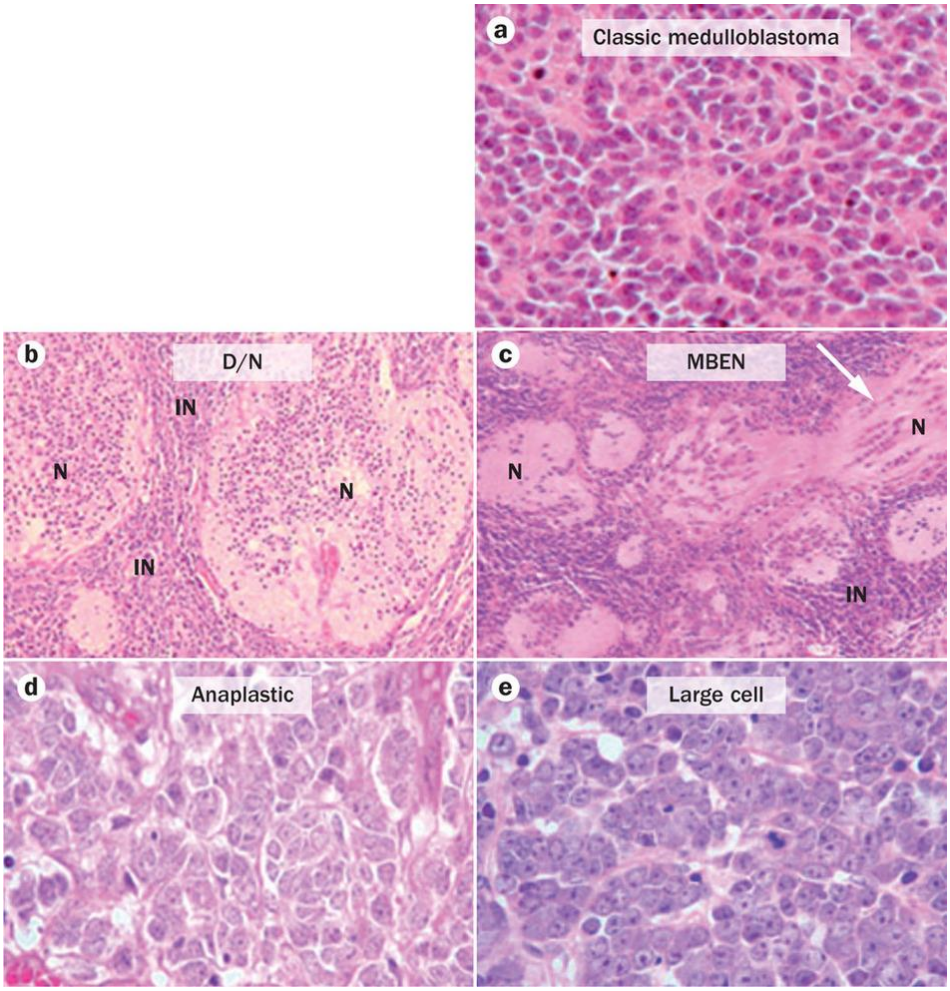

Figure 1.4. Microscopy images representing the various medulloblastoma histology variants. **a)** Classic medulloblastoma, characterised by sheets of small cells with a high nuclear-cytoplasmic ratio and mild nuclear polymorphism. **b)** D/N medulloblastoma tissue contains nodules (N) of differentiated nerve cells. Internodular (IN) regions consist of undifferentiated embryonal cells and strands of collagen. **c)** MBEN medulloblastoma is similar in appearance to D/N histology, and also consists of nodular (N) and internodular (IN) regions. The N regions differ in that they are greater in abundance and often contain streaming cells (as depicted by arrowhead). **d)** Anaplastic medulloblastomas show nuclear pleomorphism, a higher mitotic count and a greater number of apoptotic cells. Tumours must contain extensive regions with this histology to be classified as anaplastic. **e)** Large cell medulloblastoma showing characteristically monomorphic cells with both large nuclei and nucleoli. This histology is commonly observed in regions of anaplasia, resulting in the combined LCA grouping. Excerpt from Gajjar and Robinson [52].

Molecular subtype	Proportion of all medulloblastomas	5-year survival rate	Histology	Commonly mutated genes
Wnt	~10%	~90%	Classic	CTNNB1, DDX3X
SHH	~30%	~75%	All	PTCH1, TP53
Group 3	~25%	~50%	Classic/LCA	MYC/PVT1 amplification
Group 4	~35%	~75%	Classic	KDM6A, SNCAIP gain

Table 1.1. Summary of observed differences between the four molecular subgroupings of medulloblastoma in terms of prevalence, survival, histology, and driver mutations. Values derived from Gajjar and Robinson [52].

This aggressive treatment fails to cure around two thirds of those with subgroup 3 medulloblastoma, and is believed to over-treat those with Wnt-subgroup medulloblastomas, as the survivors consistently suffer long-term cognitive and endocrine defects [60, 82]. This represents a large margin for potential improvement of therapies in regard to both mortality and toxicity, and a need for increased treatment specificity to the individual molecular subgroups of medulloblastoma. The brain is too fragile an organ, particularly during development in early childhood and adolescence, to handle damaging side effects, and this needs to be addressed accordingly.

1.8. The role of E-cadherin in medulloblastoma tumourigenesis

The loss of *CDH1* has been implicated in several tumours of the central nervous system. It has previously been shown that *CDH1* expression was often absent in malignant meningiomas [87]. This has been validated by a separate study, in which negative immunostaining of E-cadherin was observed in all meningiomas [88].

Aberrant methylation of CpG islands within promoter regions is associated with the inactivation of tumour suppressor genes in many tumour types [89], and one particular study found aberrant methylation of *CDH1* in approximately 8% of investigated medulloblastoma samples, as well as one of four medulloblastoma cell lines [90].

Mutations in *CTNNB1*, with which *CDH1* interacts closely, have been reported in sporadic medulloblastoma [91]. This *CTNNB1* role in medulloblastomas is further supported by Robinson *et al.* [92], as they found that Wnt-subgroup medulloblastomas commonly contain mutations which stabilise β-catenin. Mutations have also been found in chromatin modifiers that are recruited to TCF/LEF Wnt-responsive genes by β-catenin [92], providing additional

evidence for the importance of this pathway in medulloblastomas. It is believed that the development of Wnt-subgroup medulloblastomas may be a result of altered function of chromatin remodeling at Wnt-responsive genes.

Robinson *et al* found that a small number of Wnt-subgroup medulloblastoma samples (3 of 11) did not contain mutations in *CTNNB1*, suggesting that other disruptions of this pathway could be responsible for tumour formation. One of these samples harboured an inactivating *APC* mutation, and two of these samples contained missense mutations in *CDH1* [92]. Because E-cadherin isolates β-catenin at the cell membrane [93], and prevents migration to the nucleus where β-catenin can promote Wnt-signaling, these mutations may allow β-catenin localisation to the nucleus and aberrant Wnt-signaling activation.

Importantly, mutant *CTNNB1* has been shown to initiate Wnt-subgroup medulloblastoma in mice. This prevents the migration of lower rhombic lip progenitors (LRLPs) from the embryonic dorsal brainstem, to the pontine grey nucleus (PGN) (Figure 1.5.). When this occurs, the LRLPs proliferate at the dorsal brainstem, adjacent to the cerebellum, and result in medulloblastoma tumourigenesis [83].

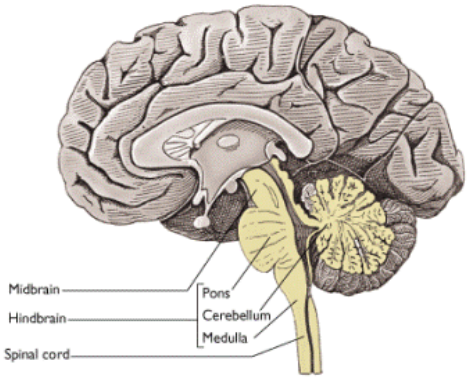

Figure 1.5. Anatomical layout of the cerebellum relative to the pons, which harbours the PGN. Wnt-subgroup medulloblastoma is initiated by the lack of LRLPs migrating from the cerebellum to the PGN. Original image by Carone [94].

Robinson *et al*. confirmed in mice that *CDH1* missense mutations, as observed within the two medulloblastoma samples mentioned above, could substitute for a mutant *CTNNB1* gene in the formation of Wnt-subgroup medulloblastomas, using short hairpin RNA (shRNA) knockdown of *CDH1* in embryonic mouse LRLPs. This resulted in upregulation of TCF/LEF-controlled gene expression in the LRLPs, and increased their self-renewal capacity by greater than two-fold. In addition to this, *in utero* electroporation of LRLPs was used to deliver *CDH1* shRNAs. This impeded LRLP migration from the dorsal brainstem to the PGN at a similar efficiency to that of mutant *CTNNB1*. These data support the hypothesis that *CDH1* is involved in the suppression of Wnt-subgroup medulloblastomas by indirectly regulating Wnt-signaling in LRLPs, through isolation of β-catenin at the cellular membrane [92].

The *DDX3X* gene is also mutated in approximately 50% of Wnt-subgroup medulloblastomas [52]. *DDX3X* is known to associate with the promoter region of *CDH1* and is capable of down-regulating E-cadherin via this binding [95]. It is unknown what effect on *CDH1*

expression these mutations induce, but this represents another link between *CDH1* and the Wnt-subgroup of medulloblastomas.

The specific downstream targets of interest from abnormal Wnt-signaling in the context of Wnt-subgroup medulloblastoma have not yet been identified. However, both c-MYC and Cyclin D1, previously described as oncogenes [96, 97], were identified as TCF/*CTNNB1* transcriptional targets in colon cancer. Both of these genes are frequently overexpressed but not amplified in Wnt-subgroup medulloblastoma, implying that *CTNNB1* plays a role in this upregulation [98, 99]. Whether these genes are involved in medulloblastoma tumourigenesis has not yet been determined. Further investigation into the molecular changes induced by aberrant Wnt-signaling is necessary to further explain tumourigenesis resulting in these Wnt-subgroup medulloblastomas.

This evidence of a biological role for *CDH1* loss in the formation of Wnt-subgroup medulloblastomas shows promise for targeted therapies against *CDH1* and its synthetic lethal partners. This could potentially be exploited in an attempt to improve current therapeutic techniques and survival in medulloblastoma, as well as decreasing the toxicity and morbidity of side-effects which result from current therapies.

1.9. Summary

The relatively high mortality and incidence of medulloblastomas in comparison to other paediatric cancers, combined with the current toxicity of treatments, warrants further research towards the development of drugs targeting the defined molecular mechanisms which drive this disease. Drugs which are able to induce a synthetic lethal interaction between *CDH1* and a candidate gene for a tumour type such as Wnt-subgroup medulloblastomas would allow for

the selective destruction or reduced fitness of tumour cells, possibly improving prognosis and decreasing treatment morbidity. The importance of improving medulloblastoma treatment specificity and prognosis through targeted molecular therapies has been illustrated here, along with potential strategies which this study will utilise to address this issue.

1.10. Aim of this project

This project aims to make use of publicly available microarray expression data to first identify a *CDH1*-low subgroup of medulloblastomas, which can then be used to identify potential synthetic lethal interactions with *CDH1*. This will be accomplished using a computational strategy outlined previously (Figure 1.2.). These putative synthetic lethal candidate genes will be compared to experimental data which has been previously produced by our laboratory with the goal of identifying synthetic lethal interactions with *CDH1*, to give greater confidence in the results of this *in silico* screen. Following this, experimental validation of the proposed synthetic lethal candidates will involve shRNA knockdown of identified candidate genes within a cell line pair representing a model of E-cadherin loss. This will be accompanied by quantitative real-time PCR (qPCR) to confirm gene knockdown. Finally, drug inhibition of candidate genes will be used as support to the above data within the same cell lines, and to provide a clinically relevant example of synthetic lethality and the implications this may hold for cancer treatment.

2. Methods and Materials

2.1. Materials

2.1.1. Reagents

0.05% trypsin solution - Prepared in lab (Appendix 5.1.1.)

0.2 µm hydrophilic syringe filter - Sartorius, Spain

0.25% trypsin solution - Prepared in lab (Appendix 5.1.1.)

0.45 µm PVDF syringe filter - Sigma-Aldrich, USA

0.5% EDTA trypsin - Invitrogen, USA

2-Mercaptoethanol - Sigma-Aldrich, USA

30% Acrylamide/Bis solution, Bio-Rad, USA

Actrapid Penfil Neutral Insulin - Novo Nordisk Pharmaceuticals Ltd, New Zealand

Ammonium persulfate (APS) - Sigma-Aldrich, USA

Anti-α-tubulin monoclonal mouse antibody - Sigma-Aldrich, USA

Anti-E-cadherin polyclonal rabbit antibody - Santa Cruz, USA

Agar bacteriology grade - Applichem, USA

Agar plates - Prepared in lab (Appendix 5.1.2.)

Ampicillin sodium salt - Sigma-Aldrich, USA

Cell culture lysis 5x reagent - Promega, USA

Cholera toxin - Sigma-Aldrich, USA

Dimethyl sulfoxide (DMSO) - Sigma-Aldrich, USA

Donkey anti-rabbit antibody, peroxidise linked - Amersham Biosciences, UK

Dulbecco's modified Eagle's medium - Invitrogen, USA

Dulbecco's modified Eagle's medium and F12 medium (DMEM-F12) - Invitrogen, USA

Eagle's minimum essential medium (RPMI-1640) - Invitrogen, USA

Epidermal growth factor (EGF) - PeproTech, USA

Foetal bovine serum (FBS) - Invitrogen, USA

Freezing medium - Prepared in lab (Appendix 5.1.3.)

Gel running buffer - Prepared in lab (Appendix 5.1.6.)

GIPZ lentiviral shRNA vector - Thermo Fisher Scientific, USA

Glycine - Sigma-Aldrich, USA

Goat anti-rabbit antibody, Alexa Fluor 488 - Thermo Fisher Scientific, USA

Goat serum - Invitrogen, USA

Harsh stripping solution - Prepared in lab (Appendix 5.1.6.)

Hoechst 33342 dye - Thermo Fisher Scientific, USA

Horse serum - Invitrogen, USA

Hydrocortisone - Sigma-Aldrich, USA

KAPA SYBR FAST qPCR Master Mix Universal - KAPA Biosystems, USA

L-glutamine - Invitrogen, USA

Laemmli sample buffer – Bio-Rad, USA

Lipofectamine 2000 - Thermo Fisher Scientific, USA

Lysogeny broth (LB) - Prepared in lab (Appendix 5.1.2.)

Non-essential amino acids - Invitrogen, USA

NucleoSpin Plasmid EasyPure - Machery-Nagel, Germany

PageRuler prestained protein ladder - Thermo Fisher Scientific, USA

Paraformaldehyde (PFA) - BDH Limited, England

Phosphate buffered saline (PBS) solution - Prepared in lab (Appendix 5.1.4.)

Phosphate buffered saline (Dulbecco A) tablets - Oxoid Limited, England

Pierce ECL Plus Western Blotting Substrate - Thermo Fisher Scientific, USA

PrimeScript RT Reagent Kit - Takara Bio Inc., Japan

Propidium iodide (PI) - Thermo Fisher Scientific, USA

psPAX2 lentiviral packaging plasmid - Addgene, UK

Puromycin - InvivoGen, USA

qPCR primers - Integrated DNA Technologies, USA

Reduced serum media (optiMEM) - Thermo Fisher Scientific, USA

RNAGEM Tissue Plus extraction kit - Zygem, New Zealand

ROX high - KAPA Biosystems, USA

SDS-PAGE gel - Prepared in lab (Appendix 5.1.5.)

Sheep anti-mouse antibody, peroxidise-linked - Amersham Biosciences, UK

Skim milk powder - Pams, New Zealand

Sodium chloride (reagent grade) - Scharlau, Spain

Sodium dodecyl sulfate (SDS) - Sigma-Aldrich, USA

Sodium pyruvate - Invitrogen, USA

Tetramethylethylenediamine (TEMED) - Thermo Fisher Scientific, USA

Transfer buffer - Prepared in lab (Appendix 5.1.6.)

Tris-buffered saline and tween-20 (TBST) - Prepared in lab (Appendix 5.1.6.)

Tris ultrapure - Applichem, USA

Triton X-100 - Sigma-Aldrich, USA

Tryptone - Scharlau, Spain

Tween-20 - Sigma-Aldrich, USA

VECTASHIELD Mounting Medium with DAPI - Vector Laboratories, USA

VSVG lentiviral envelope plasmid - Addgene, UK

Yeast extract - Merck, Germany

2.1.2. Equipment

0.6 mL microtubes - Axygen, USA

1 mL cryovials - Nunc, Denmark

1.5 mL microtubes - Axygen, USA

6 well clear walled, flat, clear bottom tissue culture plates - Greiner Bio-One, Germany

10 mL serological pipettes - Greiner Bio-One, Germany

15 mL Falcon tubes - BD Biosciences, USA

22x22 mm glass cover slips - Menzel-Glaser, Germany

25 mL cell culture flasks - Greiner Bio-One, Germany

25 mL serological pipettes - Greiner Bio-One, Germany

50 mL Falcon tubes - BD Biosciences, USA

500 mL filter system - Corning, USA

75 mL cell culture flasks - Greiner Bio-One, Germany

75x25 mm Gold Seal microscope slides - Thermo Fisher Scientific, USA

96 well black walled, flat, clear bottom tissue culture plates - Corning, USA

Applied Biosystems 7900HT Fast Real-Time PCR system - Thermo Fisher Scientific, USA

Centra 3C centrifuge - International Equipment Company, USA

CO_2 cell culture incubator - Binder, Germany

Cytell Cell Imaging System - Thermo Fisher Scientific, USA

Dual chamber cell counting slides - Bio-Rad, USA

Eclipse Ti Inverted Microscope System - Nikon, USA

Fuji LAS-3000 ECL Imaging System - Thermo Fisher Scientific, USA

Immobilon-P membrane, PVDF, 0.45 µm - Merck Millipore, USA

IncuCyte FLR - Essen BioScience, USA

MicroAmp Optical 384 well reaction plate - Thermo Fisher Scientific, USA

Milli-Q Ultrapure Water Purification System - Millipore, USA

Mr. Frosty 5100 Cryo 1°C Freezing Container - Thermo Fisher Scientific, USA

Nanodrop ND-1000 Spectrophotometer - Nanodrop Technologies, USA

Olympus CK2 Microscope - Olympus, New Zealand

TC10 Automated Cell Counter - Bio-Rad, USA

Tissue culture hood - EMAIL, Australia

Water bath - Semco, USA

2.1.3. Resources

Publicly available microarray expression data for medulloblastoma, Ewing's sarcoma and rhabdomyosarcoma were sourced from GEO [7]. Gene expression data for all three datasets has been generated on the Affymetrix U133 Plus 2.0 microarray platform.

The medulloblastoma dataset contains microarray expression data for 62 medulloblastoma tumour samples. This study was carried out with the aim of improving the specificity of molecularly classifying medulloblastoma tumours [100]. These data can be accessed at GEO, accession number GSE10327.

The Ewing's sarcoma dataset contains microarray expression data for 44 Ewing's sarcoma tumour samples. This dataset was generated for investigating the relationship between expression patterns of immune system-related genes with prognosis in Ewing's sarcoma [101]. These data can be accessed at GEO, accession number GSE17679.

The Rhabdomyosarcoma dataset contains microarray expression data for 13 rhabdomyosarcoma cell lines. These data were originally used to characterise copy number

variations in rhabdomyosarcoma cell lines, and the resulting effect on gene expression levels [102]. These data can be accessed at GEO, accession number GSE8840.

The large multi-cohort dataset containing microarray expression data from 2116 breast tumour samples was assembled by Assoc. Prof. Mik Black from 15 independent cohorts. These were acquired from publicly available microarray databases, as described by Soon *et al* [103]. The RMA algorithm [13] was used for array normalisation for each of the 15 individual datasets, prior to the use of COMBAT [14] to adjust for cross-cohort effects.

2.1.4. Software

ImageJ - National Institute of Health, USA

IncuCyte software - Essen BioScience, USA

R version 3.1.2 - R Foundation for Statistical Computing [8]

R packages installed from Bioconductor [104], most notably affy [105], limma [106] and affyQCReport [107] packages.

Windows Command Prompt

2.1.5. Cell lines

The MCF10A and MCF10A *CDH1*$^{-/-}$ isogenic pair of cell lines were purchased from Sigma-Aldrich, USA. MCF10A is an immortalised, non-tumorigenic mammary epithelial breast cell line, and this isogenic pair of cell lines represents a model of *CDH1* loss in a relatively normal biological background. MCF10A *CDH1*$^{-/-}$ cells harbour a deletion of four base pairs in exon 11 of the *CDH1* gene, accomplished with zinc finger nuclease (ZFN) technology (Appendix 5.4.).

The DAOY cell line was purchased from the American Type Culture Collection (ATCC), USA. DAOY is a cancerous medulloblastoma cell line derived from a tumour of the cerebellum in a 4-year old Caucasian male [108].

The 293FT cell line was purchased from Invitrogen, USA. This cell line is derived from human embryonal kidney cells, and is suitable for generating high-titer virus, and was selected for lentivirus production in this study.

2.2. Methods

2.2.1 Bioinformatics

All bioinformatic analyses were carried out in the computational environment R.

2.2.1.1. Dataset manipulation

Windows Command Prompt was used to generate a list of the separate tumour sample gene expression files, and this list was used to load expression data into R in the form of a matrix of expression values. The affyQCReport package was utilised for microarray quality control within the medulloblastoma microarray expression dataset [100]. Microarray expression data were normalised using the RMA algorithm [13].

2.2.1.2. Determination of CDH1 probe pair similarity

Microarray probes were annotated using the hgu133plus2.db R package [109]. The two *CDH1* probe pairs within the medulloblastoma dataset were reviewed to ensure similar measurements were exhibited by both. Linear correlation between the two probe pairs was measured with the Pearson product-moment correlation coefficient. The distribution of intensity measurements from both probe pairs was also plotted for visual examination of

similarity. Comparison of this measure of probe pair similarity was made to two separate paediatric cancer datasets of microarray expression data, containing Ewing's sarcoma and rhabdomyosarcoma samples. The reviewing of *CDH1* probe pair similarity within these two datasets was performed with identical methodology to medulloblastoma data. Subsequent to confirmation of *CDH1* probe similarity in medulloblastoma data, intensity measurements from both probe pairs were averaged to give a single mean expression value for all further data processing.

To determine whether a *CDH1*-low subgroup of tumours existed within the medulloblastoma dataset, medulloblastoma samples were separated into three equally sized classes based on *CDH1* probe intensity: *CDH1* low, *CDH1* medium and *CDH1* high. For visual representation of the three classes and the respective spread of *CDH1* intensity, the distribution of all probe pairs was plotted, including histograms representing the *CDH1* intensity values of both *CDH1* low and *CDH1* high classes.

2.2.1.3. Identification of putative synthetic lethal partnerships with CDH1

Potential synthetic lethal partnerships with *CDH1* were identified from microarray expression data within the medulloblastoma dataset using a novel bioinformatic strategy, as designed by Tom Kelly, BSc (Hons) student, and Assoc. Prof. Mik Black (Figure 1.2.) [16]. Firstly, this approach averages the intensity measurements from probe pairs of each probe set (all probe pairs for a gene) to give a mean expression value for each individual gene. Following this, all tumour samples were divided into 3-quantiles of low, medium and high expression classes for each gene.

One gene is selected as the gene of interest, or query gene, in this case *CDH1*. Provided that there is evidence of synthetic lethality with *CDH1*, a non-random distribution of tumour samples between the two genes is to be expected. For example, classification into *CDH1*-low and candidate-low groupings should be rarely observed, if at all, if a synthetic lethal partnership exists between the two genes. Additionally, if a tumour is *CDH1*-low, it is expected that a synthetic lethal partner of *CDH1* would be expressed at a greater level than normal, thus falling into the candidate-high category. A chi-squared test on data outlined in Figure 1.2. provides a measure of significance for gene-gene expression relationships. Putative synthetic lethal partners are defined as a significant chi-squared test (p-value ≤ 0.05) in conjunction with a less frequent than expected *CDH1*-low/candidate-low combination of classes, and a more frequent than expected *CDH1*-low/candidate-high combination. Correction for multiple testing was achieved using the False Discovery Rate (FDR) controlling approach of Benjamini and Hochberg [110].

All candidate genes for synthetic lethality identified by these criteria were compared against genome-wide small interfering RNA (siRNA) screen data previously generated by our laboratory [111]. This screen was used to identify synthetic lethal candidates with *CDH1* within an MCF10A model of *CDH1* loss. Any candidate genes which were not supported by the siRNA screen as synthetic lethal with *CDH1* were removed from further analyses.

The same novel bioinformatic strategy for detection of synthetic lethal partnerships was applied to a large multi-cohort dataset of 2116 breast cancer tumour samples, by Assoc. Prof. Mik Black, to validate *RARB* and *PDGFD* synthetic lethal relationships with *CDH1*.

2.2.1.4. Determination of RARB and PDGFD probe pair similarity

Following selection as synthetic lethal candidates for further investigation, the two *PDGFD* probe pairs and the five *RARB* probe pairs within the medulloblastoma dataset were reviewed to ensure similar measurements were exhibited by both. Linear correlation between the probe pairs were measured with the Pearson product-moment correlation coefficient. The distribution of intensity measurements from both probe sets was also plotted for visual examination of similarity.

2.2.2. Cell culture

2.2.2.1. Complete growth medium

DAOY cells were cultured in Eagle's minimum essential medium (RPMI-1640), supplemented with 10% foetal bovine serum (FBS). Pre-mixed medium was filter sterilised using a 0.22μm polyethersulfone filter, then aliquoted into 50mL Falcon tubes.

MCF10A cells were cultured in Dulbecco's modified Eagle's medium and F12 medium (DMEM-F12), supplemented with 5% horse serum, 20 ng/mL epidermal growth factor (EGF), 100 ng/mL cholera toxin, 0.5 μg/mL hydrocortisone and 10 μg/mL insulin. Pre-mixed complete medium was filter sterilised and aliquoted as above for DAOY.

293FT cells were cultured in Dulbecco's modified Eagle's medium (DMEM), supplemented with 10% FBS, 6mM L-glutamine, 1mM sodium pyruvate and 0.1mM non-essential amino acids. Pre-mixed complete medium was filter sterilised and aliquoted as above for DAOY.

2.2.2.2. Cell culture maintenance

DAOY, MCF10A WT, MCF10A *CDH1*$^{-/-}$ and 293FT cells were grown at 37°C, with 5% CO_2 in respective growth medium (Chapter 2.2.2.1.). Cells were regularly passaged when 90% confluency was reached.

Phosphate buffered saline (PBS), trypsin and complete growth medium was pre-warmed in a 37°C water bath prior to passaging. Old growth medium was aspirated from the flask and 5 mL of PBS used to wash the cells. PBS was then aspirated and 2 mL of trypsin added, with the concentration depending upon cell line. For DAOY, 0.25% trypsin was used. For MCF10A WT, MCF10A *CDH1*$^{-/-}$ and 293FT cells, 0.05% trypsin was used. Cells were then returned to the incubator for 5 min for both DAOY and 293FT cells, and 25 min for MCF10A WT and MCF10A *CDH1*$^{-/-}$ cells. 5 mL of complete growth medium was added to inactivate trypsin activity, then cells were transferred into 15 mL Falcon tubes and centrifuged for 5 min at 600 rpm. Supernatant was aspirated and cells resuspended in 5 mL of complete growth medium. DAOY and 293FT cells were subcultured at a 1:6 ratio. MCF10A WT and MCF10A *CDH1*$^{-/-}$ cells were counted following resuspension, and plated at $1.0x10^5$ and $1.5x10^5$ respectively, in 5 mL total of growth medium, in 25 mL culture flasks. For 75 mL culture flasks, cells were instead plated at $3.0x10^5$ and $4.5x10^5$ respectively. Additionally, when 75 mL culture flasks were used, 5 mL of trypsin was added instead of 2 mL, and cells were plated in 13.5 mL complete growth medium instead of 4.5 mL. Flasks were then returned to the incubator.

2.2.2.3. Cell counting

Cells were counted by adding 10 µL of resuspended cells to each side of a dual chamber counting slide, then counted using the TC10 Automated Cell Counter. Cell density was

measured three times for each chamber, then counts were averaged to determine the density of cell suspensions.

2.2.2.4. Resurrection of cell lines

The following applies to MCF10A WT, MCF10A *CDH1*$^{-/-}$ and DAOY cells. Cells were removed from liquid nitrogen storage and thawed in a 37°C water bath. Cells were resuspended in 9 mL of pre-warmed complete growth medium, centrifuged for 5 min at 600 rpm, then the supernatant was discarded (as this contains residual Dimethyl sulfoxide (DMSO) from the freezing medium). Cells were then resuspended in 4.5 mL complete growth medium and transferred to a 25 mL culture flask. Cells were returned to the incubator. Complete growth medium was changed after 24 hr.

For 293FT cells, the same methodology was used, except cells were not centrifuged, and were instead transferred directly to a 25 mL culture flask.

2.2.2.5. Cryogenic preservation of cell lines

During the passaging protocol as above, following trypsinisation and centrifugation, cells were resuspended in freezing medium at a density of $1x10^6$ cells per mL. Cell suspension was aliquoted into 1 mL cryovials, which were transferred into a 5100 Cryo 1°C Freezing Container and stored at -80°C for 24 hr. This freezing container causes cells to cool at a rate of 1°C per minute, which helps to preserve the viability of cells. Cryovials were then transferred into liquid nitrogen for long term storage.

2.2.3. Immunofluorescence for E-cadherin

22x22 mm cover slips were placed at the base of each well in a 6 well clear walled, flat, clear bottom tissue culture plate. Cells were seeded at $6.0x10^4$ cells per well in 2 mL complete growth medium, and grown until confluent. Confluence is suitable for the staining of E-cadherin, as cells are tightly packed and E-cadherin is clearly isolated at the cell-cell boundaries, where it is involved in cell-cell adhesion.

Cells were washed with PBS three times, then fixed with 1 mL of 4% paraformaldehyde (PFA) for 20 min in the dark, as PFA is light-sensitive. Cells were washed twice with PBS, then permeabilised with 1 mL of 0.5% Triton X-100 in PBS for 10 min. Non-specific antibody binding was blocked with 1 mL of 5% goat serum in PBS for 30 min. Cells were exposed to 40 µL of anti-E-cadherin primary antibody (polyclonal rabbit antibody, H-108), diluted 1:50 in 1% FBS, 0.05% Triton X-100 and PBS. 6 well plates were incubated at 4°C in the dark for 16 hr.

Following incubation with primary antibody, cells were washed three times with PBS, and exposed to 40 µL of anti-rabbit secondary antibody (polyclonal goat IgG antibody, Alexa Fluor 488 conjugate), diluted 1:100 in the same buffer as for the primary antibody. Cells were incubated for 1 hr at room temperature in the dark, as the secondary antibody conjugates are light-sensitive. Cells were soaked and washed with PBS three times for 5 min each. For each of the six wells, a microscope slide was retrieved, and one drop of Vectashield mounting medium with DAPI was added to each. Cover slips containing cells within each well were lowered onto microscope slides and then left overnight at 4°C. Cells were then imaged using the following channels at 20x magnification: DAPI for nuclei (Vectashield with DAPI staining) and FITC for E-cadherin antibody conjugates. Two negative controls were used:

one MCF10A WT sample with no primary antibody and one MCF10A WT sample with no secondary antibody.

2.2.4. Western blotting for E-cadherin

2.2.4.1. Protein lysate preparation

Cells were seeded into a 6 well clear walled, flat, clear bottom tissue culture plate at $6.0x10^4$ cells per well in 2 mL complete growth medium and grown until confluent. Complete growth medium was aspirated from wells, and cells were washed with PBS. Cells were then lysed with 1x cell culture lysis buffer and wells were scraped to ensure protein was suspended in buffer. Lysis solution was transferred to a 1.5 mL microtube and briefly centrifuged to form a pellet of cell debris. The supernatant was transferred to a new 1.5 mL microtube. A bicinchoninic acid (BCA) assay was performed to determine the concentration of protein samples.

2.2.4.2. Gel electrophoresis

Protein samples were mixed at a 1:1 ratio with 2x Laemmli Sample Buffer and boiled at 95°C for 5 min, then centrifuged for 1 min at 16,000 rpm to remove any bubbles after boiling, as well as ensuring thorough mixing. 50 µg of protein was loaded onto an SDS-PAGE gel for each sample, as well as 10 µL of PageRuler Prestained Protein Ladder. Gel electrophoresis, to separate proteins based on size, was performed at a constant 200 V for 45 min.

2.2.4.3. Protein transfer to PVDF membrane

The PVDF membrane was briefly soaked in 100% methanol, then washed with milli-Q H_2O (mQH_2O). The PVDF membrane, fiber pads and filter paper (components of protein transfer assembly) were soaked for 15 min in 1x transfer buffer. All components of the protein

transfer assembly were assembled, including the SDS-PAGE gel, and protein was transferred to the PVDF membrane at a constant 100 V for 1 hr. Following protein transfer, the PVDF membrane was washed with mQH_2O.

2.2.4.4. Primary antibody incubation

The PVDF membrane was washed three times for 10 min each in Tris-buffered saline and tween-20 (TBST). To block non-specific antibody binding, the membrane was blocked using 5% w/v milk powder in TBST at room temperature for 1 hr. The PVDF membrane was incubated at 4°C overnight in solution consisting of anti-E-cadherin antibody (polyclonal rabbit antibody, H-108) at a 1:200 dilution in TBST.

2.2.4.5. Secondary antibody incubation

The PVDF membrane was washed three times in TBST for 10 min each, then incubated for 1 hr at room temperature with anti-rabbit secondary antibody (polyclonal donkey IgG antibody, peroxidase-linked, NA934) diluted 1:5000 in TBST. The membrane was then washed three times in TBST for 10 min each, and incubated with enhanced chemiluminescence (ECL) reagent as per manufacturer's protocol. Chemiluminescence from the PVDF membrane was then imaged on the Fuji ECL imaging system.

2.2.4.6. Loading control: α-tubulin

The PVDF membrane was incubated at 50°C for 1 hr in a stripping solution to remove previous antibodies from the membrane, then washed for 1 hr under mQH_2O. The membrane was then washed for 10 min in TBST. The membrane was blocked for non-specific binding, incubated in primary and secondary antibodies, incubated with ECL reagent and imaged using the above methodology for anti-E-cadherin antibody. The primary antibody used was

anti-α-tubulin antibody (monoclonal mouse IgG antibody, peroxidase-linked, T6199), diluted 1:2500 in TBST. The secondary antibody used was anti-mouse antibody (polyclonal sheep IgG antibody, peroxidase-linked, NA931) at a 1:5000 dilution in TBST. Negative controls included an MCF10A WT sample with no primary antibody, and an MCF10A WT sample with no secondary antibody.

2.2.5. qPCR

2.2.5.1. RNA extractions

RNA was extracted from cells in each well of a 6 well or 96 well plate (dependent upon experiment), using the RNAGEM Tissue Plus extraction kit according to manufacturer's protocol, including deoxyribonuclease (DNase) treatment.

2.2.5.2. cDNA synthesis

cDNA synthesis from extracted RNA samples was performed immediately following RNA extraction, using the PrimeScript RT Reagent Kit, according to the manufacturer's protocol. cDNA was used immediately for quantitative real-time PCR (qPCR), or kept at -80°C for long term storage. Negative controls included samples with no reverse transcriptase (RT) enzyme, and a no template control which contained no RNA.

2.2.5.3. qPCR

qPCR was performed in MicroAmp Optical 384 well reaction plates using the Applied Biosystems 7900HT Fast Real-Time PCR system. cDNA samples were diluted 1 in 5 in mQH_2O, and each sample was investigated in triplicate. Each individual reaction had a total volume of 8 μL (Table 2.1.).

All qPCR experiments were performed with primers for *PPIA* and *GAPDH*, used as housekeeper genes. *PPIA* and *GAPDH* were established in the laboratory as housekeeper genes prior to this study commencing. These housekeepers were selected due to their consistent expression levels between MCF10A and MCF10A *CDH1*$^{-/-}$ cell lines, as determined through RNA sequencing [112]. Although not performed during this study, a thorough evaluation of potential housekeeping genes would have proven beneficial. This evaluation would include the testing of at least 7 different housekeeping genes following treatment with lentivirus particles, as this treatment may induce effects on housekeeper gene expression, thus confounding any RT-qPCR results.

qPCR steps included heating to 95°C for 3 min, followed by 40 cycles of: 95°C for 10 sec, 58°C for 10 sec, 72°C for 10 sec. qPCR negative controls include a sample with mQH_2O substituted for cDNA, and the controls described above for cDNA synthesis, as none of these should be amplified.

Component	Volume (µL)
PCR-grade water	0.06
2x KAPA SYBR FAST qPCR Master Mix Universal	4
50x ROX High	0.16
Primer mix (20 µM stock)	0.08
cDNA	3.7
Total volume per reaction	8

Table 2.1. Components of the qPCR reaction mastermix.

2.2.6. Lentiviral-mediated shRNA knockdown

2.2.6.1. Plasmid preparation

DH5α competent *E. coli* cells which have been transformed with pGIPZ lentiviral vectors containing shRNAs of interest were streaked onto agar plates containing 100 µg/mL ampicillin. These colonies were cultured for 16 hr at 37°C. Isolated colonies were

individually inoculated into 50 mL Falcon tubes containing 16 mL of lysogeny broth and 100 µg/mL ampicillin. Culture were then incubated at 37°C for 24 hr to allow for sufficient propagation. Two 8 mL aliquots of the lysogeny broth were used for plasmid DNA purification using the NucleoSpin Plasmid EasyPure kit according to the manufacturer's protocol. Total plasmid DNA in solution was quantified with the NanoDrop, and stored at -20°C.

2.2.6.2. Lentivirus particle production

293FT cells were seeded into one 75 mL culture flask per shRNA to be packaged into lentiviruses, at a density of $5.4x10^6$ cells in 10 mL complete growth medium. All following steps were performed for each 75 mL culture flask. 24 hr post-seeding, a plasmid mixture containing 18.6 µg of shRNA plasmid (or non-silencing (NS) plasmid), plasmids required for lentivirus packaging (psPAX2 and VSVG at 9.6 µg and 4.8 µg respectively) and optiMEM was filtered through a 0.2 µM hydrophilic filter directly into a mixture of Lipofectamine 2000 and filtered optiMEM, to produce a final transfection mixture. 293FT cells were washed once with PBS, then incubated in 8 mL of 5% FBS in optiMEM, which was pre-warmed and filtered through a 0.2 µM hydrophilic filter. The transfection mixture was incubated for 20 min at room temperature, then added dropwise to the 75 mL culture flask. Culture flasks were then returned to the incubator.

24 hr later, cells were washed with PBS, old growth medium aspirated, and 6 mL of fresh complete growth medium added. After a further 24 hr, 293FT complete growth medium containing lentivirus particles was removed from culture flasks and transferred into 15 mL falcon tubes, followed by centrifugation at 3000 rpm for 15 min. Supernatant containing

lentivirus particles was removed and filtered through a 0.45 μm PVDF filter, aliquoted into 1.5 mL microtubes at 500 μL each, then frozen immediately at -80°C.

2.2.6.3. Determining lentivirus titer

To determine the titer of produced lentivirus particles, MCF10A WT cells were seeded into a 96 well black walled, flat, clear bottom tissue culture plate at 4,000 cells per well in 100 μL complete growth medium. At 24 hr post-seeding, serial dilutions of the virus stocks were performed with MCF10A complete growth medium, and 100 μL of diluted virus stock was added to MCF10A cells to give a final dilution range of 1/2 – 1/32 of original virus stocks within the 96-well plate. MCF10A complete growth medium without virus was added to the cell only (CO) negative controls. This CO control was used to confirm that no GFP fluorescence is exhibited by these cells without transduction of shRNAs.

At 48 hr post-seeding, old growth medium was aspirated and replaced with 100 μL of MCF10A complete growth medium.

At 72 hr post-seeding, cells were examined at 10x magnification using the GFP channel on the Eclipse Ti Inverted Microscope System, and five images were taken per well. The dilution of lentivirus particles used for further titer determination was 1/32 for all productions of lentivirus, as our laboratory had previously observed that this dilution results in approximately 50% transduction efficiency (data not shown). A transduction efficiency of approximately 50% ensures that a sufficient number of cells per well are GFP-expressing, increasing the accuracy of counting, but higher efficiencies result in multiple transducing events in some cells, thus causing counting to underestimate the lentiviral titer.

Images were exported into ImageJ for counting of GFP-expressing cells using the Cell Counter plugin. These cell counts across five different images were averaged to give the average number of GFP-expressing cells per image, then multiplied by the factor of the image area relative to the entire well area, essentially giving a number of GFP-expressing cells per well. Following this, the number of GFP-expressing cells per well was multiplied by the reciprocal of the dilution used (i.e. multiplied by 32), and converted from GFP cells per 100 µL to GFP cells per mL. This is the same as the number of transducing units per mL for each lentivirus stock, a measure of lentivirus titer.

2.2.6.4. shRNA knockdown in MCF10A WT and MCF10A CDH1$^{-/-}$ cells

MCF10A WT and MCF10A *CDH1*$^{-/-}$ cells were seeded at 1,000 cells and 2,000 cells per well respectively, into a 96 well black walled, flat, clear bottom tissue culture plate, in 100 µL of complete growth medium. 24 hr post-seeding, lentivirus stocks were diluted in complete growth medium to adjust the titer, and cells were transduced with a multiplicity of infection (MOI) of 15, adding 50 µL total of diluted virus to each well. shRNA knockdown controls used were CO and NS plasmid. The NS control does not specifically target any mRNA sequence within the human genome, but is still processed by the RNA interference pathway. Any knockdown resulting from the NS control represents non-specific responses within the cell, and is used as a baseline for measuring specific knockdown of genes of interest. Accordingly, all results from shRNA knockdown experiments, both qPCR and viability measurements, are normalised to the NS control.

Old growth medium was aspirated at 48 hr post-seeding, and replaced with 100 µL of complete growth medium with 1 µg/mL puromycin for selection of transduced cells. CO

controls were not treated with puromycin, and instead an equal volume of complete growth medium was added to these wells.

At 96 hr post-seeding, RNA was extracted and cDNA synthesised from this as described in Chapter 2.2.5.1. and 2.2.5.2. respectively. 100 µL of a staining mixture containing 1 µg/mL Hoechst 33342 and 1 µg/mL propidium iodide (PI) in PBS was added to each well and incubated at room temperature, in the dark, for 30 min. Within each well, 20 fields of view were automatically imaged at 10x magnification using DAPI and Cy3 channels by the Cytell Cell Imaging System, which is capable of automatically imaging and counting stained cells. The Cytell Cell Imaging System counts total nuclei in the DAPI channel (Hoechst 33342 staining), and PI-stained nuclei, a measure of cell death, in the Cy3 channel. Within the output, both a total nuclei count, and the percentage of dead cells, as determined by comparing numbers of PI- and Hoechst-stained nuclei, are returned.

qPCR to confirm gene knockdown with respective shRNAs was performed according to Chapter 2.2.5.3.

2.2.7. Drug inhibition

2.2.7.1. Drug suspension and storage

Both CD2665 and SU6668 were reconstituted in DMSO to create stock solutions at a concentration of 80mM. These were aliquoted and stored in 1.5 mL microtubes at -80°C.

2.2.7.2. IncuCyte assay

MCF10A WT and MCF10A *CDH1*$^{-/-}$ cells were seeded into a 96 well, black walled, flat, clear bottom tissue culture plate at a density of 4,000 cells per well in 100 µL complete

growth medium. 24 hr post-seeding, cells were treated with 10 µL of varying concentrations of either CD2665 or SU6668, or with 0.07% DMSO for controls. Immediately following drug treatment, tissue culture plates were incubated within the IncuCyte apparatus for 48 hr of real-time imaging at 2 hr intervals. Resulting data was analysed using the IncuCyte software which utilises cell surface area to estimate the confluence of each well at any given time point.

Because IncuCyte assays were performed prior to end-point nuclei counting experiments, drug concentrations were yet to be optimised. Therefore, serial dilutions of 1/5 were performed for both CD2665 and SU6668, starting at 786 µM, the maximum possible concentration considering the volume of drug stock aliquots. Serial dilution concentrations were therefore: 786 µM, 157.2 µM, 31.44 µM, 6.29 µM, 1.26 µM, 0.25 µM, 0.05 µM, and 0.01 µM.

2.2.7.3. End-point nuclei counting

MCF10A WT and MCF10A *CDH1*$^{-/-}$ cells were seeded into a 96 well, black walled, flat, clear bottom tissue culture plate at a density of 4,000 cells per well in 100 µL complete growth medium. 24 hr post-seeding, cells were treated with 10 µL of either CD2665, SU6668, or 0.07% DMSO for controls. For SU6668, the same serial dilution of drug was performed as in Chapter 2.2.7.2. For CD2665, because a synthetic lethal effect had been observed at 31.44 µM from the IncuCyte assay, further end-point nuclei counting assays utilised drug concentrations of 20 µM – 55 µM.

72 hr post-seeding, 100 µL of a staining mixture containing 1 µg/mL Hoechst 33342 in PBS was added to each well and incubated at room temperature, in the dark, for 30 min. Within

each well, 20 fields of view were automatically imaged at 10x magnification using the DAPI channel on the Cytell Cell Imaging System. The Cytell counts total nuclei in the DAPI channel (Hoechst 33342 staining), and these counts were used for analyses.

3. Results

3.1. Identifying putative synthetic lethal partners with *CDH1* in medulloblastoma

The mRNA expression profiles of 62 medulloblastomas were used for the identification of synthetic lethal partners with *CDH1*. This dataset was produced by Kool *et al*. [100] through expression profiling with Affymetrix microarrays, with the aim of improving the specificity of molecular classification of medulloblastomas. This dataset was acquired from GEO (accession number GSE10327) [7]. All of the following bioinformatic analyses were carried out in the computational environment R [8].

Initial quality control checks are a necessity when dealing with a new microarray dataset, to ensure that there is no significant variation in probe intensities due to variables such as differences in sample preparation. Probe intensity is a measure of gene expression levels, with greater intensity representing a greater level of probe hybridisation to sample RNA, therefore reporting increased gene activity. The affyQCReport package [107] for R was utilised for microarray quality control, and no anomalies were found amongst the 62 microarrays (Appendices 5.2.1.-5.2.3.). This shows that, prior to normalisation, the microarrays contained no significant differences in relation to variables such as hybridisation differences, and are therefore sufficiently comparable for biological analyses. It's important that internal quality control is carried out prior to this normalisation, to ensure that the data does not contain anomalies that will affect further analyses, as these may be obscured during the normalisation process (Appendix 5.2.4.). Following quality control checks, microarray expression data was normalised using the RMA algorithm [13], considered to be the de facto standard for this application. As a result of the processing used in the RMA normalisation algorithm, probe intensities are measured on the log scale.

The correlation and density plots for the two *CDH1* probe pairs used by the microarray dataset were reviewed to ensure that probes had similar intensity measurements, and were therefore reliable for further analyses. A Pearson's correlation coefficient of 0.69, as well as visual similarity of probe set distributions (Figure 3.1.) suggests that these probes are generating relatively similar measurements for each sample. Two additional, separate microarray datasets were processed to compare *CDH1* probe correlations, and to determine relative *CDH1* probe quality in the medulloblastoma dataset. These datasets contained Ewing's sarcoma [101] and rhabdomyosarcoma [102] tumour and cell line samples respectively, also interrogated with an identical microarray platform (GEO accession number GSE17679 and GSE8840 respectively). *CDH1* probes from the medulloblastoma dataset were far more comparable to each other, relative to those of these two additional datasets with *CDH1* probe correlations of 0.4 and -0.15 respectively (Appendices 5.3.1.-5.3.2.). This is important as it suggests that the *CDH1* probes are performing relatively well within the medulloblastoma dataset, compared to alternative datasets. Subsequent to this, *CDH1* intensity values from both probe sets for each individual tumour sample in the medulloblastoma dataset were averaged for all further data processing, as probe similarity was deemed sufficient.

For the proposed synthetic lethality detection strategy to be effective, a subgroup of the tumours of interest must express *CDH1* at relatively low levels, representing tumours that exhibit *CDH1* loss. If *CDH1* expression spans a 2-fold range amongst the 62 medulloblastoma samples, this provides a reasonable degree of evidence for variation in *CDH1* expression, and may reveal a *CDH1*-low subgroup of samples. The 62 medulloblastoma samples were separated into three equally sized classes based on the level of *CDH1* expression in each tumour: *CDH1* low, *CDH1* medium, and *CDH1* high. As

intensity is now measured on the log scale, a range of at least 1 in intensity will represent a two-fold range of *CDH1* expression. The lowest intensity for the *CDH1* probe set detected amongst the samples measured at 6.44, with the highest at 8.25 (Table 3.1.). This range of 1.81 in intensity amongst all samples tested provides evidence of variance in *CDH1* expression within the dataset, and appears to reveal a subset of *CDH1*-low medulloblastoma tumours. This therefore enables the use of the proposed bioinformatic strategy for detecting synthetic lethal relationships. The distinct, narrow subgrouping of *CDH1*-low tumour samples may represent Wnt-subgroup medulloblastomas (Figure 3.2.).

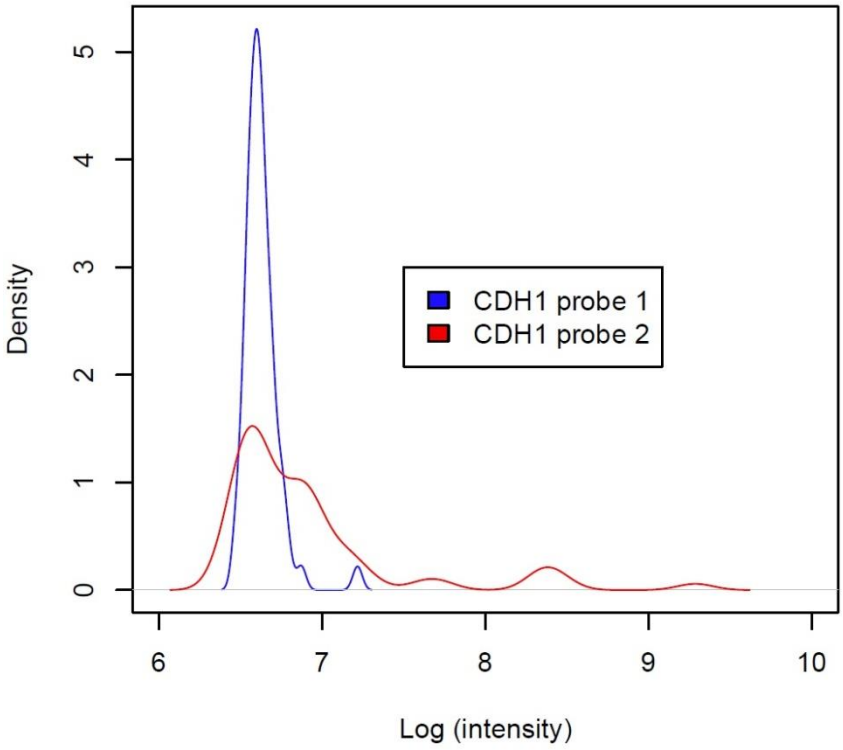

Figure 3.1. Distribution of probe intensities from both *CDH1* probe pairs as measured in all 62 medulloblastoma tumour samples. There appear to be several outlying intensity readings from probe 2, however the majority of readings lie within the same range as probe 1.

	***CDH1* expression classes**		
	Low	**Medium**	**High**
Log (intensity) range	**6.44 - 6.60**	**6.60 - 6.76**	**6.76 - 8.25**

Table 3.1. Range of *CDH1* intensity measurements for each *CDH1* expression class.

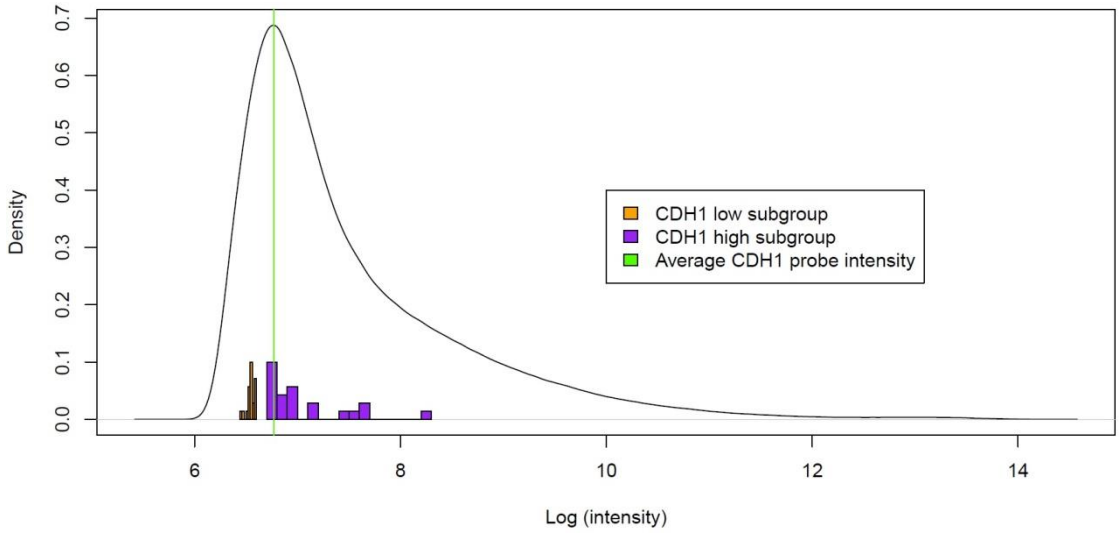

Figure 3.2. Distribution of *CDH1* probe set intensities for both *CDH1* low (orange histogram) and *CDH1* high (purple histogram) subgroups are depicted here, as well as intensity measurements for all probe targets within the dataset (distribution curve). Average *CDH1* intensity is depicted with a vertical green line, and a clear range of *CDH1* intensities amongst the dataset can be observed. Additionally, a distinct *CDH1*-low subgroup of tumours has been revealed within a narrow range of intensity readings.

Putative synthetic lethal interactions were identified using an approach designed by Tom Kelly, BSc (Hons) student, and Assoc. Prof. Mik Black (Figure 1.2.) [16]. An example of the output from this approach is shown below (Table 3.2.), presenting three candidate genes which exhibit a gene expression relationship with *CDH1* that is indicative of synthetic lethality, and three genes which do not appear synthetic lethal with *CDH1*. This analysis detected 73 significant (adjusted p-value ≤ 0.05) potential synthetic lethal partners with *CDH1*, after correcting for multiple testing with the false discovery rate (FDR) approach (Table 3.3.).

	Gene	ObsLow	ExpLow	ObsHigh	ExpHigh	SynLethal	adjPval_FDR
Indicative of synthetic lethality	CREB3L2	3.00	7.11	14.00	7.11	1	0.00
	RARB	2.00	7.11	9.00	7.11	1	0.05
	PDGFD	2.00	7.11	13.00	7.11	1	0.05
Not indicative of synthetic lethality	FGF11	8.00	7.11	7.00	7.11	0	0.93
	CVID4	8.00	7.11	6.00	7.11	0	0.96
	METTL12	8.00	7.11	7.00	7.11	0	0.99

Table 3.2. Output from bioinformatic approach used to identify synthetic lethal partnerships. ObsLow represents the number of tumour samples in which the candidate gene was expressed at low levels in conjunction with *CDH1*. ExpLow represents the expected number of tumour samples in which the candidate gene was expressed at low levels in conjunction with *CDH1*, assuming there is no existing gene-gene relationship. ObsHigh and ExpHigh represent the same as ObsLow and ExpLow, except these depict the number of, or expected number of tumours with high expression of the candidate gene. If ObsLow is significantly lower than the ExpLow value, and ObsHigh is significantly higher than the ExpHigh value, this is indicative of synthetic lethality with *CDH1*, presented here with SynLethal = 1 (see top three candidate genes). If ObsLow is significantly greater than the ExpLow value, or ObsHigh is significantly lower than ExpHigh, or no significant difference is observed between the values, this is not indicative of synthetic lethality with *CDH1*, presented here with SynLethal = 0 (see bottom three candidate genes). The associated p-values, corrected for multiple testing (adjPval_FDR), are determined from a chi-squared test of the data outlined in Figure 1.2.

Gene	FDR-adjusted p-value
CREB3L2	0
HSCB	0.01
SDC2	0.01
SLC1A5	0.01
ITPRIPL2	0.01
EIF3K	0.02
QTRTD1	0.02
COL4A5	0.02
RPS19	0.02
VAMP1	0.02
MSC	0.02
SLC25A37	0.02
RPL18A	0.02
RPL36A	0.02
EMP3	0.02
REST	0.03
NTAN1	0.03
RPL36AL	0.03
TLK1	0.03
TYW3	0.03
EPHB4	0.04
LGALS1	0.04
ANO6	0.04
NOL10	0.04
RPL35A	0.04
RPS16	0.04
STARD4	0.04
DLG1	0.04
LPP	0.04
PRDX4	0.04
SUMF1	0.04
EIF3E	0.04
SFXN4	0.04
RPL31	0.05
C1orf198	0.05
IER3	0.05
SIX5	0.05

Gene	FDR-adjusted p-value
ATP11C	0.05
CCL2	0.05
RARB	0.05
SAG	0.05
METTL9	0.05
PBX1	0.05
PABPC1	0.05
RNF7	0.05
LPAR6	0.05
GPBP1L1	0.05
PBX3	0.05
PPA1	0.05
COX6B1	0.05
R3HDM1	0.05
POLQ	0.05
WWP1	0.05
FAM175A	0.05
PDGFD	0.05
AFF1	0.05
RPS2	0.05
SQLE	0.05
MRPL36	0.05
APOL4	0.05
EIF4A1	0.05
SNRPD2	0.05
MRPL51	0.05
DERA	0.05
ADSL	0.05
AGTRAP	0.05
CALD1	0.05
SKIL	0.05
SLC44A3	0.05
RPL36	0.05
SERPINF1	0.05
MTBP	0.05
TSPO	0.05

Table 3.3. List of all significant candidate genes for synthetic lethality with *CDH1*, identified from microarray expression data of 62 medulloblastoma tumour samples, in order of significance.

3.2. Synthetic lethal candidate selection

These candidate genes for synthetic lethality with *CDH1* were then compared to experimental data previously generated by our laboratory. This data consists of a genome-wide small interfering RNA (siRNA) screen, performed by PhD student Bryony Telford at the Victorian Centre for Functional Genomics, Peter MacCallum Cancer Centre, Melbourne [111]. An isogenic MCF10A cell line pair of non-tumorigenic, epithelial breast cells were used for this screen: one of the pair expresses *CDH1* at wild-type (WT) levels, whilst the other has had *CDH1* expression abrogated (Appendix 5.4.). siRNA knockdown of 18,175 genes, using four pooled siRNAs each, was performed in these cell lines. Changes in cell numbers, a measure of cell viability, were measured metabolically using CellTiter-Glo. Synthetic lethality was defined as at least a 15% reduction in cell viability in the MCF10A $CDH1^{-/-}$ cell line relative to the MCF10A WT cells following gene knockdown. To this end, a total of 2,160 candidate synthetic lethal partners with *CDH1* were identified for further investigation. This screen is currently used as a resource for a variety of projects within our laboratory.

Any candidate genes achieving the thresholds for synthetic lethality in the siRNA screen were compared against the significant candidate genes identified from the *in silico* screen. All candidate synthetic lethal partners from the *in silico* screen were removed unless also synthetic lethal in the siRNA screen. Seven of the remaining candidate genes were also supported by the siRNA screen (Figure 3.3., Table 3.4.). This provides additional confidence in the selection of candidate genes for experimental validation, as there has been experimental evidence in the past which supports all seven of these genes as synthetic lethal partners of *CDH1*.

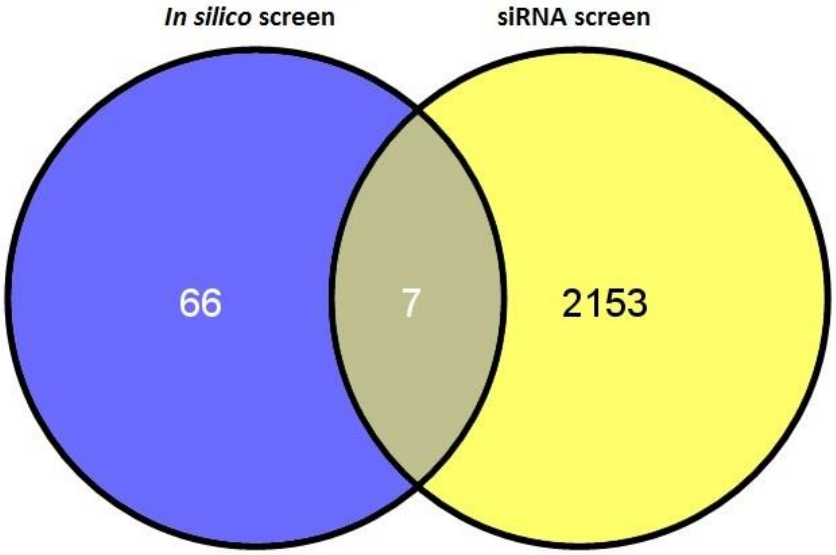

Figure 3.3. Venn diagram [113] representing the 73 significant synthetic lethal candidates identified in the *in silico* screen, the 2,160 synthetic lethal candidates from the siRNA screen, and the 7 candidates from the *in silico* screen which are supported by the siRNA screen.

From the seven synthetic lethal candidates which were supported by both screens, *RARB* and *PDGFD* were selected for further experimental validation. Within the siRNA screen, *RARB* and *PDGFD* induced the greatest synthetic lethal effect out of the seven genes, with a 26% and 29% difference in viability between cell lines respectively (Table 3.4.). Knockdown of all seven candidate genes also caused minimal harm to healthy MCF10A WT cells. This combination of characteristics for *RARB* and *PDGFD* is suitable in a clinical setting for the reduction of toxic side effects following treatment.

Additionally, the same bioinformatic strategy utilised for the medulloblastoma dataset showed relationships between *CDH1* and both *RARB* and *PDGFD* that were consistent with synthetic lethality in a breast cancer dataset (Assoc. Prof. Mik Black, personal communication). This breast cancer dataset is a large multi-cohort dataset of approximately 2000 breast cancer tumours, assembled from publicly available microarray data by Assoc. Prof. Mik Black [103]. Both *RARB* and *PDGFD* have been selected for further validation as

candidate genes for a synthetic lethal relationship with *CDH1* based on a number of characteristics (Table 3.7.).

Gene	FDR-adjusted p-value	MCF10A viability	MCF10A WT : *CDH1*$^{-/-}$ ratio
EIF3K	0.02	0.92	0.80
TLK1	0.03	1.04	0.75
EPHB4	0.04	0.98	0.79
DLG1	0.04	1.04	0.75
RARB	0.05	0.82	0.74
PDGFD	0.05	0.90	0.71
DERA	0.05	0.92	0.82

Table 3.4. List of all significant synthetic lethal candidates for *CDH1* identified by the *in silico* screen and also supported by siRNA screen data. P-values for the *in silico* screen, corrected for multiple testing to control the False Discovery Rate (FDR), are shown. MCF10A WT : *CDH1*$^{-/-}$ ratio represents the relative viability of *CDH1*$^{-/-}$ cells to MCF10A WT cells within the siRNA screen. For example, with *EIF3K* knockdown with siRNAs, MCF10A WT cells decreased in viability by 8% compared to controls, and a difference of 20% in viability was observed when comparing *CDH1*$^{-/-}$ cells to WT cells.

RARB encodes retinoic acid receptor beta (RARβ), a nuclear receptor for retinoic acid, and one of three known retinoic acid receptors (RARs), including RARα and RARγ [114]. The three different isotypes are similar, but not identical in structure. As a result, some functional redundancies exist between RARs, but each isotype is also associated with unique functions [115-117]. These retinoic acid receptors are part of the nuclear hormone receptor family, characterised by the binding of DNA enhancer elements, referred to as hormone-response elements, within or adjacent to the promoters of target genes to regulate transcription [118]. The presence of retinoic acid stimulates the dimerisation of RARs and retinoid X receptors (RXRs), which bind to retinoic acid response elements (RAREs) to regulate transcription of target genes [119]. RARs play a role in mediating embryogenesis [117], cell differentiation [120] and matrix homeostasis [121].

The platelet-derived growth factor (PDGF) family consists of four different PDGFs, PDGF-A, -B, -C and -D. These are inactive in their monomeric forms, but form homo- and heterodimers when active: PDGF-AA, PDGF-AB, PDGF-CC and PDGF-DD. The platelet-

derived growth factor receptors (PDGFRs) themselves come in two forms: PDGFRα and PDGFRβ. These also form homo- and heterodimers: PDGFR-αα, -αβ and –ββ. PDGFD homodimerises to form PDGF-DD, which is regarded as specific to PDGFR-ββ, although has a minor affinity to PDGFR-αβ also. *PDGFD* has been shown to play key roles in cell differentiation, macrophage recruitment and blood vessel maturation [122, 123].

Following the selection of *RARB* and *PDGFD* for further validation as synthetic lethality candidate genes, probe correlations were reviewed in the same manner as for *CDH1*. Both *PDGFD* probes were especially comparable, with a Pearson's correlation coefficient of 0.82. Visual representation was also in support of this, as probe 1 covered a similar range of intensity values to probe 2, with the exception of some outlying greater intensities (Figure 3.4.). This microarray platform contains five probe pairs interrogating *RARB*, making a comparison by Pearson's correlation difficult as none of the probe pairs exhibit broad similarity to all other *RARB* probe pairs, and instead display sufficient correlation to a subset of these. Upon visual observation, a clear similarity can be seen amongst the *RARB* probes collectively (Figure 3.5.). From this, it can be inferred that values derived from each individual probe were reliable as well as, by extension, the previous analyses which used these values to identify *RARB* and *PDGFD* as synthetic lethal partners to *CDH1*.

Affymetrix probe identifier	Designated name
201130_s_at	*CDH1* probe 1
201131_s_at	*CDH1* probe 2
219304_s_at	*PDGFD* probe 1
222860_s_at	*PDGFD* probe 2
205080_at	*RARB* probe 1
208412_s_at	*RARB* probe 2
208413_at	*RARB* probe 3
208530_s_at	*RARB* probe 4
217020_at	*RARB* probe 5

Table 3.5. Affymetrix probe identifiers and the designated names as they are referred to throughout this study.

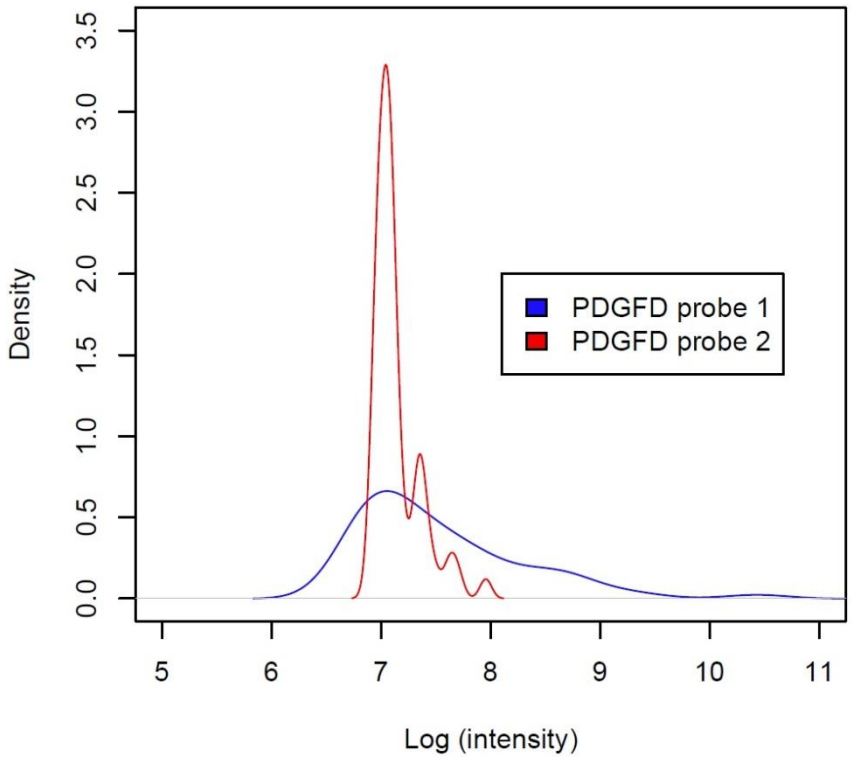

Figure 3.4. Distribution of probe intensities from both *PDGFD* probe pairs as measured in all 62 medulloblastoma samples.

RARB probe set correlation					
	Probe 1	Probe 2	Probe 3	Probe 4	Probe 5
Probe 1	1.00	0.08	0.08	0.90	0.11
Probe 2	0.08	1.00	0.44	0.17	0.32
Probe 3	0.08	0.44	1.00	0.11	0.39
Probe 4	0.90	0.17	0.11	1.00	0.13
Probe 5	0.11	0.32	0.39	0.13	1.00

Table 3.6. Pearson correlation coefficients of the average intensity values for all five *RARB* probe pairs.

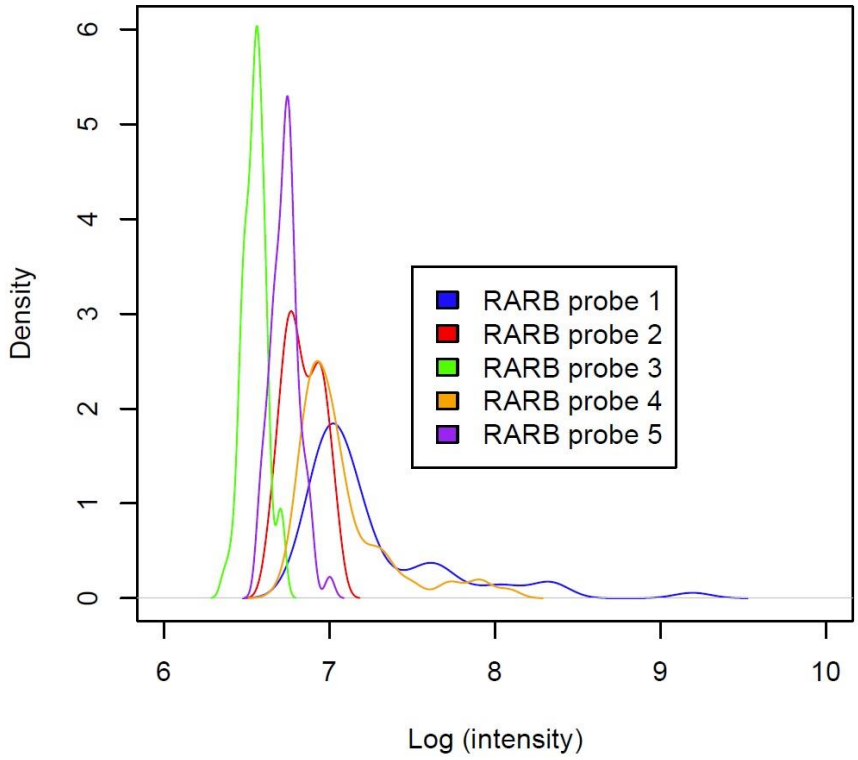

Figure 3.5. Distribution of probe intensities from all five *RARB* probe pairs as measured in all 62 medulloblastoma samples.

Characteristics	RARB	PDGFD
siRNA screen: MCF10A WT viability	0.82	0.9
siRNA screen: MCF10A *CDH1*$^{-/-}$ viability	0.61	0.64
siRNA screen: MCF10A WT viability : MCF10A *CDH1*$^{-/-}$ viability ratio	0.74	0.71
Synthetic lethal detection strategy: FDR-adjusted p-value	0.05	0.05
Synthetic lethal detection strategy: Supported by breast cancer dataset	Yes	Yes
Synthetic lethal detection strategy: Supported by Ewing's sarcoma dataset	No	Yes

Table 3.7. Summary of *RARB* and *PDGFD* characteristics leading to selection as synthetic lethal partners of *CDH1* for experimental validation. These characteristics include viability values from the siRNA screen as well as bioinformatic analyses using a novel synthetic lethal detection strategy.

3.3. Cell lines for experimental validation of candidate genes

The isogenic pair of MCF10A cells are mammary epithelial breast cells, and are therefore not of the same biological background as medulloblastomas. However, these cells have been well established and characterised by our laboratory through cell-based assays and genome-wide RNAseq [112], and represent a model of *CDH1* loss in a relatively normal biological background.

The need to conduct validation experiments in a cell line with a similar genetic background to medulloblastoma led to the investigation of various medulloblastoma cell lines. E-cadherin expression was a requirement for cell line selection, as the proposed method for reproducing synthetic lethality involved transiently knocking down *CDH1* expression via shRNAs, thereby producing a *CDH1*$^{-/-}$ cell line for comparison with the *CDH1*$^{+/+}$ cells. In this regard, the cell line pair would be utilised in the same way as the MCF10A isogenic cell line pair for viability experiments, and the determination of synthetic lethality between *RARB* and *PDGFD* with *CDH1*.

The DAOY cell line was selected for this purpose. DAOY is a cancerous cell line derived from a tumour of the cerebellum, originating from a 4-year old Caucasian male [108], and exhibits adherent culture properties (Figure 3.6.). Adherent properties were preferable during

cell line selection as MCF10A shares this characteristic, and both cell lines have analogous culturing protocols. This has useful implications for the comparison of results between DAOY and MCF10A cell lines, as confounding factors such as culture technique are reduced. Importantly, E-cadherin expression had previously been shown in the DAOY cell line through western blotting [124].

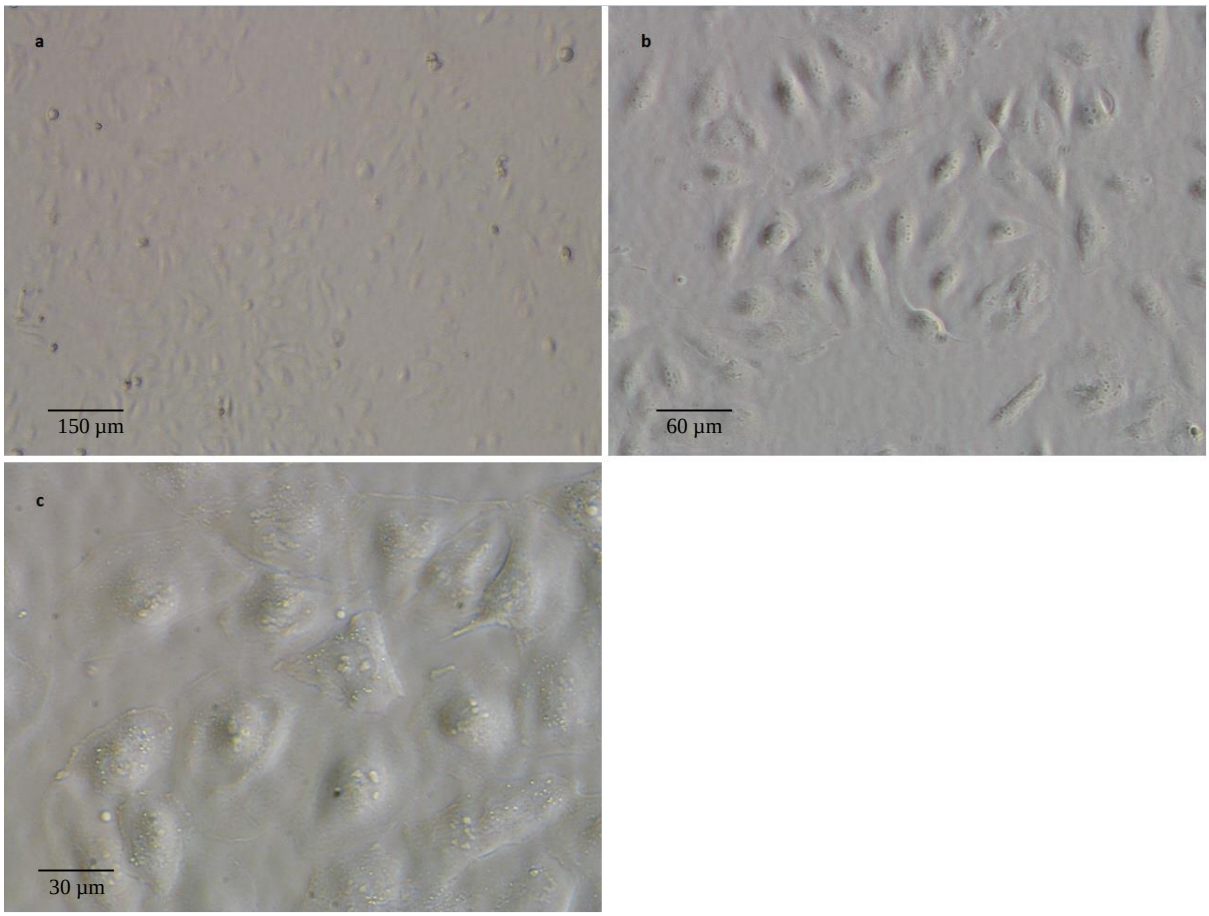

Figure 3.6. Microscopy illustrating the morphology of medulloblastoma cell line DAOY at 4x (a), 10x (b) and 20x (c) magnification. DAOY is derived from a medulloblastoma originating in a 4-year old Caucasian male, and exhibits adherent culture properties, as illustrated above.

3.4. Confirming *CDH1* expression in the DAOY cell line

As mentioned above, *CDH1* expression has already been shown in DAOY in a previous study [125]. Attempts to reproduce this observation of *CDH1* expression were made within our laboratory before further DAOY experimentation. However, immunofluorescence staining for E-cadherin in DAOY cells was inconclusive (Figure 3.7.). As expected, clear

localisation of E-cadherin to the cellular boundaries of MCF10A WT cells can be seen, in concordance with the role of E-cadherin in cell-cell adhesion, and MCF10A *CDH1*$^{-/-}$ cells did not exhibit E-cadherin staining. DAOY cells appear to show a lesser degree of E-cadherin staining relative to MCF10A WT cells, but this apparent staining is not localised to cell boundaries. It is possible that this was due to autofluorescence of DAOY cells, as the staining was not localised, and appears consistent across the entirety of the cell body. However, if this was the case, staining in MCF10A *CDH1*$^{-/-}$ cells should exhibit a similar pattern of fluorescence. Alternatively, this could have been due to the lack of E-cadherin localisation to cell boundaries, resulting in an even distribution of E-cadherin protein across the cellular membrane or cytoplasm.

CDH1 expression was further investigated through western blotting with E-cadherin antibody (Figure 3.8.). As anticipated, and in concordance with the immunofluorescence staining, E-cadherin expression was clearly exhibited by MCF10A WT cells, and absent in MCF10A *CDH1*$^{-/-}$ cells. DAOY also lacked E-cadherin protein. This was unexpected as E-cadherin expression had been clearly shown by western blotting in the earlier study [125]. Although the loading control shows that protein lysates were not consistent between samples, this reinforces the lack of E-cadherin protein in DAOY, as considerably more protein from DAOY cells was loaded in comparison to MCF10A WT.

As western blotting for E-cadherin expression in DAOY cells provided an unanticipated result, and immunofluorescence also showed an E-cadherin deficit, quantitative real-time PCR (qPCR) of *CDH1* activity was performed as a final measure of *CDH1* expression in DAOY cells (Figure 3.9.). As anticipated, *CDH1* mRNA in MCF10A WT cells was abundant. As a result, *CDH1* mRNA levels from DAOY and MCF10A *CDH1*$^{-/-}$ cells were

normalised to MCF10A WT levels for comparison. *CDH1* transcripts were scarcely detected in MCF10A *CDH1*$^{-/-}$. Some degree of *CDH1* transcript was expected in the MCF10A *CDH1*$^{-/-}$ cells, as RNAseq experiments used to characterise these cells by our laboratory [112] also detected low levels of transcript (despite this, no E-cadherin protein is produced in these cells due to the 4 bp deletion in *CDH1*). Within the DAOY cell line, *CDH1* activity was comparable to the MCF10A *CDH1*$^{-/-}$ sample. This scarce level of *CDH1* transcript detected is perhaps purely an artefact of the qPCR methodology, or *CDH1* is expressed at particularly low levels in this cell line. When examining raw cycle threshold (Ct) values, a difference of one Ct between samples represents a two-fold change in expression, as Ct is measured on the log scale. Raw Ct values showed that DAOY expresses *CDH1* at approximately 6.25% the level of MCF10A *CDH1*$^{-/-}$, and approximately 0.20% the level of MCF10A WT (Table 3.8.). It should be noted that this is not an accurate measurement, as this is only taking into account the raw Cts value for *CDH1*, and not normalising to housekeeper genes to control for cDNA concentration. However, this further illustrates the particularly low level of *CDH1* expression within DAOY cells.

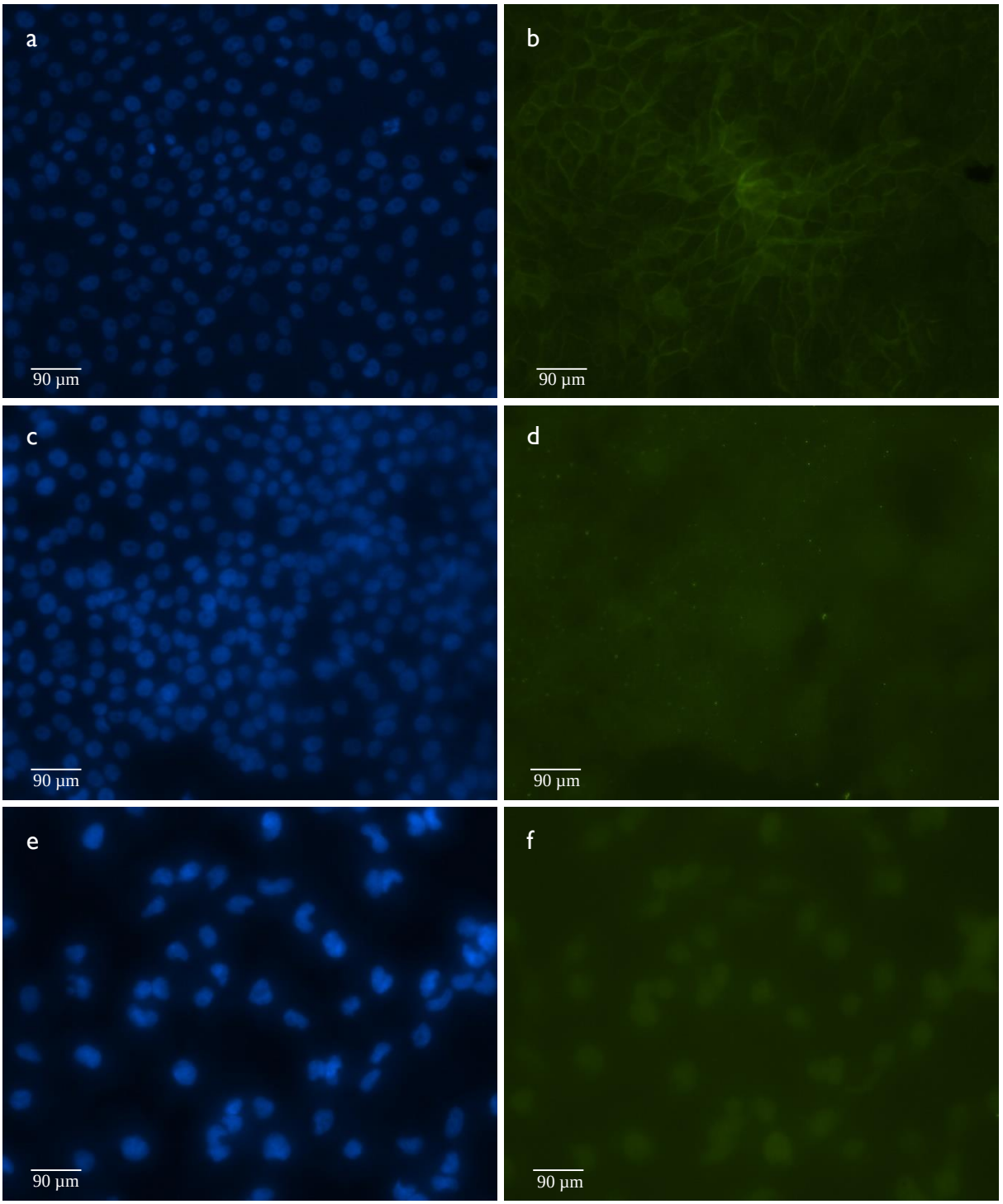

Figure 3.7. Microscopy of immunofluorescence staining for E-cadherin at 20x magnification. **a)** DAPI staining of MCF10A WT nuclei. **b)** Fluorescence emitted from the E-cadherin antibody conjugate in MCF10A WT cells. Clear localisation of E-cadherin to cell boundaries was observed. **c)** DAPI staining of MCF10A *CDH1*$^{-/-}$ nuclei. **d)** Fluorescence emitted from the E-cadherin antibody conjugate in MCF10A *CDH1*$^{-/-}$ cells. No E-cadherin staining was detected. **e)** DAPI staining of DAOY nuclei. **f)** Fluorescence emitted from the E-cadherin antibody conjugate in DAOY cells. Faint E-cadherin staining was exhibited by DAOY cells, although this was not localised to cell boundaries.

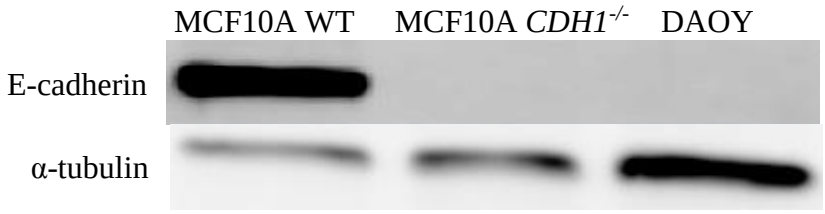

Figure 3.8. Western blotting with E-cadherin antibody shows clear expression of E-cadherin in the MCF10A cell line, and a distinct lack of protein in both DAOY and MCF10A *CDH1*$^{-/-}$ cells. Loading control α-tubulin shows that the MCF10A WT protein lysate contained considerably less protein.

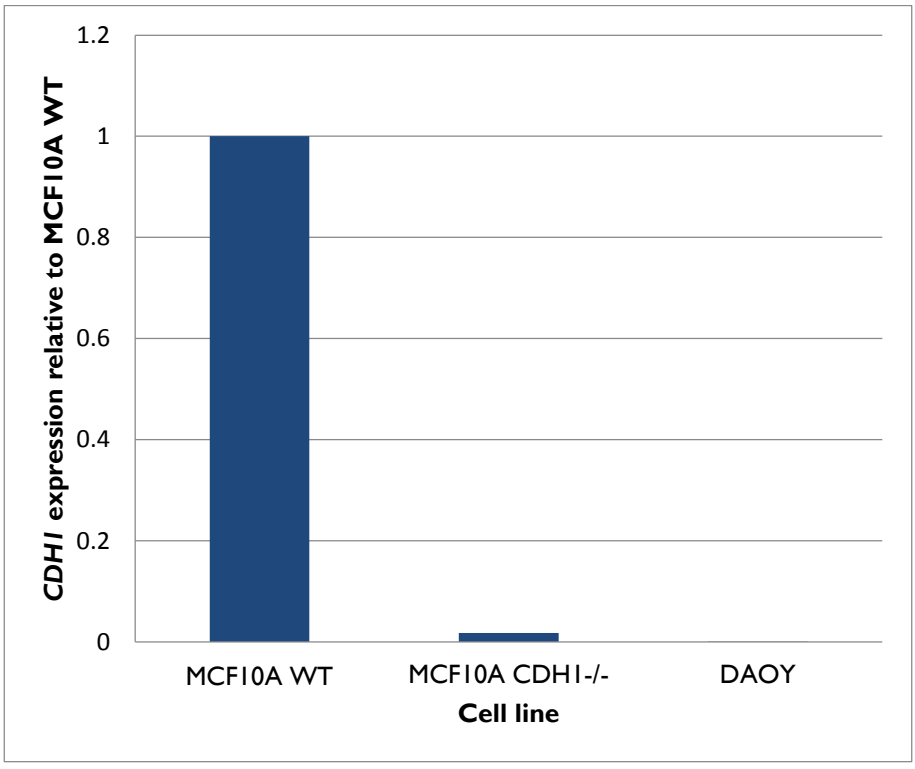

Figure 3.9. qPCR of *CDH1* activity, normalised to *CDH1* mRNA expression in the MCF10A WT cell line. Both MCF10A *CDH1*$^{-/-}$ and DAOY cells exhibit scarcely detectable levels of *CDH1* transcript.

Cell Line	Average Ct for *CDH1*
MCF10A WT	21.87
MCF10A *CDH1*$^{-/-}$	27.18
DAOY	31.03

Table 3.8. Raw Ct values from qPCR of *CDH1* activity. DAOY clearly exhibits extremely low levels of *CDH1* expression, about 16-fold lower than that of MCF10A *CDH1*$^{-/-}$.

Subsequently, it was concluded that DAOY could not be used to create a medulloblastoma-derived pair of cell lines with high and low *CDH1* expression. As a consequence, experimental validation of synthetic lethal partners *RARB* and *PDGFD* was performed solely in the MCF10A isogenic cell line pair.

3.5. Cell viability following shRNA knockdown of synthetic lethality candidate genes

In addition to *RARB* and *PDGFD*, a third gene, *MAPRE3*, was elected for knockdown as a potential positive control for synthetic lethality with *CDH1*. Microtubule-associated protein RP/EB family member 3 (MAPRE3) is a microtubule plus end binding protein which is involved in regulating the attachment and stabilisation of microtubule ends at the cell cortex as well as their interactions with the mitotic kinetochore, and is believed to affect the structure of growing microtubule tips [126]. This gene was a compelling candidate gene for synthetic lethality with *CDH1*, as determined from the genome-wide siRNA screen. In addition to the results from the siRNA screen, *MAPRE3* is of interest due to its close involvement with the cellular microtubule network, a characteristic that *CDH1* shares, providing a biological link which may explain the mechanism of synthetic lethality, should this relationship exist.

Prior to the shRNA knockdown experiments performed in this study, Bryony Telford (PhD student) and James Frick (Masters student) established and optimised the Neon®

Transfection System for siRNA knockdown of candidate synthetic lethal partners in the MCF10A isogenic cell line pair. However, a balance between sufficient transfection efficiency and acceptable cell death induced by electroporation was not achieved, and as a result, lentiviral-mediated small hairpin RNA (shRNA) knockdown was utilised by this study. Lentiviral-mediated shRNA knockdown of *RARB*, *PDGFD* and *MAPRE3* was performed separately in the MCF10A isogenic cell line pair. Differences in cell numbers 72 hr after transduction were observed, and synthetic lethality was defined as a significant reduction in MCF10A *CDH1*$^{-/-}$ cell numbers relative to MCF10A WT cell numbers. Four unique shRNA clones were used for *MAPRE3* knockdown (A1-A4), whilst *RARB* and *PDGFD* were interrogated with two unique clones each (R1-R2 and P1-P2 respectively). The activity of shRNA clones targeting *MAPRE3*, *RARB* and *PDGFD* resulted in 31-56% (Figure 3.10.), 40-73% and 24-69% (Figure 3.11.) mRNA knockdown respectively.

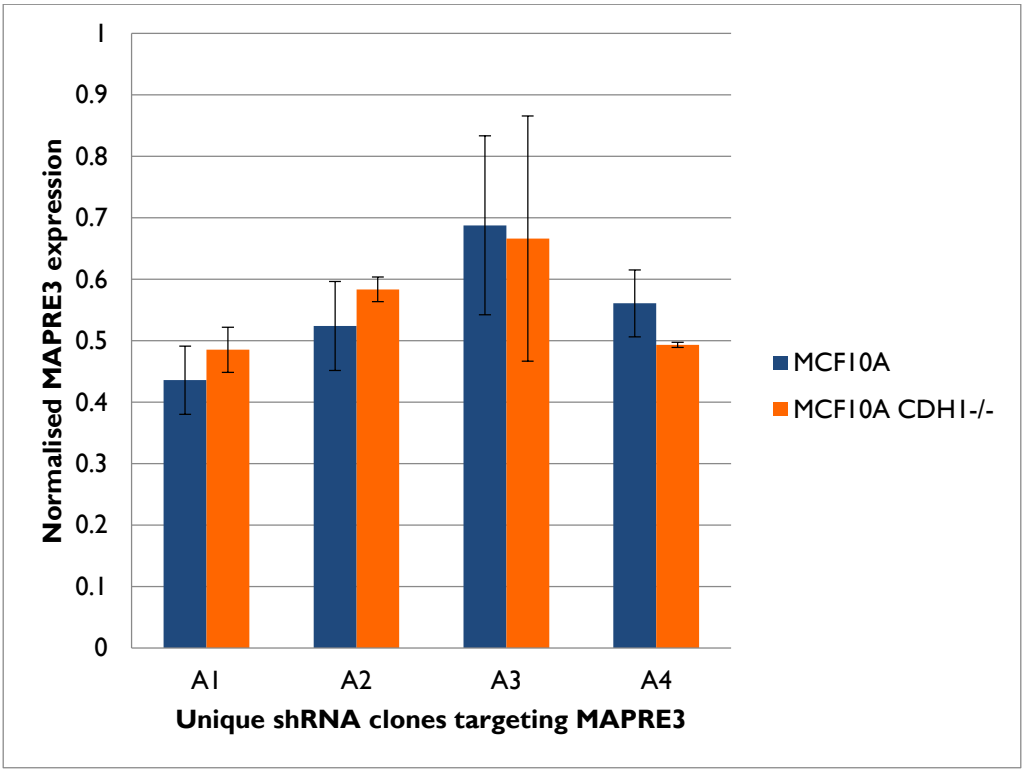

Figure 3.10. Level of *MAPRE3* expression, normalised to a non-silencing (NS) plasmid control, following knockdown with four unique shRNA clones in both MCF10A cell lines. Error bars represent ± 1 standard deviation, as derived from two technical replicates.

It should be noted that controls for both *PDGFD* and *RARB* mRNA expression did not behave as expected. If normalised to the non-silencing (NS) control, both R1 and R2 shRNAs have induced mRNA transcript knockdown. However, the cell only (CO) control exhibits *RARB* expression at comparable levels to samples treated with shRNAs when normalised to the NS control. This was unexpected, as the CO control should have similar levels of *RARB* expression to the NS control. Initially this was thought to be a result of variability in qPCR reactions for *RARB*, as it's expressed at very low levels in MCF10A WT and *CDH1*$^{-/-}$ cells [112], possibly resulting in PCR biases. However, upon repetition of this experiment, very similar results were obtained when identical RNA samples were used (Appendix 5.6.).

A similar effect was observed for *PDGFD* (Appendix 5.7.), which is also expressed at low levels in MCF10A WT and *CDH1*$^{-/-}$ cells, although more abundant than *RARB*. The CO control was more comparable to the NS control for *PDGFD* knockdown than for *RARB* knockdown, however there was still an apparent decrease in expression. Additionally, *PDGFD* knockdown induced by the P2 shRNA clone was observed in only one of two experiments. These observed anomalies are most likely due to the low levels of transcript in the cell population as a whole, resulting in potential significant fluctuation of these levels at any one time point. This could be further investigated through repeating of shRNA experiments, and obtaining new RNA samples for testing. Due to time constraints, this was not completed.

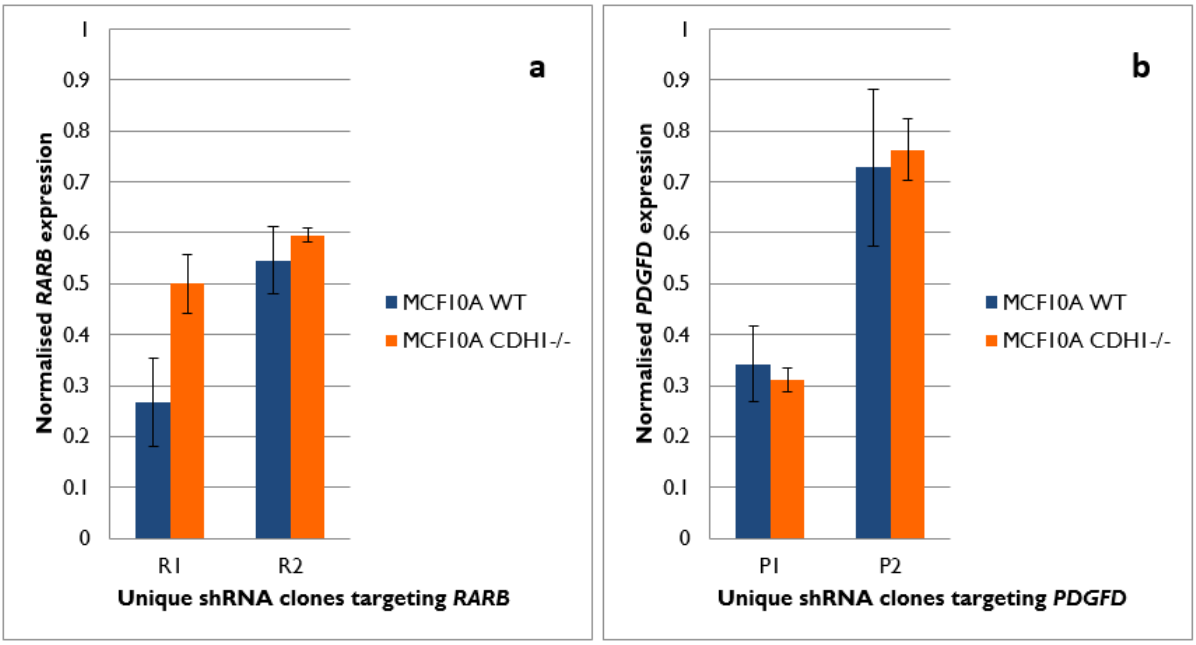

Figure 3.11. a) Level of *RARB* expression is depicted here, following shRNA knockdown with clones R1 and R2. **b)** Level of *PDGFD* expression is depicted here, following shRNA knockdown with clones P1 and P2. All mRNA quantifications are normalised to a NS plasmid control. Error bars represent ± 1 standard deviation, as derived from two technical replicates.

72 hr after transduction, cell viability was measured by total nuclei counting as well as propidium iodide (PI) staining (a marker for cell death), to determine the percentage of non-viable cells. Knockdown of *MAPRE3* in the MCF10A isogenic pair using the A1 shRNA clone induced a significant (p-value = 0.03) 15% decrease in cell numbers, (Figure 3.12.) for MCF10A *CDH1*$^{-/-}$ cells relative to MCF10A WT cells. Additionally, PI staining of cells showed that the A1 shRNA clone induced an 87% increase in cell death within the MCF10A *CDH1*$^{-/-}$ cells compared to MCF10A WT cells (Figure 3.13.), trending towards significance (p-value = 0.07), whilst the WT cells suffered no increased death compared to the NS plasmid control. Knockdown of *MAPRE3* using the A3 shRNA clone appears to have induced a synthetic lethal effect at a lesser differential of 5% between cell lines, but this was not sufficient for significance (p-value = 0.21), and was not reflected by PI staining. No synthetic lethal effect was observed for A2 and A4 clones.

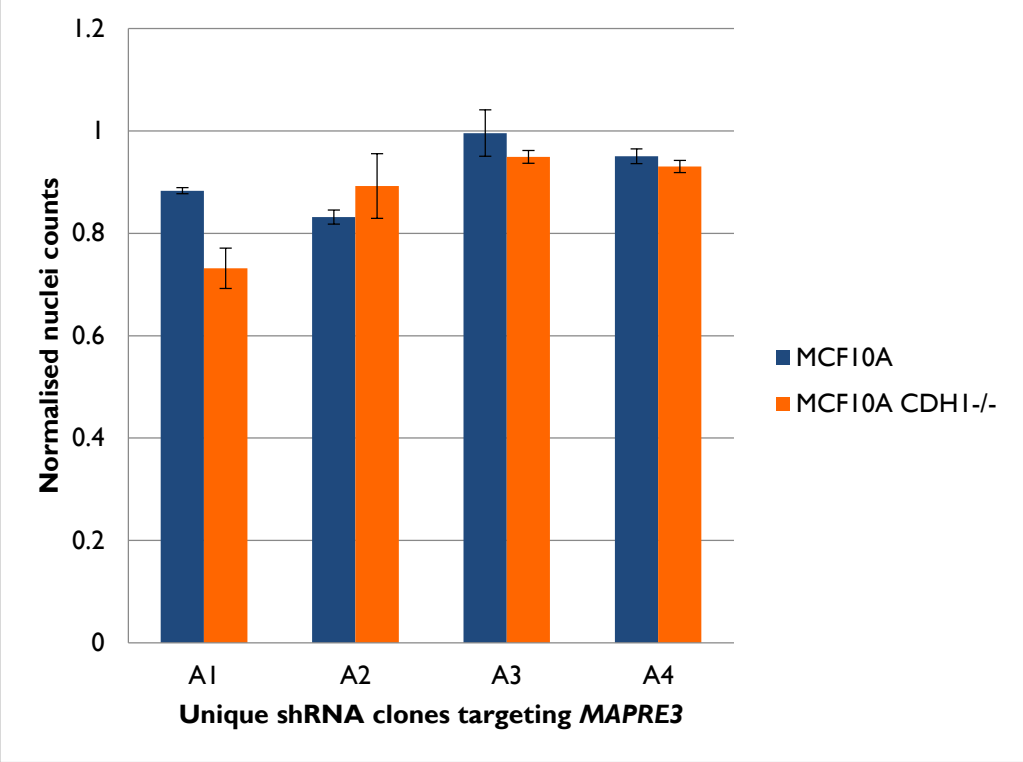

Figure 3.12. Cell numbers, normalised to the NS plasmid control, as measured by total nuclei counting following MAPRE3 knockdown with four unique shRNA clones. A significant synthetic lethal effect was induced by the A1 shRNA clone. The A3 shRNA clone appears to have induced a lesser synthetic lethal effect, but this effect was not significant. Error bars represent ± 1 standard error, as derived from the biological replicates of two separate experiments.

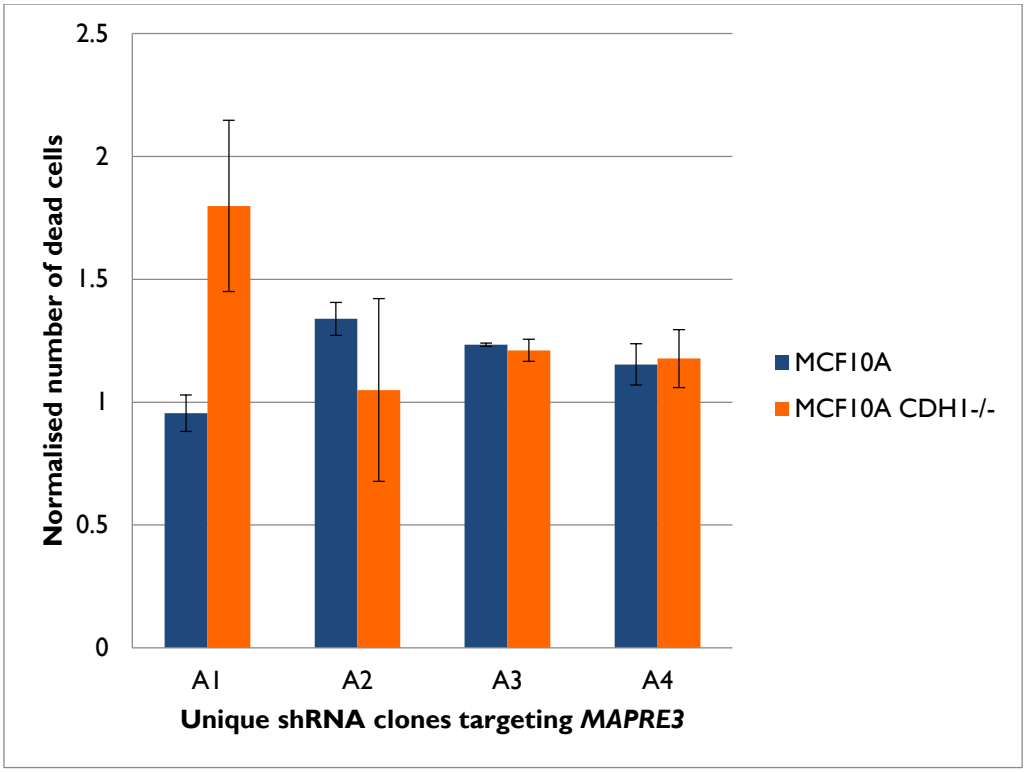

Figure 3.13 Counting of PI-stained nuclei to represent cell death, normalised to NS plasmid control, following MAPRE3 knockdown with four unique shRNA clones. The A1 shRNA clone induced an increase in cell death within MCF10A *CDH1*$^{-/-}$ cells relative to MCF10A WT. No other shRNA clones for *MAPRE3* have induced a synthetic lethal effect. Error bars represent ± 1 standard error, as derived from biological replicates from two separate experiments.

No evidence of synthetic lethal interactions with *CDH1* were observed by total nuclei counting following shRNA knockdown of either *RARB* or *PDGFD* (Figure 3.14.). However, PI staining of nuclei showed that knockdown of *RARB* with the R1 shRNA clone induced a significant (p-value = 0.05) increase of 19% cell death within *CDH1*$^{-/-}$ cells relative to the NS control (Figure 3.15.), amounting to a significant (p-value = 0.03) difference in cell death of 38% between cell lines. The P2 shRNA clone has induced 23% greater death in MCF10A WT cells compared to the NS control, but a significant (p-value = 0.004) increase of 66% in *CDH1*$^{-/-}$ cells. This represents a significant (p-value = 0.01) difference in cell death of 43% between cell lines. Neither synthetic lethal candidate induced a synthetic lethal effect as prominent as observed for *MAPRE3*, the positive control for synthetic lethality. Regardless, significant changes in cell death were observed between WT and *CDH1*$^{-/-}$ cells following

shRNA knockdown of candidate genes, consistent with a synthetic lethal relationship between these candidates and *CDH1*. Although not backed up by total nuclei counts, clear evidence supporting the identification of these genes as synthetic lethal partners with *CDH1* from the *in silico* screen has been observed.

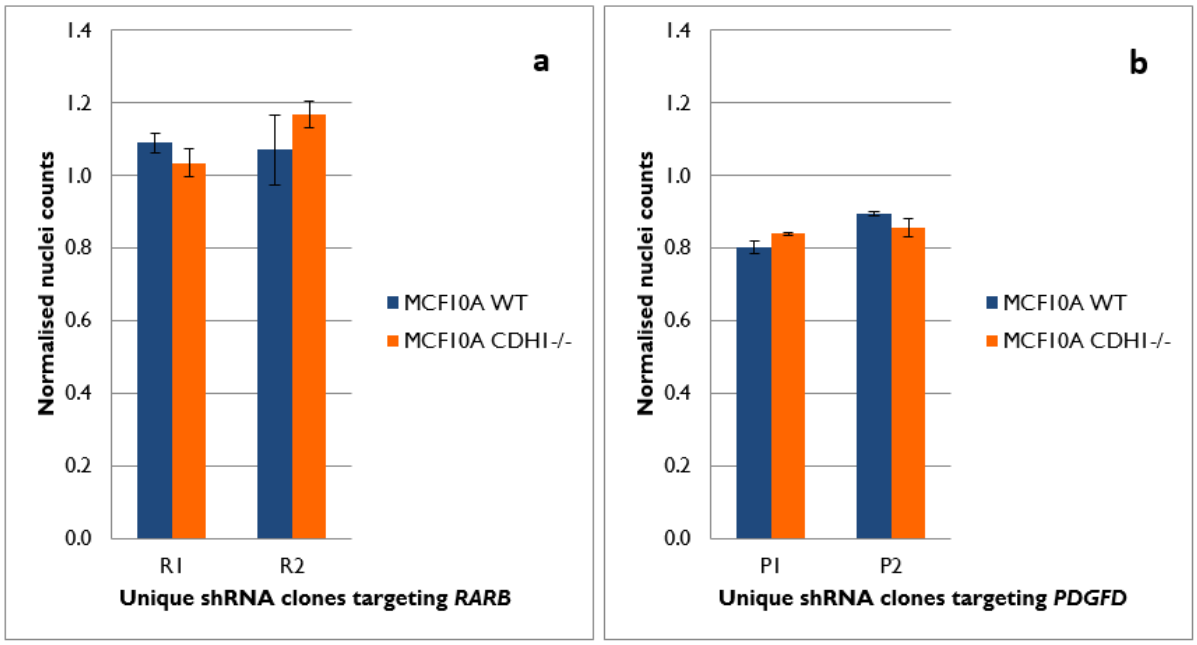

Figure 3.14. Cell numbers, normalised to NS plasmid control, as measured by nuclei counting following knockdown of **a)** *RARB* or **b)** *PDGFD* with two unique shRNA clones each. None of the shRNA clones appear to have induced a synthetic lethal effect. Error bars represent ± 1 standard error, as derived from the biological replicates of two separate experiments.

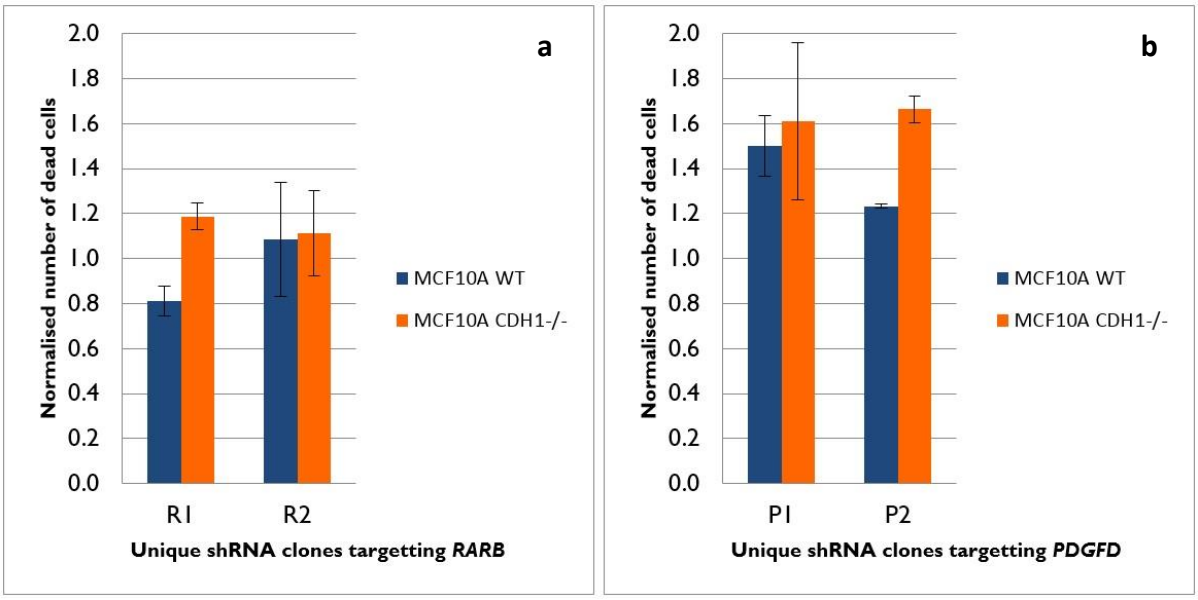

Figure 3.15. Counting of PI-stained nuclei to represent cell death, normalised to the NS plasmid control, following knockdown of **a)** *RARB* or **b)** *PDGFD* with two unique shRNA clones each. The R1 shRNA clone has increased cell death in *CDH1*$^{-/-}$ cells relative to the WT cells. The P2 shRNA clone has induced death in MCF10A WT cells compared to the NS control, but a greater increase in cell death for *CDH1*$^{-/-}$ cells. Neither R2 nor P1 clones induced a synthetic lethal phenotype. Error bars represent ± 1 standard error, as derived from biological replicates from two separate experiments.

3.6. Cell viability following drug inhibition of synthetic lethality candidate genes

Following the support of both *RARB* and *PDGFD* as synthetic lethal partners with *CDH1* through shRNA knockdown, these candidate genes were further investigated through drug inhibition. The use of drugs to inhibit platelet-derived growth factor D (PDGFD) and retinoic acid receptor β (RARβ) is a more clinically relevant approach to investigating these interactions, as opposed to shRNA knockdown of candidate genes.

For inhibition of RARβ, CD2665 was used, a selective antagonist of both RARβ and RARγ, encoded by the *RARB* and *RARG* genes respectively. CD2665 is capable of crossing the blood brain barrier in mice [127], an important feature of this compound for investigation in the context of brain cancers. No direct inhibitors of PDGFD currently exist, so SU6668 was used for the inhibition of PDGFRβ, the receptor for PDGFD.

Cell viability in the isogenic MCF10A cell pair following drug inhibition was determined through total nuclei counting, as for shRNA knockdown, 48 hr post-drugging. A clear synthetic lethal phenotype can be observed through the inhibition of RARβ with CD2665, with a synthetic lethality differential of approximately 20% across all concentrations investigated (Figure 3.16., Table 3.9.), achieving significance (p-value $\leq$ 0.05) at concentrations of 20-25 μM. A CD2665 concentration of 20μM appears suitable for the selective death of E-cadherin deficient cells, as only a 13% reduction in MCF10A WT cells is induced, whilst MCF10A *CDH1*$^{-/-}$ cells suffer a 30% decrease in viability.

Further to cell counting based assays, the effect of drug inhibition of synthetic lethal candidates on cell growth was measured in real-time. The IncuCyte was used for this, which utilises high throughput imaging to determine cell confluency at specified intervals. Negligible growth inhibition, relative to the dimethyl sulfoxide (DMSO) control, of MCF10A WT cells was observed following treatment with 31 μM CD2665 (this concentration was the result of a serial dilution, see Chapter 2.2.7.2.), whereas MCF10A *CDH1*$^{-/-}$ cells exhibited a marked decrease in growth rate (Figure 3.17.). At 48 hr post-drugging, a final confluency differential of approximately 10% was observed between MCF10A *CDH1*$^{-/-}$ cells treated with 31 μM CD2665 and those treated with DMSO. Therefore, assays involving end-point total nuclei counting as well as real-time measurement of cell growth provide evidence and support for the inhibition of RARβ to induce a synthetic lethal phenotype in the MCF10A model of *CDH1* loss.

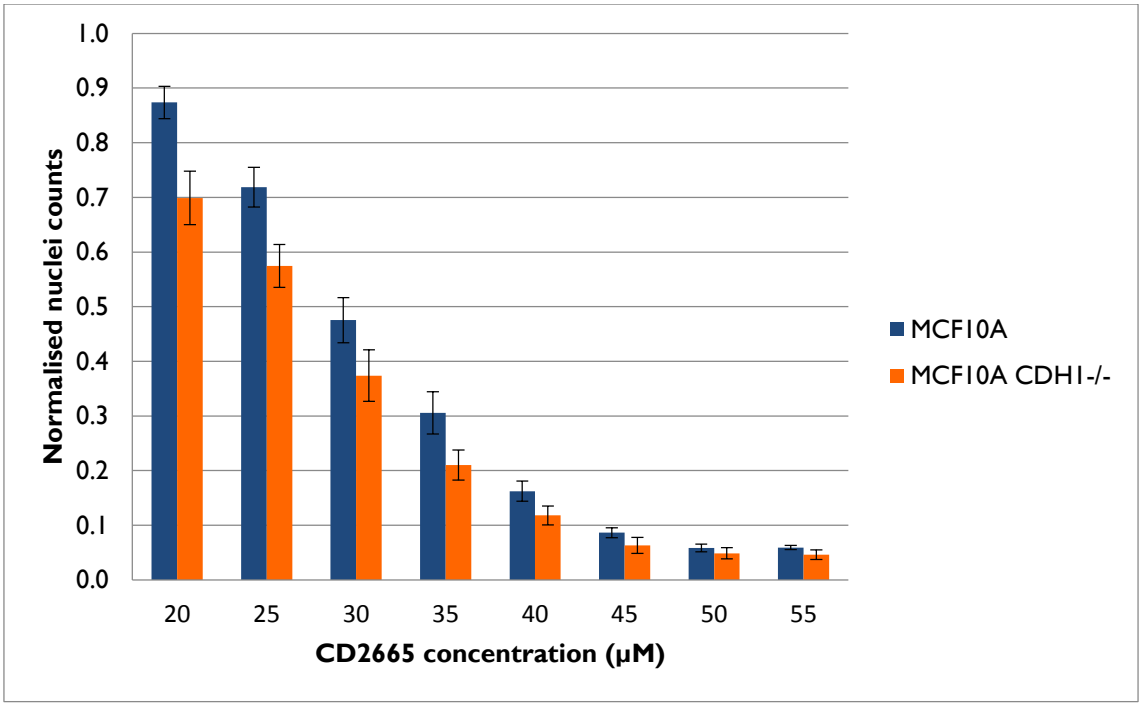

Figure 3.16. Cell numbers, normalised to DMSO control, as measured by total nuclei counting following RARβ inhibition with CD2665 at concentrations ranging from 20-55 µM. A significant synthetic lethal effect was induced at 20-25 µM. A similar synthetic lethality differential was maintained across all concentrations investigated, although these did not achieve significance at concentrations greater than 25 µM. Error bars represent ± 1 standard error, as derived from the biological replicates of three separate experiments.

CD2665 Concentration (µM)	MCF10A *CDH1*$^{-/-}$: MCF10A WT ratio	p-value
20	0.80	0.02
25	0.80	0.03
30	0.79	0.09
35	0.69	0.06
40	0.73	0.08
45	0.73	0.12
50	0.83	0.24
55	0.78	0.12

Table 3.9. Summary of synthetic lethality differentials, depicted here as the ratio of MCF10A *CDH1*$^{-/-}$ normalised nuclei counts to MCF10A WT counts across all concentrations of CD2665 investigated, in addition to the associated p-values. Concentrations of 20-25µM achieved the threshold for significance, although the MCF10A *CDH1*$^{-/-}$: MCF10A WT ratio maintains relatively constant across all concentrations of CD2665 investigated.

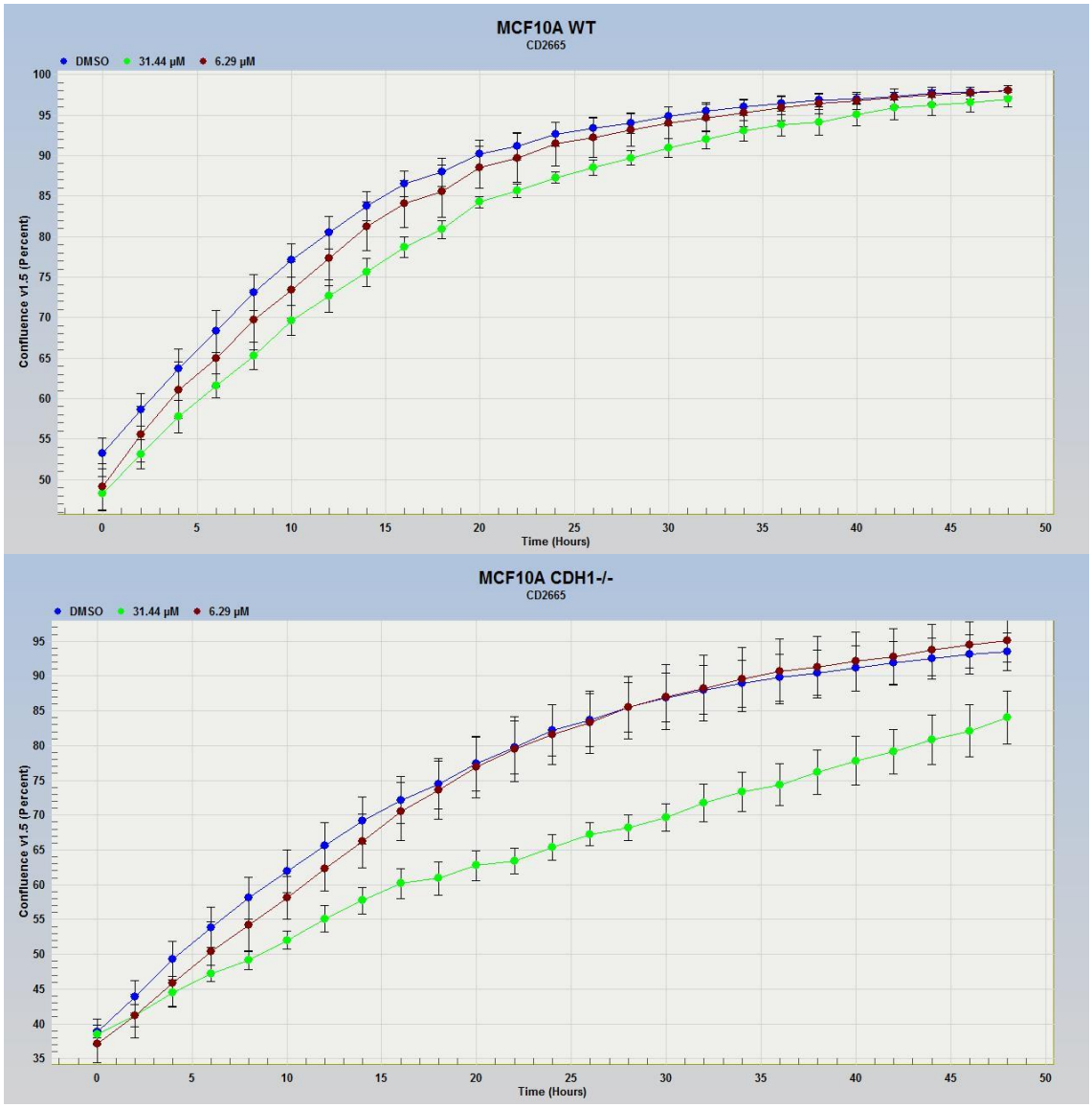

Figure 3.17. IncuCyte assay illustrating the effect of CD2665 on cell growth in both MCF10A WT and *CDH1*$^{-/-}$ cell lines. Each plot point is representative of cell confluency, with error bars depicting ± 1 standard error as derived from 6 or 3 technical replicates for DMSO and CD2665 treatment respectively. Cells were drugged at t = 0 hr and readings taken at 2 hr intervals over 48 hr total. A clear inhibition of cell growth, relative to the DMSO control, can be seen in MCF10A *CDH1*$^{-/-}$ cells treated with 31.44 µM CD2665, whereas identical treatment in MCF10A WT cells has a negligible effect on cell growth.

Following drug inhibition of PDGFRβ with SU6668 in both MCF10A cell lines, end-point nuclei counting exhibited no significant difference in cell numbers between WT and *CDH1*$^{-/-}$ cells (Figure 3.18.). Cell numbers were unaffected by treatment with SU6668 at a concentration of 1.26 µM, with a marginal decrease of approximately 5% observed in both cell lines at 6.29 µM. An approximately 50% reduction in cell numbers for both cell lines was observed at 31.44 µM SU6668.

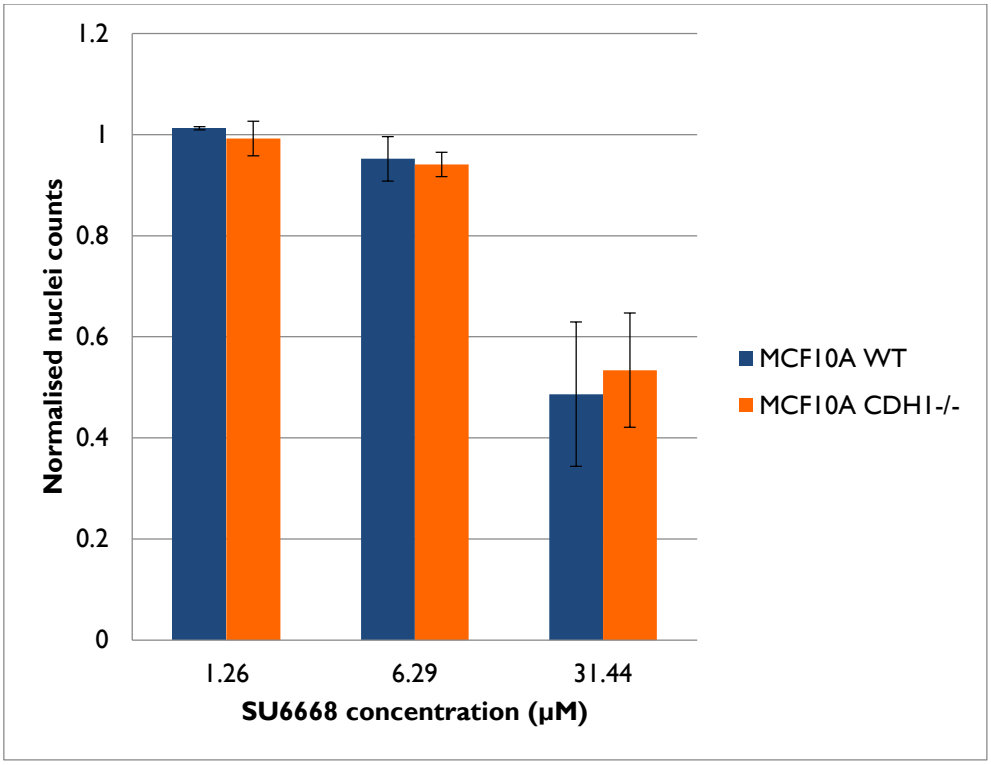

Figure 3.18. Cell numbers, normalised to the DMSO control, as measured by total nuclei counting following PDGFRβ inhibition with SU6668 at concentrations ranging from 1.26-31.44µM. No synthetic lethal phenotype was observed following treatment with SU6668, with a reduction in cell numbers for both cell lines at 31.44 µM. Error bars represent ± 1 standard error, as derived from the biological replicates of two separate experiments.

It should be noted that one of the two experiments represented by Figure 3.18. was normalised to the CO control as opposed to the DMSO control. This was due to an anomaly in DMSO nuclei counting for MCF10A WT which exhibited a decrease of 62.1% in cell numbers relative to *CDH1*$^{-/-}$ cell numbers for DMSO treatment. No significant difference between WT and *CDH1*$^{-/-}$ cells has been previously observed for DMSO controls, and this was most likely due to an accidental seeding of less MCF10A WT cells in wells treated with DMSO. It was obvious that both experiments represent the same effect of SU6668 treatment on cell numbers (Appendix 5.5), despite the fact that they are normalised to different controls.

Concordant with nuclei counting, real-time growth measurements from the IncuCyte assay showed inhibition of cell growth in both cell lines when treated with 31 µM SU6668 (Figure

3.19.). As determined through both nuclei counting and real-time cell growth, inhibition of PDGFRβ with SU6668 does not induce a synthetic lethal phenotype in this particular model of *CDH1* loss.

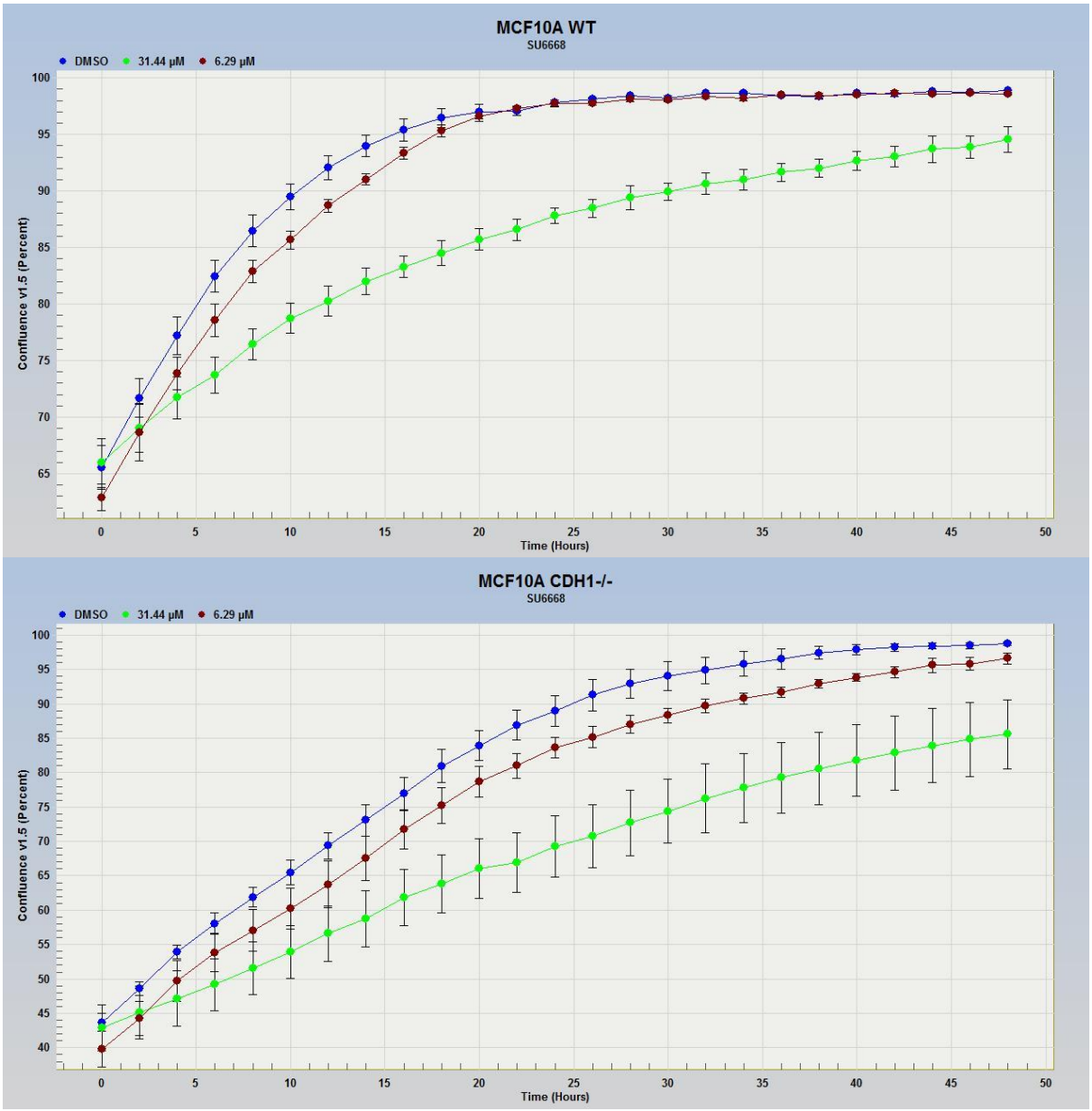

Figure 3.19. IncuCyte assay illustrating the effect of SU6668 on cell growth in both MCF10A WT and *CDH1*$^{-/-}$ cell lines. Each plot point is representative of cell confluency, with error bars depicting ± 1 standard error as derived from 3 technical replicates. Cells were drugged at t = 0 hr and readings taken at 2 hr intervals over 48 hr total. A clear inhibition of cell growth, relative to the DMSO control, can be seen in both cell lines following treatment with 31.44µM SU6668, with no presentation of a synthetic lethal phenotype.

4. Discussion

The current study performed an investigation into synthetic lethal partners with *CDH1* in medulloblastoma, utilising a novel bioinformatic approach (Figure 1.2.) [16] to identify these candidate genes using publicly available tumour expression data. Candidate genes from this initial *in silico* screen were then compared to *CDH1* synthetic lethal partnerships as previously identified by a genome-wide siRNA screen, performed by PhD student Bryony Telford in Melbourne [111]. Finally, experimental validation of putative synthetic lethal candidates included shRNA knockdown and drug inhibition of target genes and their respective proteins in an MCF10A model of *CDH1* loss.

4.1. Importance of developing novel strategies for medulloblastoma treatment

Affecting just under two people per million each year, medulloblastoma is the most common malignant brain tumour in children [51]. Prognosis varies greatly depending upon a range of clinical factors such as the presence of metastasis at patient diagnosis [58], as well as the molecular classification of the tumour [82], with an overall average 5-year survival rate of 70-75% [51]. For example, Wnt-subgroup medulloblastomas boast a remarkable 5-year survival rate of approximately 90% [52], however, survivors of this disease suffer from long-term debilitating side-effects from current, highly aggressive, therapeutic techniques. Deficits in neurocognitive and endocrine function are common side effects, as well as decreased academic ability and memory retention [53-60].

Primarily due to the development of high-throughput genomic and proteomic methods, we now have a thorough understanding of the biological mechanisms responsible for the initiation of Wnt- and SHH-subtype medulloblastomas, however our understanding of group 3 and 4 tumours remains limited [52]. Despite these advances in our understanding of the

underlying biology of these tumours, there has been no significant change in clinical practice, as all molecular subgroups continue to receive the same combination of chemotherapy, irradiation and surgery. The long-term cognitive consequences associated with current therapies, particularly in the Wnt-subgroup which is believed to be over-treated, is testament to the need for increased specificity of medulloblastoma therapies and the development of novel strategies that target the defined molecular mechanisms which differentiate cancerous cells from healthy brain tissue.

The concept of synthetic lethality has the defining characteristic of differentiating between cancerous and healthy cells, providing selective killing and leaving healthy cells relatively unharmed [2]. Synthetic lethality has already shown promise in the clinic through PARP1 inhibitors for the treatment of breast cancers harbouring *BRCA1*/*BRCA2* mutations [4, 5], and medulloblastoma patients could potentially benefit from therapies based on such concepts in an attempt to reduce the cytotoxicity of current treatment regimens. As our laboratory has previously, and is currently, carrying out research into synthetic lethal relationships with *CDH1*, and *CDH1* silencing has been identified as a mechanism for Wnt-subgroup medulloblastoma tumourigenesis [92], this provides an opportunity to apply previously generated data towards the determination of synthetic lethal partners of *CDH1* within a different cancer type, medulloblastoma.

4.2. Identification of synthetic lethal partnerships using a novel bioinformatic strategy

A novel bioinformatic approach for the detection of synthetic lethal partnerships has been utilised in this study, as developed by Tom Kelly, BSc (Hons) student, and Assoc. Prof. Mik Black (Figure 1.2.) [16]. *RARB* and *PDGFD* were identified as putative synthetic lethal candidates with *CDH1* using this approach, through analysis of a dataset containing mRNA

microarray expression profiles of 62 medulloblastomas [100]. Finding a dataset of this size was fortunate considering the rarity of medulloblastoma presentation. The experimental validation of identified synthetic lethal candidate genes *RARB* and *PDGFD* from this initial *in silico* screen provides support for the use of this algorithm in further studies involving synthetic lethality. Additionally, this study provides support for the genome-wide siRNA screen approach in determining synthetic lethal partnerships, as this data was invaluable for the selection of promising candidate genes. Further to this, support for the siRNA screen approach on its own has also been exhibited by the validation of *MAPRE3* as a synthetic lethal partner of *CDH1*. In this study, the combined effectiveness of these approaches for identifying synthetic lethal partnerships with *CDH1* has been shown, and by extension, this technique should prove useful for determining such relationships between other genes. This is significant because any cancer type which commonly loses or alters function of a particular tumour suppressor gene could be investigated in a synthetic lethal context, and interrogated using the same methodology utilised for this study.

For this particular study, we were fortunate to have access to experimental data, in the form of the genome-wide siRNA screen, to provide further confidence in selected candidate genes for synthetic lethality with *CDH1*. This likely helped to remove any statistical or biological artefacts which were not truly representative of synthetic lethality, and was an ideal method for this situation as only two candidate genes were to be further characterised and validated experimentally. As the *in silico* screen was performed on medulloblastoma samples, whereas the genome-wide siRNA screen was carried out in MCF10A breast cells, it is likely that at least some of the identified synthetic lethal candidates which were not supported by the siRNA screen would still be capable of inducing a synthetic lethal effect in a medulloblastoma or cerebellum derived cell line. The differing biological backgrounds of the

cells used for each of the aforementioned experiments will presumably result in unique weaknesses following the loss of *CDH1* function, and therefore unique synthetic lethal partnerships for the corresponding tissue type. To further investigate this, it would be of interest to examine candidate genes identified by the *in silico* screen which were not detected by the siRNA screen. However, it should also be noted that an increased number of false positive synthetic lethal partnerships is likely to occur when not using the siRNA screen to provide extra confidence in the *in silico* results.

As this study has revealed, due to the two different tissue types utilised, some synthetic lethal partnerships are retained across different cell backgrounds. This in itself has important implications for the treatment of various cancers, as *CDH1* function is commonly lost in gastric cancer, lobular breast cancer, carcinomas of both the ovary and endometrium, and medulloblastoma [19, 23, 35, 36, 38-40, 92]. By extension, if synthetic lethal therapies are developed based on partnerships with *CDH1*, such treatments may prove effective across various cancer types. In such a situation, drug development and introduction into the clinic would be far more efficient in terms of both time and cost, as a single developed compound could be utilised across several different patient groups. Importantly, for a rare cancer such as medulloblastoma, this increases the number of applicable patients, and thus improves the likelihood of the development and modification of such compounds.

4.3. Selection of the MCF10A cell line

This study required a cell line which could act as a model of *CDH1* loss to investigate and validate the identified synthetic lethal candidate genes *RARB* and *PDGFD*. An MCF10A isogenic pair of cell lines was selected for this, one of which harbours a 4 base pair deletion in *CDH1* which effectively halts E-cadherin synthesis. As mentioned previously, this

MCF10A isogenic pair is an example of *CDH1* loss in a relatively normal biological background. When MCF10A cells were originally isolated from mammary epithelial cells and established as a cell line, it was demonstrated that the cells were non-tumorigenic in nude mice, lacked anchorage-independent growth, and maintain hormone/growth factor-controlled growth in culture. These are all characteristics of normal breast epithelium [128].

Following the spontaneous immortalisation of MCF10A, cytogenetic analysis determined relatively high genomic stability, with few chromosomal rearrangements [128]. The lack of tumourigenicity is preferable when exploring the effects of synthetic lethality, as genomic stability infers that any genetic interactions within the cell line are more likely to reflect biology *in vivo*, as biological pathways have been minimally altered. If signalling pathways are significantly different in a cell line, this may enable redundancies to emerge for synthetic lethal partners of *CDH1*, and may reduce the synthetic lethal phenotype following gene inhibition. Therefore, although the MCF10A cells are not of the same tissue origin as medulloblastoma, their relatively normal genetic background makes these cells well suited for the characterisation of synthetic lethality, so they were used for validation of *RARB* and *PDGFD* as synthetic lethal partners of *CDH1*.

In addition to this model of *CDH1* loss, it would have been preferable to investigate *RARB* and *PDGFD* within a cell line of similar genetic background to medulloblastomas. The DAOY cell line was imported for this purpose, with a proposed approach of transiently knocking down *CDH1* expression via shRNAs. This would have resulted in the creation of a *CDH1*$^{-/-}$ cell line for comparison with WT cells following shRNA knockdown and drug inhibition of *RARB* and *PDGFD*. However, no convincing *CDH1* expression could be detected through immunofluorescence, western blotting or qPCR. Either *CDH1* was

expressed at particularly low levels, mutations have occurred within antibody binding sites on the E-cadherin protein, or *CDH1* expression has been silenced. This result was unanticipated as E-cadherin expression had been clearly shown by a previous study [124]. If mutations have occurred within the antibody binding sites for those used in this study, perhaps the use of different antibodies would yield markedly different results. However, this seems unlikely due to the particularly low, or absent, levels of *CDH1* expression detected via qPCR. Another possibility is that the different media used by this previous study may have induced *CDH1* expression, or perhaps genomic alterations have occurred within either our lineage of DAOY cells, or those of the other study. Alternatively, it is possible that either the cells utilised within this study, or the study presenting E-cadherin expression in DAOY [122], were not truly DAOY cells. Cells can be accidentally switched or contaminated with a different cell line, and this has been estimated to occur as frequently as 16-35% [127, 128]. As the cells used within this study were imported from ATCC, and ATCC validates all cell lines for sale, it is unlikely that these were incorrectly classified. One potential test that could have been performed to validate the DAOY cells used in this study is short tandem repeat (STR) DNA profiling. STR profiling can identify human cell lines derived from a specific individual based on the hypervariable STR regions, and the specificity of these STR genotypes to any one cell lineage [129]. STR profiling is utilised by ATCC for cell line validation. Regardless of the cause, *CDH1* expression was deemed inadequate for the proposed approach, and the DAOY cell line investigations discontinued.

Inducing *CDH1* expression within DAOY cells was considered, but disregarded for several reasons. The mechanism of *CDH1* silencing in these cells is unknown, and if repressing regulators of *CDH1* expression such as *SNAI1* [129] are upregulated, re-expression could prove difficult. Also, there is no guarantee that E-cadherin will function normally if

expression is successfully induced. Therefore, the re-expression of *CDH1* may prove inconsequential. One might argue that DAOY cells, lacking in *CDH1* expression, may be an ideal cell line for determining death induced by synthetic lethal therapies based on *CDH1* partnerships. However, without a WT control to normalise results to, measurements of cell death or growth inhibition would not be informative. As a consequence, experimental validation of synthetic lethal partners *RARB* and *PDGFD* was performed solely in the MCF10A isogenic cell line pair.

4.4. *MAPRE3* as a synthetic lethal partner of *CDH1*

As *MAPRE3* had previously been identified as a synthetic lethal partner of *CDH1* through the genome-wide siRNA screen, combined with its close association to the microtubule network, this synthetic lethal phenotype has been further investigated, and validated, by this study. A single shRNA clone, A1, induced a synthetic lethal effect in the MCF10A isogenic pair of cell lines, as observed through both total nuclei counting and PI staining for cell death. It is not clear why only one out of four shRNA clones presented this synthetic lethal phenotype, but this same anomaly has been observed within our laboratory for the shRNA clones of several synthetic lethal partners with *CDH1*, as well as for siRNA clones within the siRNA screen [111]. It is possible that some of the shRNA clones target sequences which are difficult to access due to the secondary structure of the mRNA transcript, thus not binding or binding at a lower frequency than expected. Loss of *CDH1* is associated with abnormal cytoskeletal organisation, and *MAPRE3* is involved in the dynamics and stabilisation of microtubule ends, as well as regulating the attachment and stabilisation of these ends at the cell cortex and mitotic kinetochore [126]. This provides a biological link between the two genes in cytoskeletal maintenance. As such, it is plausible that the underlying mechanism for this synthetic lethal relationship is as follows: loss of E-cadherin function causes cytoskeletal

instability, exposing a potential weakness for exploitation in tumour cells. Loss of *MAPRE3* function in addition to *CDH1* results in further cytoskeletal disarray, a phenotype which cannot be sustained by the cells, resulting in cell death. E-cadherin-expressing cells however, are viable despite this defect in microtubule function induced by decreased *MAPRE3* expression.

In this particular case, it is possible that A1 proved most effective as the level of *MAPRE3* mRNA transcript following knockdown with this clone was the lowest of all four clones (Figure 3.10.). It is plausible that a specific threshold for mRNA knockdown must be breached to generate a significant effect on the levels of MAPRE3 protein within cells, and that without achieving this, minimal or no alteration to *MAPRE3* function is caused, thus no synthetic lethal phenotype is exhibited.

This work performed for *MAPRE3* validation as a synthetic lethal partner of *CDH1* has been recently published, amongst other work conducted within our laboratory, in Molecular Cancer Therapeutics [111].

Within the *in silico* screen, although significance was not achieved (p-value = 0.16), the gene expression relationship between *CDH1* and *MAPRE3* within medulloblastoma samples was concordant with synthetic lethality according the bioinformatic strategy utilised. Further support for *MAPRE3* as a synthetic lethal partner of *CDH1* has been illustrated by this study, through experimental validation in MCF10A cells, warranting further investigation in the context of medulloblastoma.

4.5. *PDGFD* as a synthetic lethal partner of *CDH1*

PDGFD was identified as a putative synthetic lethal partner of *CDH1* from the initial *in silico* screen, and further supported by the genome-wide siRNA screen. Validation of this candidate gene was successful through shRNA knockdown in the MCF10A model of *CDH1* loss. Although not supported by total nuclei counts, PI staining for cell death showed increased death for cells lacking *CDH1* expression compared to WT cells, following knockdown of *PDGFD* expression. Similar to the phenotypes presented by *MAPRE3*, this effect was observed for only one of two shRNA clones. For *PDGFD*, the shRNA clone which induced a synthetic lethal phenotype was not the clone which induced the greatest level of mRNA knockdown.

Drug inhibition of PDGFRβ, the receptor for PDGFD, using SU6668 failed to reflect observed results for shRNA knockdown, with no synthetic lethal phenotype exhibited within the MCF10A model of *CDH1* loss. This was confirmed through both total nuclei counting, an end-point assay of cell numbers, as well as through confluence over time, a real-time assay of cell growth. The drug inhibition experiments for both PDGFRβ and RARβ would have benefited from the use of PI staining to determine the proportion of non-viable cells in addition to total cell number and confluence over time measurements. This would identify cells which are apoptotic, but yet to undergo cell lysis. Additionally, this would help differentiate between inhibition of cell growth and induced cell lysis. Drug inhibition assays were performed prior to shRNA knockdown of candidate synthetic lethal partners, and PI staining had not yet been established within the laboratory.

It is possible that the lack of a synthetic lethal phenotype through drug inhibition is due to the non-specific nature of inhibiting PDGFRβ instead of PDGFD itself. PDGF-DD is regarded as

specific to PDGFR-ββ, although has a minor affinity to PDGFR-αβ also, and so SU6668 was used to inhibit PDFGRβ. However, PDGFRα and PDGFRβ form homo- and heterodimers: PDGFR-αα, -αβ and –ββ. Therefore, the inhibition of PDFGRβ would have also reduced PDGFR-αβ activity, thereby affecting both PDGF-BB and PDGF-CC activity, as both bind this receptor [130]. As a result, the inhibition of PDGFRβ would not have induced specific reduction of *PDGFD* activity, and thus these unintended effects on other PDGFs and PDGFR-αβ dimers may be the reason for synthetic lethal phenotype presentation, as both cell lines were equally affected by this.

An alternative reason for the lack of a synthetic lethal phenotype is that various other growth factor receptors are inhibited as well as PDGFRβ: VEGFR2, FGFR1 and EGFR. The inhibition of these other growth factor receptors is likely to reduce growth in both cell lines equally, as none were synthetic lethal candidates with *CDH1* according to the *in silico* screen. EGFR inhibition is the most likely cause in this respect, as MCF10A complete growth media is supplemented with EGF, and inhibition of this would reduce cell growth for both WT and *CDH1*$^{-/-}$ cells.

PDGFRβ, the receptor for PDGF-DD, has been shown to phosphorylate and activate the activity of c-Src, encoded by the *SRC* gene [131]. c-Src forms a regulatory component of the complex that links integrins to the cytoskeleton [132], and is also involved in the regulation of actin cytoskeleton organisation [133, 134]. Because *CDH1* is also involved in cytoskeletal organisation, it is possible that the mechanism for *PDGFD* synthetic lethality is similar to that of *MAPRE3*. In this scenario, a lack of *CDH1* results in abnormal cytoskeletal organisation which is tolerated by the cell. The loss of *PDGFD* expression in addition to *CDH1* prevents PDGF-DD binding to PDGFRβ, therefore preventing the activation of c-Src

and resulting in a further decrease in cytoskeletal organisation, as well as impaired integrin-cytoskeleton interaction, a phenotype which is non-viable. Cells with normal E-cadherin expression are predicted to be less affected by this deficit in cytoskeletal and integrin organisation, as E-cadherin can counteract this effect and maintain cytoskeletal integrity.

4.6. *RARB* as a synthetic lethal partner of *CDH1*

As for *PDGFD*, *RARB* was also identified as a putative synthetic lethal partner of *CDH1* during the initial *in silico* screen, supported by genome-wide siRNA screen data, and was validated through shRNA knockdown in the MCF10A model of *CDH1* loss. Although no synthetic lethal phenotype was detected through total nuclei counting, PI staining showed that *CDH1*$^{-/-}$ cells suffered greater cell death following *RARB* knockdown. However, once again, this phenotype was observed in only one of two shRNA clones. As for *MAPRE3*, greater mRNA knockdown was achieved by the same *PDGFD* shRNA clone which induced a synthetic lethal phenotype, a possible cause of discrepancies between shRNA clones.

Additional validation of *RARB* as a synthetic lethal candidate was performed through inhibition of RARβ with CD2665, which was successful in inducing a synthetic lethal phenotype. This was observed through both end-point assaying of cell numbers, in addition to a real-time assay of cell growth. At a concentration of 20 μM, CD2665 was capable of inducing a synthetic lethal differential between cell lines of 20%, whilst causing minimal harm to MCF10A WT cells, exhibiting approximately a 10% reduction in cell numbers. This observed effect was greater in magnitude than that for shRNA knockdown of *RARB*, where no change in total cell numbers was reported. This same anomaly has been reported by a previous study, in relation to PARP1 inhibitors and the synthetic lethal interaction with *BRCA1/BRCA2*, where siRNA knockdown presented a less severe synthetic lethal phenotype

compared to drug inhibition [5]. The validation of the synthetic lethal partnership between *RARB* and *CDH1* through the use of CD2665 provides some clinically relevant support for the potential development of treatment strategies in a synthetic lethal context.

Within *RARB* shRNA experiments, PI staining showed that *CDH1*$^{-/-}$ cells were dying in significantly greater numbers than WT cells, exhibiting a convincing synthetic lethal phenotype. However, total nuclei staining presented no apparent difference in cell numbers, as for *PDGFD.* By extension, it is possible that a synthetic lethal effect would have been observed through total nuclei counts if shRNA knockdown experiments were extended in duration, as the *CDH1*$^{-/-}$ cells should have lysed in greater numbers than WT cells. However, with current experimental conditions, cells reach near-confluence which poses an issue for normalisation to the NS negative control. If a well reaches confluence, final nuclei counts are an underestimation of cell viability and inhibition of growth. Lowering initial cell numbers does not appear to be an option to counter this, as our laboratory has observed considerable variation in initial cell seeding numbers when our current seeding numbers are lowered (data not shown). If significant variation in cell numbers is initially present within wells, this difference increases exponentially with cell growth, resulting in large variation in final nuclei counting. One potential solution to this would be a 6-well plate format as opposed to 96 wells, which would allow for both greater seeding densities to reduce seeding variation, and a greater duration before cells reach confluence. This would result in lower throughput experiments, and may be best utilised to further interrogate already promising shRNA clones, such as those for *PDGFD* and *RARB*.

There are a number of possible lines of reasoning behind the lesser synthetic lethal phenotype following shRNA knockdown of *RARB* compared to drug inhibition of RARβ. As drug

inhibition directly targets RARβ, this likely induces a prompt reduction in RARβ activity and thus cell function. However, shRNA knockdown is not as direct, as it reduces mRNA expression of *RARB*, thereby potentially reducing the quantity of RARβ synthesised, if knockdown is sufficient. It is possible that a greater level of mRNA knockdown, in any of the three candidate synthetic lethal partners investigated, would result in a greater synthetic lethality differential between WT and *CDH1*$^{-/-}$ cells. Support for this can be deduced from *MAPRE3* and *RARB* shRNA knockdown results, as for both candidates, a greater level of mRNA knockdown corresponded with a synthetic lethal phenotype, whereas shRNA clones inducing lesser degrees of knockdown did not exhibit this phenotype. Presumably, increasing the multiplicity of infection (MOI) for shRNA knockdown experiments would increase the level of mRNA knockdown achieved, and by extension, increase the magnitude of synthetic lethal effects presented by this study. Greater MOIs were tested within our laboratory during initial establishment of this lentiviral-mediated shRNA knockdown approach, but an unacceptable level of non-specific cell death was observed with an increased MOI, particularly for *CDH1*$^{-/-}$ cells. Where possible, there is a necessity to reduce death induced through transduction of lentiviral particles alone, especially in this case where cell lines are differentially affected, to avoid confounding of results.

An additional factor to consider is the half-life of the RARβ protein. If a sufficient level of RARβ is still active after 72 hr, the period from transduction with shRNA through to cell counting, then a decrease in mRNA expression and protein synthesis may have minimal effect on levels of RARβ, and therefore cell function. This could be investigated through western blotting or immunofluorescence for RARβ, but this was not explored due to a combination of a lack of antibodies targeting RARβ within our laboratory, and time constraints associated with importing these. If it is determined that protein levels have not

sufficiently been lowered after 72 hr, one method of accounting for this would be to extend the duration of shRNA knockdown experiments, as mentioned above.

The increased synthetic lethal phenotype observed with CD2665 inhibition of RARβ compared to shRNA knockdown of *RARB* may also be due to the dual inhibition of both RARβ and RARγ, encoded by the *RARG* gene. Although *RARG* has not been implicated as a synthetic lethal partner of *CDH1* through either screen, it is possible that the combined inhibition of *RARG* and *RARB* activity reduces further redundancies in retinoid signalling, thus inducing a more severe synthetic lethal phenotype than a reduction in *RARB* activity alone.

The addition of retinoic acid (RA) induces the activity of RARs such as RARβ, and RA addition to skeletal muscle cells has been shown to induce cytoskeletal rearrangement through the AMPK pathway [135]. RARs also play a role in the regulation of matrix metalloproteinases (MMPs), which are involved in degradation of the extracellular matrix, an essential step towards tumour invasion and metastasis [136-139]. Within aggressive melanoma and squamous cell carcinoma cell lines, a mixture of agonists and antagonists of RARs were capable of inhibiting MMPs and therefore blocking invasion of these aggressive cells [140]. Further to this role of RARs in extracellular matrix maintenance, the addition of RA has been shown to reduce MMP activity and inhibit tumour cell invasion of colon cancer cell lines [141], and in fibroblasts has been shown to stimulate extracellular matrix production [142]. RARs appear to regulate the extracellular matrix, and by extension repress invasion, and also play a role in cytoskeletal organisation. Although the exact mechanism behind these functions has not been delineated, including the specific RARs responsible for each particular role, it is possible that these functions are the mechanism behind the synthetic

lethal relationship between *RARB* and *CDH1*. However, further study is required to define the specific mechanisms behind this synthetic lethal relationship.

4.7. Implications for CD2665 treatment

Wnt-subgroup medulloblastomas currently have an approximate 90% 5-year survival rate, implying that current treatments are effective at killing medulloblastoma cells. However, current chemotherapy is inadequate for the specific targeting of cancerous cells, instead causing irreparable damage to healthy and developing brain tissue. Therefore, in the context of improving current medulloblastoma therapies, drugs which are proven to induce a synthetic lethal effect with a tumour suppressor gene which is commonly lost, for example CD2665 for *CDH1*, provide a rational approach to address this issue, as healthy cells are minimally affected.

In a perfect situation, drugs that are able to induce a synthetic lethal effect would replace current chemotherapy, and result in complete elimination of cancerous cells whilst causing minimal harm to healthy cells. Although, as observed for CD2665, this particular drug does not induce absolute killing of *CDH1*$^{-/-}$ cells at doses which present a synthetic lethal phenotype. However, it should be noted that the efficacy of CD2665 may be greater than the observed effect in cell lines, as clinical treatment would not consist of a short 48 hr treatment as used in this study. Instead, treatment would consist of cycles of chemotherapy, with each cycle longer than this 48 hr period, potentially inducing a greater synthetic lethal phenotype. Depending on the efficacy of CD2665 within patients, perhaps a more pragmatic aim is to develop therapies for medulloblastoma patients lacking normal *CDH1* function, which use current chemotherapy drugs in combination with synthetic lethal drugs. The clinical aim of this would be to lower doses of the currently used (and more harmful) compounds, whilst still

inducing sufficient death of cancerous cells. Additionally, this approach may result in the potential for lower radiation doses during the initial phases of medulloblastoma treatment, as the tumour is more effectively handled through chemotherapy regimens. This would be a significant advance in therapy development, as much of the damage to healthy cells is caused by irradiation [61-63].

4.8. Future research

To further the findings of this study in the context of medulloblastomas, confirmation of results should be carried out in biologically relevant cell lines. Initial steps would involve the use of a cell line derived from the cerebellum, with sufficient *CDH1* expression to generate a WT and *CDH1*$^{-/-}$ isogenic pair. The use of TALENs or CRISPR/Cas systems [143, 144] could be used to directly edit the sequence of *CDH1*, thus stably repressing E-cadherin expression, or shRNAs could be used for transient knockdown of *CDH1*, if the effect on protein levels is sufficient, as outlined previously (Chapter 3.3.). Alternatively, if *CDH1* expression proves inadequate across cerebellum cell lines, inducing *CDH1* expression is a possibility. However, as previously discussed, there is no guarantee that E-cadherin will function normally, and thus the expression of *CDH1* may prove inconsequential. The initial use of a cerebellar cell line as opposed to a medulloblastoma cell line follows the same reasoning as the use of MCF10A cells. Non-cancerous cell lines exhibit a relatively normal genetic background, which is preferable for the initial phases of synthetic lethality studies. In addition to assessing synthetic lethality in a medulloblastoma context, this work may provide further support for *MAPRE3*, *PDGFD* and *RARB* as synthetic lethal partners of *CDH1*. The work presented here is consistent with a synthetic lethal partnership between these candidate genes, however, inconsistencies were apparent, such as the variable exhibition of synthetic lethal phenotypes with different shRNA clones.

Following validation within a cerebellar cell line, further investigation of promising synthetic lethal partners, such as *RARB* and *PDGFD*, within a medulloblastoma-derived cell line would provide support for the knockdown or drug inhibition of candidate genes within cells containing tumour-like genetic makeups, a necessary step if the long term goal is to use such drugs for patient therapies. Of course, such a cell line must express *CDH1* at sufficient levels for the creation of a *CDH1*$^{-/-}$ cell line, unlike the DAOY cells used in this study.

Within the bioinformatic approach utilised for this study, multiple probe pairs corresponding to each gene were averaged to give a single median measure of gene expression per gene. However, some information may be lost through this approach, such as different probe pairs targeting splice variants of a particular gene. It would be of interest to investigate synthetic lethal partners with *CDH1* using individual probe pairs, and determine whether similar results are obtained, or if additional synthetic lethal interactions are identified. It is plausible that splice variants of *CDH1* or a putative synthetic lethal partner will have differential effects in regard to synthetic lethality. However, some inaccuracies are to be expected with this approach, as a single probe pair may over or underestimate gene expression, but as an entire probe set be considered an accurate measurement of gene expression.

For this study, the pGIPZ plasmid was used for the expression of shRNAs in gene knockdown experiments, which is a non-inducible system. This means that upon transduction, shRNAs are expressed and active, but only within the subset of the cell population which has been successfully transduced. Although selection with puromycin was used, this is only active over the latter 48 hr of the experiment, and a subset of the cell population remains both live and non-transduced (data not shown). Because only a subset of total cells are transduced, many cells do not express shRNAs, and therefore retain normal

gene function, without exhibiting a synthetic lethal phenotype. If only a subset of the cell population is affected by synthetic lethality, the synthetic lethal phenotype proves difficult to detect. Increasing the MOI would increase the proportion of transduced cells, however, increased cell death has been reported with increasing MOIs, as outlined previously.

An alternative to increasing MOI is to substitute the pGIPZ plasmid for an inducible system, such as the pTRIPZ plasmid. Because pTRIPZ requires the addition of doxycycline to induce expression of shRNAs, shRNA activity could be repressed until desired. This would allow for the selection of transduced cells until 100% of the population contains the shRNA of interest. Following this, induction of shRNAs through doxycycline would allow for a more accurate measurement of cell death due solely to shRNA knockdown of synthetic lethal candidate genes, eliminating confounding factors such as cell death in non-transduced cells due to puromycin selection or the initial transduction of shRNAs. Additionally, cells could be seeded in greater numbers, as the time from seeding to end-point assays would be reduced from 96 hr to 72 hr. Alternatively, instead of increasing cell numbers, experiments could be extended in duration, with less limitations regarding cell confluency.

In this particular study, synthetic lethal interactions with *CDH1* have been investigated, as our laboratory has a current interest in these interactions across several cancer types, and this allowed the utilisation of the genome-wide siRNA screen, which is based on synthetic lethality with *CDH1*, to aid in selection of candidate genes for further validation. A potential shift in focus for this project would be the investigation of synthetic lethal interactions with *CTNNB1*. *CTNNB1* encodes β-catenin, and is mutated in approximately 90% of Wnt-subgroup medulloblastomas [92, 145-147]. As such, this proves an attractive target for molecularly targeted therapies in the context of medulloblastoma. Synthetic lethal partners of

CTNNB1 could be investigated in addition to those of *CDH1*, in an attempt to target the majority of Wnt-subgroup medulloblastomas. As the initial *in silico* screen has been proven an effective tool for identifying synthetic lethal partnerships, this methodology could be utilised for *CTNNB1* also.

Mutations in *CTNNB1* within Wnt-subgroup medulloblastomas commonly result in β-catenin migration to the nucleus, and prevent interaction with E-cadherin through changes in the *armadillo* repeat region. This prevents linking of E-cadherin to the actin cytoskeleton, and may effectively imitate E-cadherin loss in the context of the cytoskeleton. Our laboratory has previously shown that E-cadherin loss alters cytoskeletal organisation [112], and it is plausible that this loss of β-catenin binding causes weaknesses relating to the cytoskeleton, due to altered E-cadherin activity, that can be exploited through synthetic lethal therapies based off interactions with *CTNNB1*. Additionally, because E-cadherin function is essentially altered through these *CTNNB1* mutations, it is possible that such mutations can also expose medulloblastomas to synthetic lethal therapies based on *CDH1*, even in tumours where *CDH1* does not contain mutations itself, due to these cytoskeletal weaknesses. If true, this would broaden the applicability of synthetic lethal drugs designed through interactions with *CDH1* and cytoskeletal components to include the majority of Wnt-subgroup medulloblastomas.

Cell lines do not always reflect *in vivo* biology, and as such, mouse models are commonly used for testing anti-cancer medication, and for confirmation of proposed molecular concepts. If *CTNNB1* was to be further investigated in a synthetic lethal context for medulloblastomas, the use of a mouse model would be possible, as a model exists which harbours *CTNNB1* mutations [148, 149]. To this end, promising drugs for synthetic lethality with *CTNNB1*

could be tested in this mouse model, and perhaps even synthetic lethal drugs in the context of *CDH1*, if the above hypothesis is correct regarding *CTNNB1* mutations and resulting weaknesses to synthetic lethal therapies which exploit *CDH1* loss.

4.9. Summary

This study has demonstrated the effectiveness of a combined novel bioinformatic approach for the identification of synthetic lethal partnerships, in this case with *CDH1*, with experimental validation of these partnerships. *RARB* and *PDGFD* were chosen from this initial *in silico* screen, as well as *MAPRE3* from the genome-wide siRNA screen, and validated as synthetic lethal partners of *CDH1* through shRNA knockdown in an MCF10A model of *CDH1* loss, where synthetic lethal phenotypes were confirmed. Additionally, one of the synthetic lethal candidates, *RARB*, was also validated through drug inhibition of RARβ with CD2665 within this same MCF10A model, and was capable of inducing a synthetic lethal phenotype with minimal harm to WT cells. The aforementioned genome-wide siRNA screen was valuable for the selection of synthetic lethal candidates from the *in silico* screen, and reduced the chance of false positive results. Plans were made to reproduce these synthetic lethal phenotypes in DAOY, a medulloblastoma cell line, but insufficient *CDH1* expression for the proposed approach meant that this was discontinued. Although the findings in this study are consistent with a synthetic lethal relationship between *CDH1* and these synthetic lethal partners, further validation in a different system, such as a medulloblastoma cell line, is necessary to definitively validate these findings.

The combination of breast and medulloblastoma tissue types utilised within this study extend the application of these results to both medulloblastoma and lobular breast cancer. As this study has revealed, synthetic lethal partnerships with *CDH1* can be shared across tissue types,

perhaps allowing the application of synthetic lethal partners *RARB* and *PDGFD* to other cancer types which are defective in E-cadherin function. Furthermore, in addition to identifying novel targets for potential medulloblastoma treatment, this study has validated previous work from the genome-wide siRNA screen which was initially carried out in the context of lobular breast cancer.

The findings presented in this study are in support of the development of drugs designed in a synthetic lethal context, and addresses the need for therapies that differentiate between healthy and cancerous cells, causing minimal damage to healthy tissue. This study sheds light on the potential use for synthetic lethal drugs, such as CD2665, as novel treatment options for medulloblastoma, and following further validation, could be explored as an alternative to current treatment, or in combination with current treatments, in an effort to lower the dose of the harmful compounds used, and thereby decrease treatment morbidity.

Acknowledgements

I would like to thank all of the staff and students of the Cancer Genetics Laboratory for the support I've received over the last two years. My time spent in the laboratory has been invaluable. I have enjoyed getting to know all of you, and have also learnt a great deal from you.

In particular, I would like to thank Parry Guilford and Mik Black for the guidance offered throughout my study, and the constant availability of support. Both of you have greatly stimulated my interest in this field, and I cannot thank you enough for all of your help.

Further gratitude towards the Synthetic Lethal group: Parry Guilford, Augustine Chen, Bryony Telford, Henry Beetham, Andrew Single, Tom Kelly and James Frick. Our weekly collaborations were very effective for trouble-shooting problems when assistance was needed, and for the gaining of knowledge.

To my friends both inside and outside of the lab, thank you for helping me maintain my sanity during this write-up period, we have some great stories from the last two years, and I'm sure there are many more to come.

To my partner Amelia, thank you for your love and support throughout the last two years, particularly during stressful periods of experiments or writing.

Finally, to Mum and Dad, thank you for your love and support throughout my university studies, through both good and bad, and your keen interest in the path I have chosen.

5. Appendix

5.1. Reagent preparation

5.1.1. Trypsin preparation

0.5% trypsin was diluted in PBS 1 in 2 and 1 in 10 for 0.25% and 0.05% trypsin respectively.

5.1.2. Lysogeny broth and agar plate preparation

To make 500 mL lysogeny broth, the following were thoroughly mixed with mQH_2O: 5 g tryptone, 2.5 g yeast extract, and 5 g sodium chloride. For agar plates, 7.5 g agar was also added. Lysogeny broth mixture was autoclaved, then well mixed after cooling. For agar plates, 100 µg/mL ampicillin was added prior to pouring.

5.1.3. Freezing medium

Freezing medium for DAOY cells consisted of 95% complete growth medium with 5% DMSO.

Freezing medium for MCF10A cells consisted of 70% complete growth medium with 20% horse serum and 10% DMSO.

Freezing medium for 293FT cells consisted of 90% complete growth medium and 10% DMSO.

5.1.4. PBS preparation

PBS was prepared by adding 1 PBS tablet per 100 mL in mQH_2O, then autoclaved for sterilisation.

5.1.5. SDS-PAGE gel preparation

The resolving gel consisted of: 8.03 mL mQH_2O, 5 mL of 1.5 M Tris-Cl at pH 8.8, 6.6 mL of 30% acrylamide, 200 µL of 10% sodium dodecyl sulfate (SDS), 20 µL tetramethylethylenediamine (TEMED) and 150 µL of 10% ammonium persulfate (APS).

The stacking gel consisted of: 4.54 mL mQH_2O, 2mL of 0.5M Tris-Cl at pH 6.8, 1.3mL of 30% acrylamide, 80 µL of 10% SDS, 20 µL TEMED and 60 µL of 10% APS.

5.1.6. Western blot buffer preparation

For 1 L of 10x running buffer, the following was thoroughly mixed in mQH_2O: 135.2 g glycine, 24.16 g Tris, and 8 g SDS.

For 1 L of 20x transfer buffer, 150.1 g glycine and 24.1 g Tris was thoroughly mixed in mQH_2O. To make 1 L of 1x transfer buffer, 50 mL of 20x buffer was mixed with 850 mL mQH_2O and 100 mL methanol.

For 1 L of 10x TBST, the following was mixed thoroughly in 800 mL mQH_2O: 24.23 g Tris, 87.66 g NaCl and 10 mL tween-20. pH was then adjusted to 7.5, and volume made to 1 L with mQH_2O. 10x TBST was diluted 1 in 10 with mQH_2O to make 1x TBST stock.

For 100 mL of harsh stripping solution, the following were mixed thoroughly in mQH_2O: 20 mL of 10% SDS, 12.5 mL of 0.5M Tris-Cl at pH 6.8 and 0.8 mL 2‑Mercaptoethanol.

5.2. Microarray quality control

5.2.1. Average PM intensity

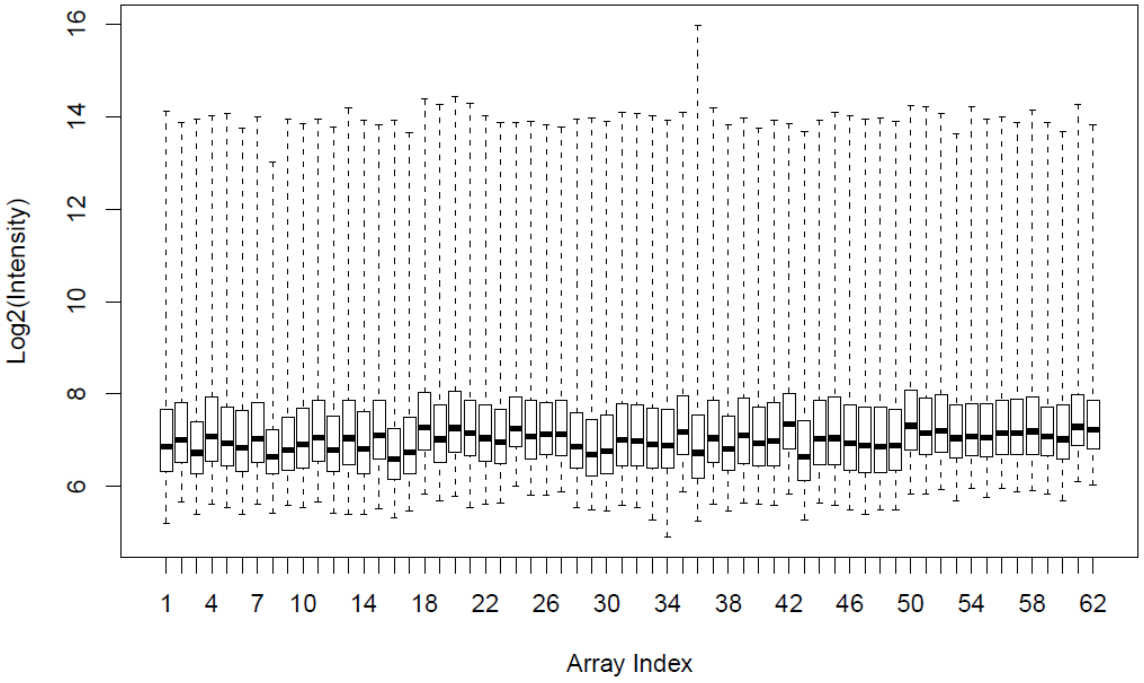

An excerpt from the affyQCReport package output. This represents all PM probe intensities across each microarray sample. An array with a low average intensity would be of suspect quality, however all 62 samples are acceptable in this dataset.

5.2.2. Distribution of probe intensities

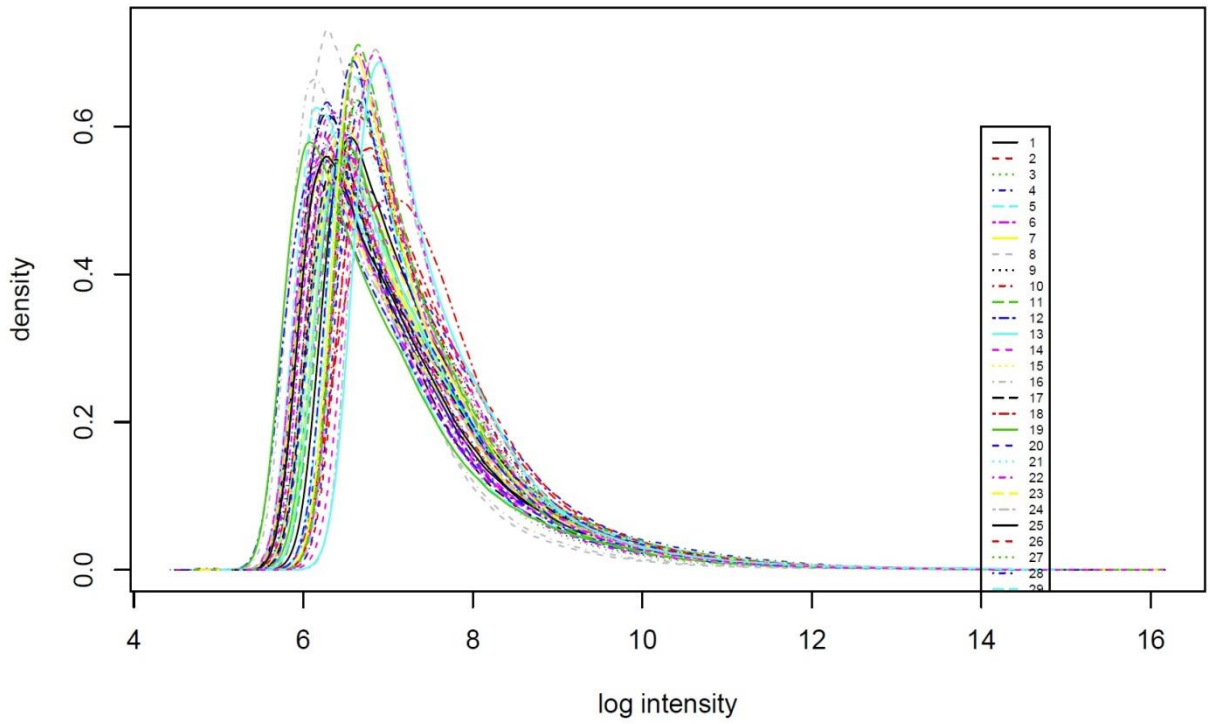

An excerpt from the affyQCReport package output. Each individual microarray is depicted here with all PM probe intensities. Quality would be of concern if any individual sample significantly differed in distribution, which is not the case here.

5.2.3. Uniformity of hybridisation

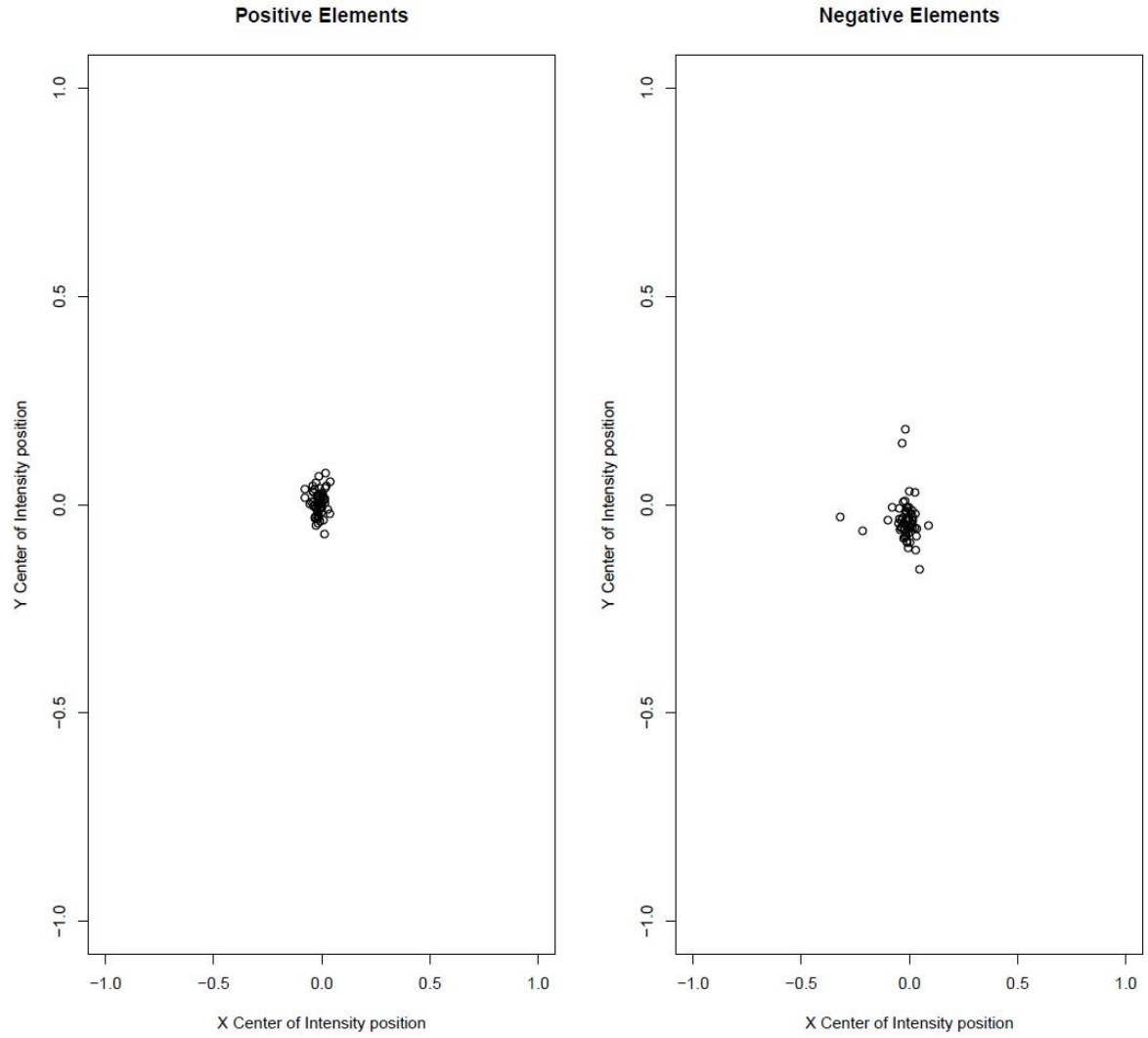

An excerpt from the affyQCReport package output. Individual microarray cells are separated based on which edge of the microarray they are located. Following this, the average values for each physical edge are calculated for both positive and negative controls. A centre of intensity (COI) can then be calculated based on the average of controls located on each individual edge. Positive and negative controls are presented separately as positive and negative elements respectively, as seen above. For positive controls, if hybridisation was uniform across the microarray, no significant differences would be observed on each of the four edges, and the COI would be located in the physical centre of the array. The COI can be shifted due to variables such as bubbles being present during hybridisation. For negative

controls, this tests the uniformity of background intensity over the microarray. For both controls, any array with a COI coordinate greater than 0.5 away from 0 is flagged, and deemed suspect. As shown above, this was not an issue for any of the 62 medulloblastoma samples.

5.2.4. Effect of RMA normalisation on average PM intensity

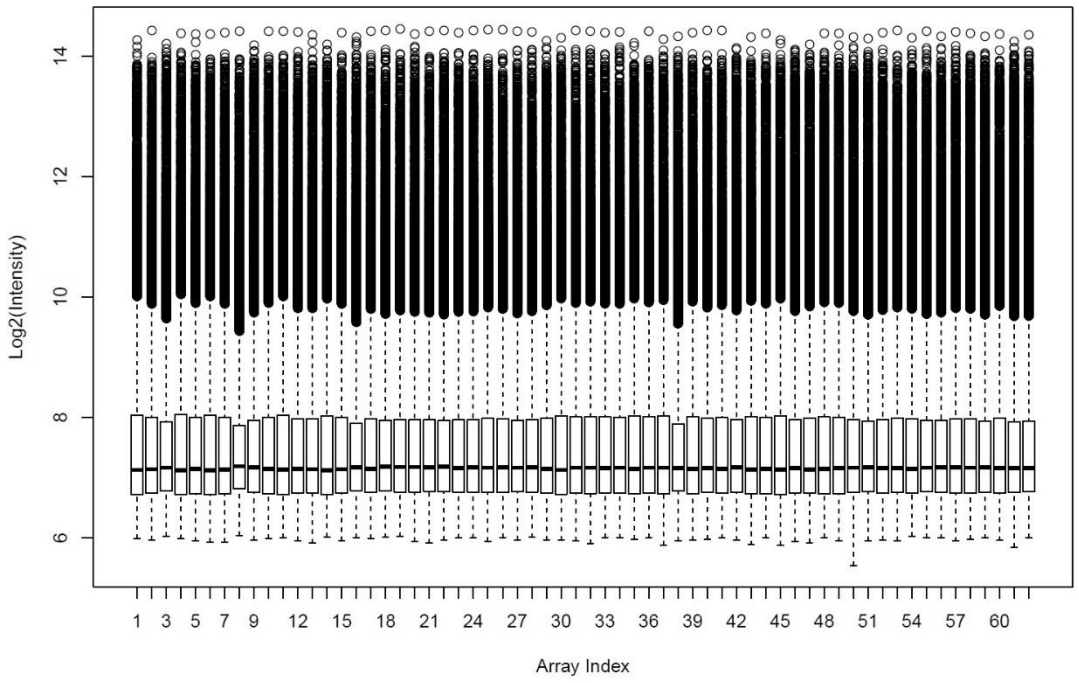

Boxplot representing all PM probe intensities, as in Appendix 5.2.1., post-normalisation with the RMA algorithm. When compared with Appendix 5.2.1., this illustrates the effect RMA normalisation has upon the dataset, and further stresses the importance of quality control tests prior to normalisation.

5.3. Evaluation of *CDH1* probe performance in other datasets

5.3.1. Visual distribution of CDH1 probe intensities: Ewing's sarcoma dataset

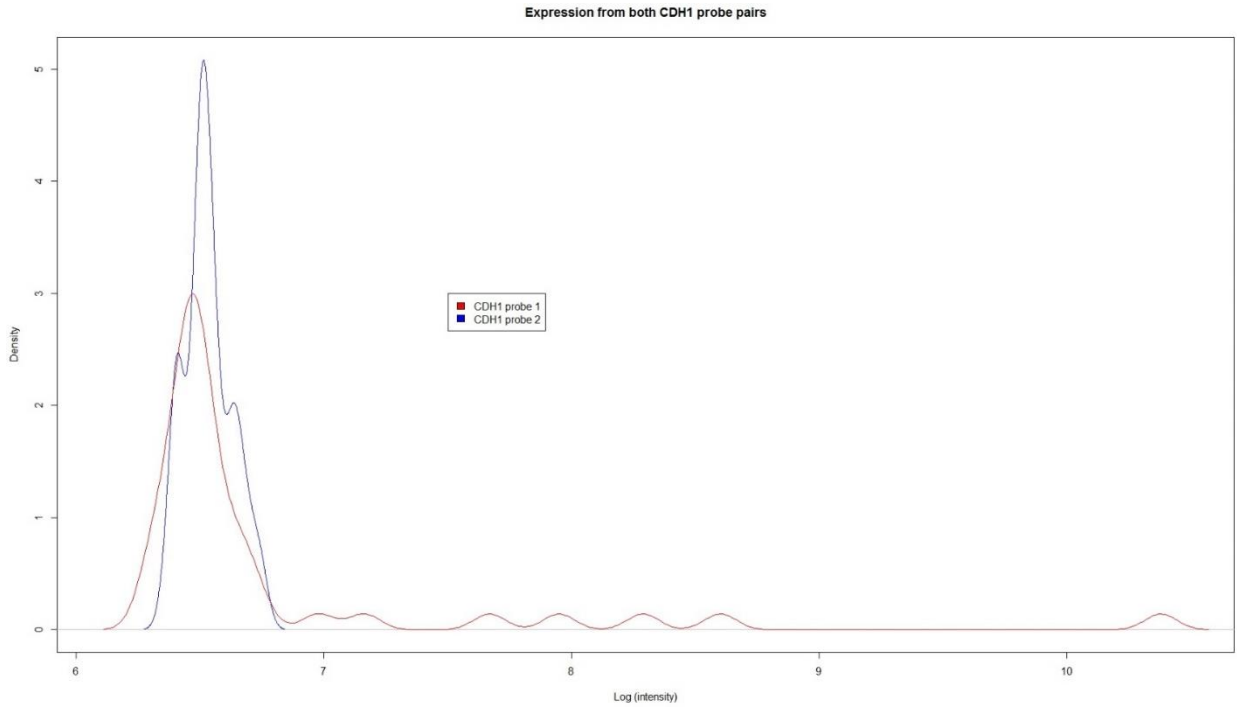

Distribution of probe intensities from both *CDH1* probe pairs as measured in all 44 Ewing's sarcoma tumour samples. The low Pearson correlation coefficient of 0.4 is most likely due to the outlying samples with high intensity readings from probe 1.

5.3.2. Visual distribution of CDH1 probe intensities: Rhabdomyosarcoma dataset

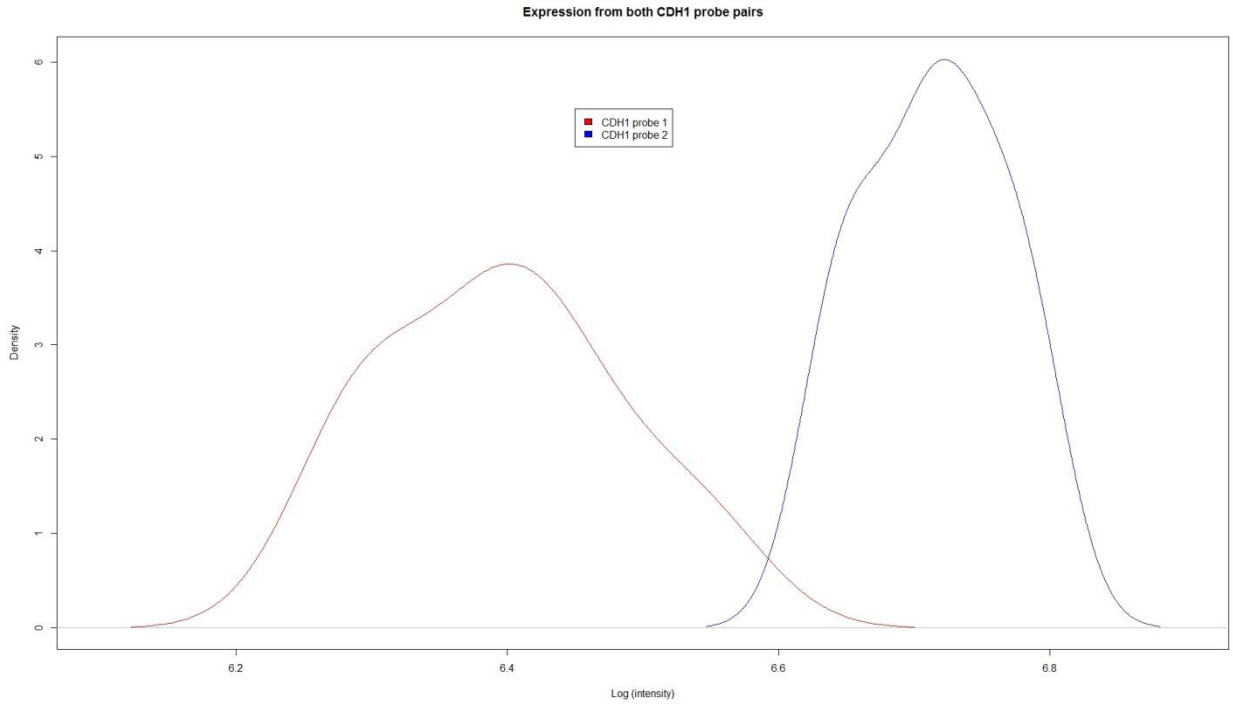

Distribution of probe intensities from both *CDH1* probe pairs as measured in all 13 rhabdomyosarcoma cell lines. The particularly low Pearson correlation coefficient is clearly represented here, with both probes exhibiting decidedly different intensity readings.

5.4. MCF10A *CDH1*$^{-/-}$ cell line

A homozygous 4 bp deletion in exon 11 of *CDH1* was accomplished with zinc finger nuclease (ZFN) technology. This successfully abrogated *CDH1* expression in the MCF10A cell line.

ATAACTGAAGAAGCGCTTAAGCCGTTTTCAGCTACA
TGTTGTTTGCTGGTCCTATTC**TAAAAGCCAGAGCT**
TGTCCCCGTTCAGATATCGGATTTGGAGAGACACT
GCCAACTGGCTGGAGATTAATCCGGACACTGGTGC
CATTTCCACTCGGGCTGAGCTGGACAGGGAGGATT
TTGAGCACGTGAAGAACAGCACGTA**CACAGCCCTA**
ATCATAgctaca**GACAATGGTAAGGGG**GCCTCATCT
GAGCCTTTGCTGCCTCGACCTCCTAGCTAGTTCAG
TTCCTTGCCCCTCCCTTCTTTTGGAGGGAAGAGTT
CATTCTTTTTCTTTTAT**CCTTTTTGTTTGCTGGATTG**
ATTTGTATAAATGTATGGAGTACAAGGGTAATTTTG
TTACATGCATAGATGTGTAGTGGTAAAGTC

Schematic of the genomic sequence at the target region (exon 11) recognized by the ZFN pair; the resulting deletion, and the CEL-I primer sequences:

CEL-I Primers - **Bolded and underlined**

ZFN binding site - **UPPER CASE, BOLDED RED**

ZFN cut site - lower case red

Deletion - yellow highlighted

(Excerpt from Sigma-Aldrich product data sheet)

5.5. DMSO nuclei counting anomaly following SU6668 treatment

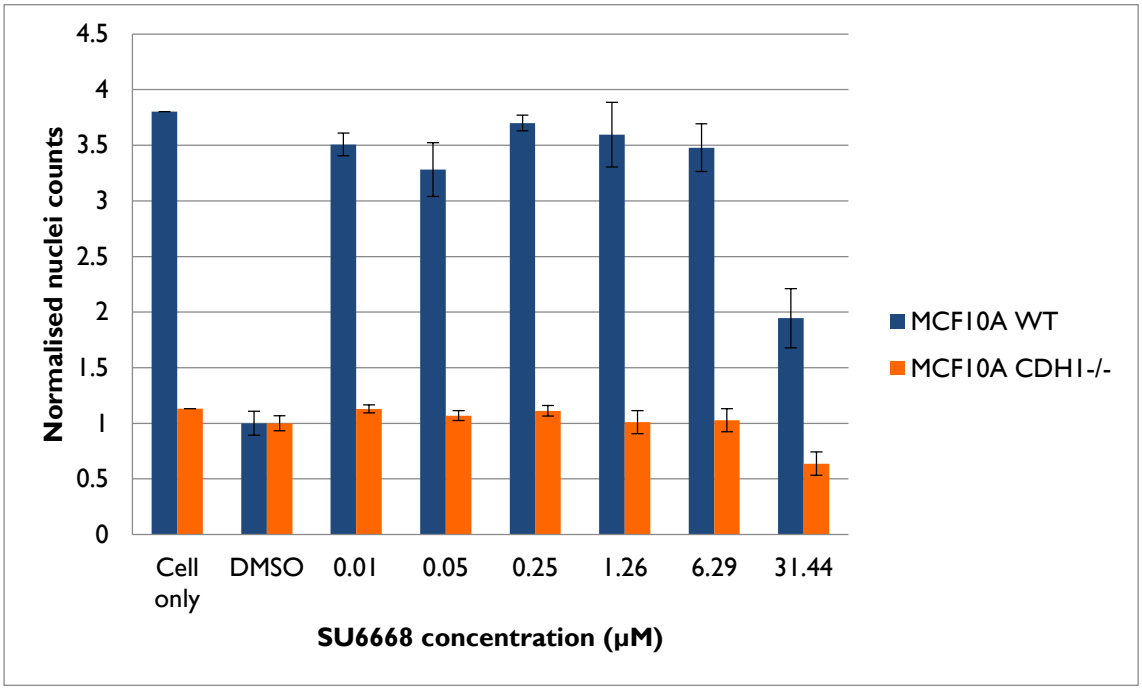

Above is the nuclei counting result from the first SU6668 experiment, normalised to the DMSO control.

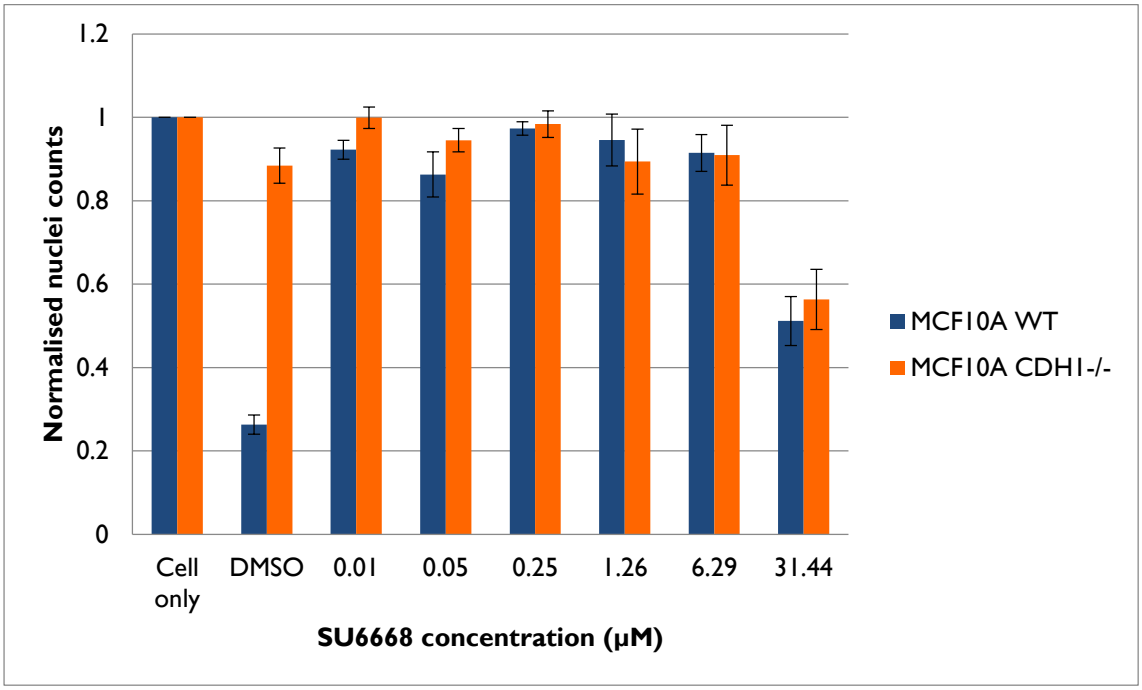

Above is the nuclei counting result from the first SU6668 experiment, normalised to the cell only (CO) control.

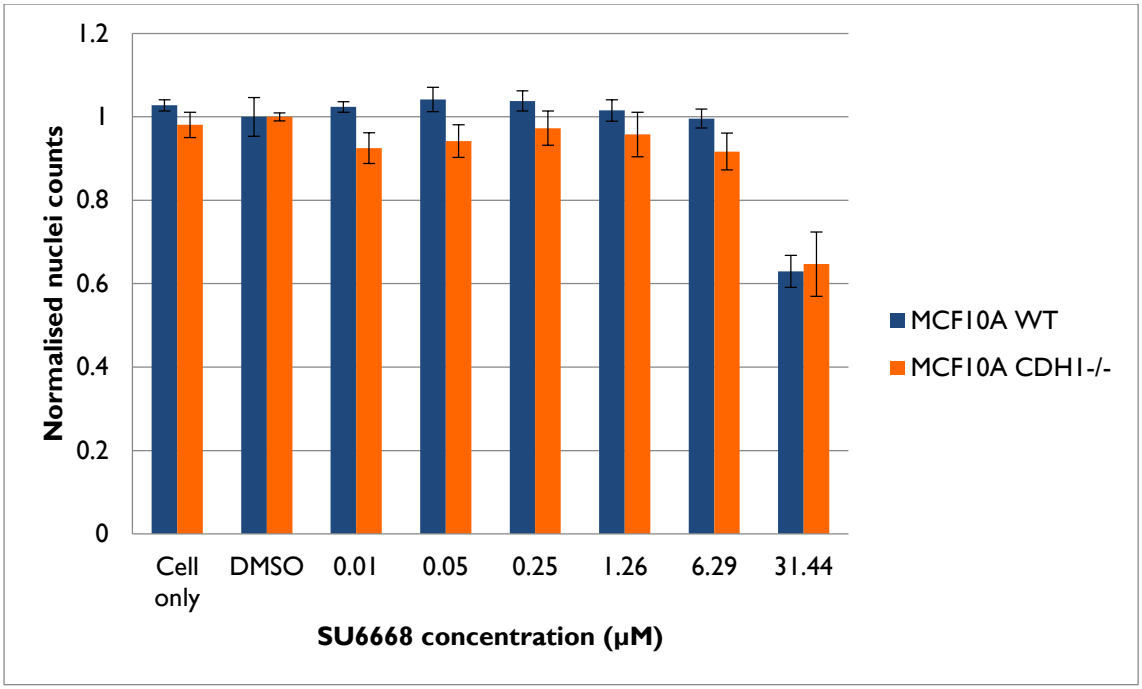

Above is the nuclei counting result from the second SU6668 experiment, normalised to the DMSO control.

It is clear that the DMSO control for MCF10A WT in the first SU6668 experiment exhibits lower cell numbers than expected, as every other condition for MCF10A WT, including the 31.44 µM SU6668 condition which has been shown to decrease cell numbers, show significantly higher nuclei counts (first graph). When these results are instead normalised to the CO control, the trend in cell numbers is clearly similar to that of the second SU6668 experiment (second and third graphs). From this, it was concluded that both experiments exhibit the same result, and so both results were used, although the first experiment was normalised to the CO control instead of the DMSO control.

5.6. qPCR controls for *RARB* expression

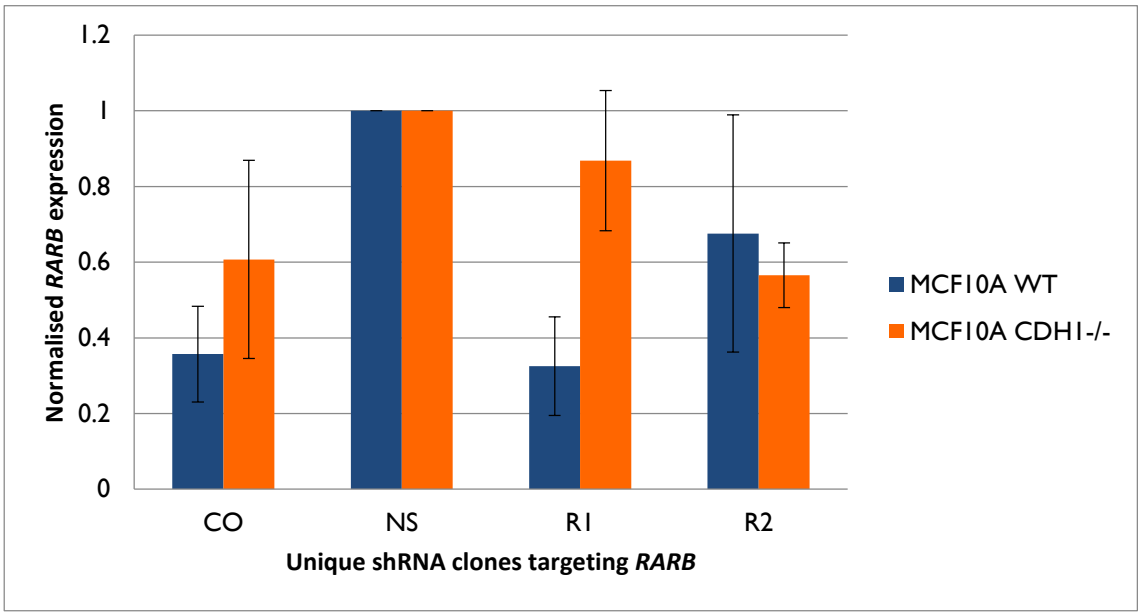

First *RARB* qPCR experiment: *RARB* mRNA transcript levels as detected through qPCR, normalised to the NS control.

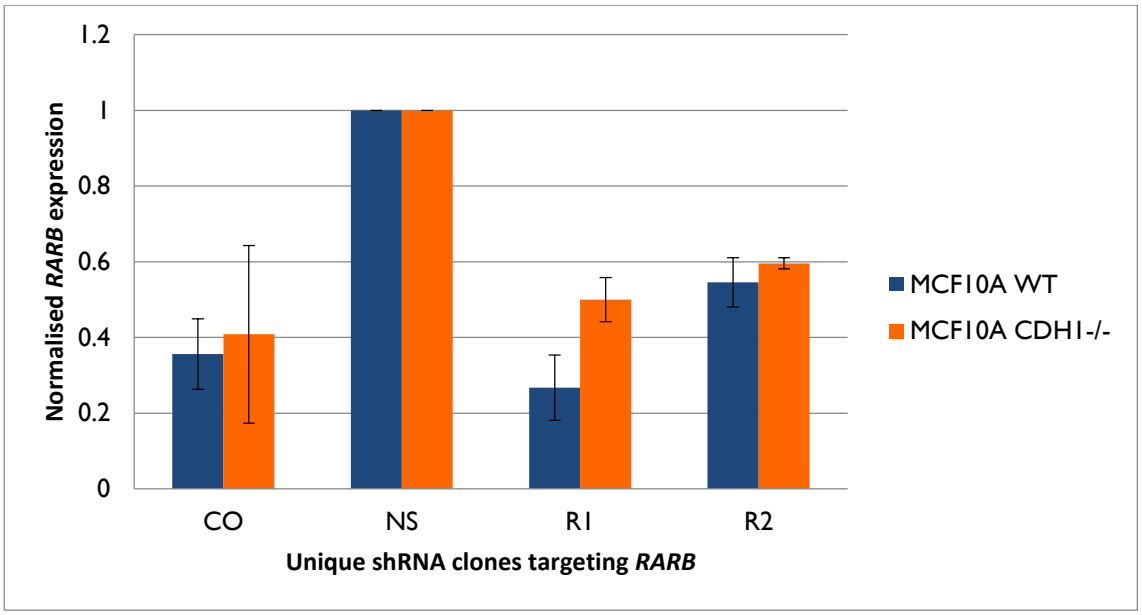

Second *RARB* qPCR experiment: identical to the first *RARB* qPCR experiment.

5.7. qPCR controls for *PDGFD* expression

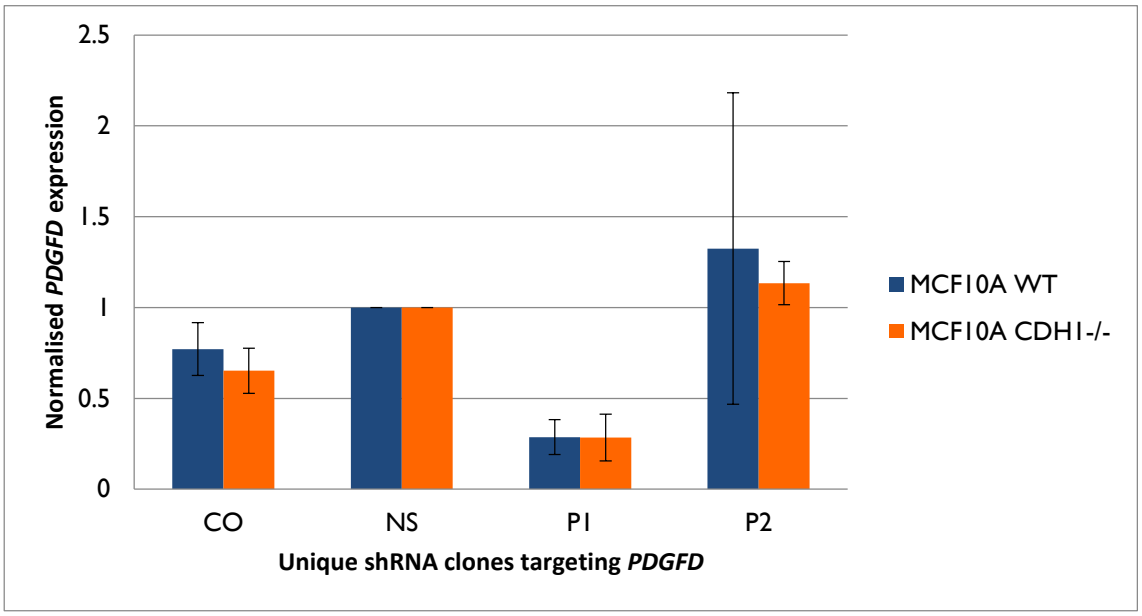

First *PDGFD* qPCR experiment: *PDGFD* mRNA transcript levels as detected through qPCR, normalised to the NS control.

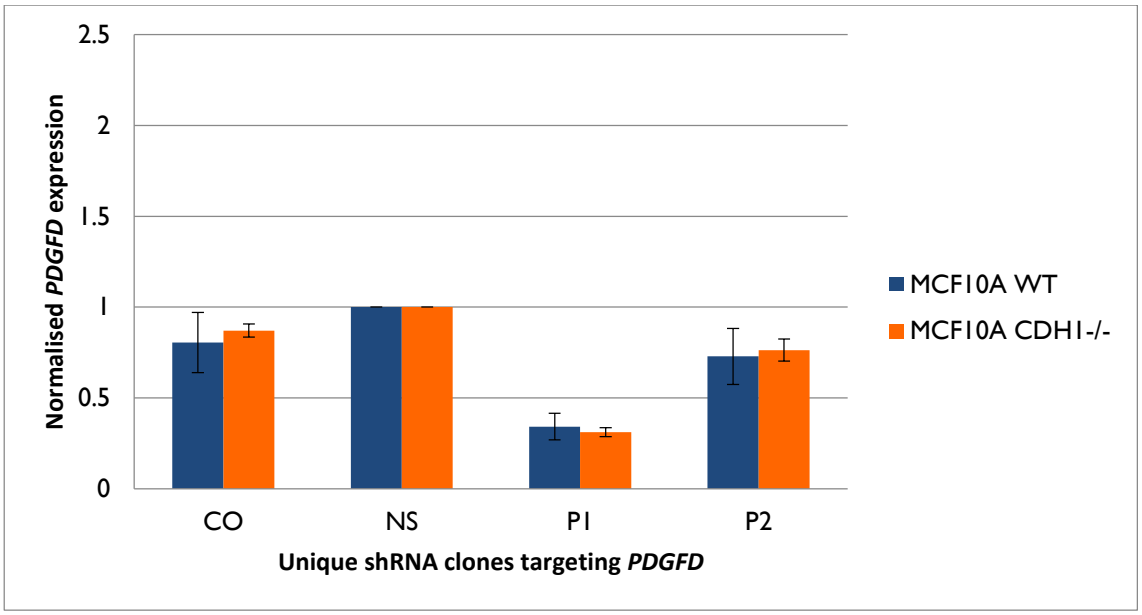

Second *PDGFD* qPCR experiment: identical to the first *PDGFD* qPCR experiment.

5.8. shRNA clone sequences

Listed below are the mature antisense sequences for each of the shRNA clones utilised in this study:

shRNA clone	Antisense sequence
MAPRE3 (A1)	CTCACCCATTCTAATTTAT
MAPRE3 (A2)	CCTGTTATCTCAGGCATCA
MAPRE3 (A3)	ACATTATAGTCCTTTCCTA
MAPRE3 (A4)	GTGATCAGATCTTCAACAA
RARB (R1)	TAACACAGTTCTTATCTCG
RARB (R2)	ATAACACAGTTCTTATCTC
PDGFD (P1)	TGAAATGTAATTTGTACGG
PDGFD (P2)	TATATTGACCGAGTAATTC
Non-silencing (NS)	CTTACTCTCGCCCAAGCGAGAG

References

1. Dobzhansky, T., *Genetics of Natural Populations. Xiii. Recombination and Variability in Populations of Drosophila Pseudoobscura.* Genetics, 1946. **31**(3): p. 269-90.
2. Kaelin, W.G., Jr., *The concept of synthetic lethality in the context of anticancer therapy.* Nat Rev Cancer, 2005. **5**(9): p. 689-98.
3. Tong, A.H., et al., *Global mapping of the yeast genetic interaction network.* Science, 2004. **303**(5659): p. 808-13.
4. Ashworth, A., *A synthetic lethal therapeutic approach: poly(ADP) ribose polymerase inhibitors for the treatment of cancers deficient in DNA double-strand break repair.* J Clin Oncol, 2008. **26**(22): p. 3785-90.
5. Bryant, H.E., et al., *Specific killing of BRCA2-deficient tumours with inhibitors of poly(ADP-ribose) polymerase.* Nature, 2005. **434**(7035): p. 913-7.
6. Dufva, M., *Introduction to microarray technology.* Methods Mol Biol, 2009. **529**: p. 1-22.
7. Barrett, T., et al., *NCBI GEO: mining millions of expression profiles--database and tools.* Nucleic Acids Res, 2005. **33**(Database issue): p. D562-6.
8. R Development Core Team, *R: A language and environment for statistical computing*. 2013, R Foundation for Statistical Computing: Vienna, Austria.
9. Heller, M.J., *DNA microarray technology: devices, systems, and applications.* Annu Rev Biomed Eng, 2002. **4**: p. 129-53.
10. Pease, A.C., et al., *Light-generated oligonucleotide arrays for rapid DNA sequence analysis.* Proc Natl Acad Sci U S A, 1994. **91**(11): p. 5022-6.
11. Speed, T.P., *Expression monitoring by hybridization to high-density oligonucleotide arrays.* Biostatistics, 1996. **14**(13): p. 1675-80.
12. Lockhart, D.J., et al., *Expression monitoring by hybridization to high-density oligonucleotide arrays.* Nat Biotechnol, 1996. **14**(13): p. 1675-80.
13. Irizarry, R.A., *Exploration, normalization, and summaries of high density oligonucleotide array probe level data.* 2003. **4**(2): p. 249-64.
14. Johnson, W.E., C. Li, and A. Rabinovic, *Adjusting batch effects in microarray expression data using empirical Bayes methods.* Biostatistics, 2007. **8**(1): p. 118-27.
15. Kapur, K., et al., *Cross-hybridization modeling on Affymetrix exon arrays.* Bioinformatics, 2008. **24**(24): p. 2887-93.
16. Kelly, T., *Statistical prediction of synthetic lethal interactions in cancer*. 2013, University of Otago: Unpublished.
17. Takeichi, M., *The cadherins: cell-cell adhesion molecules controlling animal morphogenesis.* Development, 1988. **102**(4): p. 639-55.
18. Semb, H. and G. Christofori, *The tumor-suppressor function of E-cadherin.* Am J Hum Genet, 1998. **63**(6): p. 1588-93.
19. Behrens, J., et al., *Dissecting tumor cell invasion: epithelial cells acquire invasive properties after the loss of uvomorulin-mediated cell-cell adhesion.* J Cell Biol, 1989. **108**(6): p. 2435-47.
20. Perl, A.K., et al., *A causal role for E-cadherin in the transition from adenoma to carcinoma.* Nature, 1998. **392**(6672): p. 190-3.
21. Shino, Y., et al., *Clinicopathologic evaluation of immunohistochemical E-cadherin expression in human gastric carcinomas.* Cancer, 1995. **76**(11): p. 2193-201.

22. Lewis, J.E., P.J. Jensen, and M.J. Wheelock, *Cadherin Function Is Required for Human Keratinocytes to Assemble Desmosomes and Stratify in Response to Calcium.* J Investig Dermatol, 1994. **102**(6): p. 870-877.
23. Guilford, P., et al., *E-cadherin germline mutations in familial gastric cancer.* Nature, 1998. **392**(6674): p. 402-5.
24. Hirokawa, N. and J.E. Heuser, *Quick-freeze, deep-etch visualization of the cytoskeleton beneath surface differentiations of intestinal epithelial cells.* J Cell Biol, 1981. **91**(2 Pt 1): p. 399-409.
25. Miyaguchi, K., *Ultrastructure of the zonula adherens revealed by rapid-freeze deep-etching.* J Struct Biol, 2000. **132**(3): p. 169-78.
26. Farquhar, M.G. and G.E. Palade, *Junctional complexes in various epithelia.* J Cell Biol, 1963. **17**: p. 375-412.
27. Meng, W. and M. Takeichi, *Adherens junction: molecular architecture and regulation.* Cold Spring Harb Perspect Biol, 2009. **1**(6): p. a002899.
28. McCrea, P.D., C.W. Turck, and B. Gumbiner, *A homolog of the armadillo protein in Drosophila (plakoglobin) associated with E-cadherin.* Science, 1991. **254**(5036): p. 1359-61.
29. Mosimann, C., G. Hausmann, and K. Basler, *Beta-catenin hits chromatin: regulation of Wnt target gene activation.* Nat Rev Mol Cell Biol, 2009. **10**(4): p. 276-86.
30. van Roy, F. and G. Berx, *The cell-cell adhesion molecule E-cadherin.* Cell Mol Life Sci, 2008. **65**(23): p. 3756-88.
31. Hsu, S.C., J. Galceran, and R. Grosschedl, *Modulation of transcriptional regulation by LEF-1 in response to Wnt-1 signaling and association with beta-catenin.* Mol Cell Biol, 1998. **18**(8): p. 4807-18.
32. Korinek, V., et al., *Constitutive transcriptional activation by a beta-catenin-Tcf complex in APC-/- colon carcinoma.* Science, 1997. **275**(5307): p. 1784-7.
33. Molenaar, M., et al., *XTcf-3 transcription factor mediates beta-catenin-induced axis formation in Xenopus embryos.* Cell, 1996. **86**(3): p. 391-9.
34. Yost, C., et al., *The axis-inducing activity, stability, and subcellular distribution of beta-catenin is regulated in Xenopus embryos by glycogen synthase kinase 3.* Genes Dev, 1996. **10**(12): p. 1443-54.
35. Berx, G., et al., *E-cadherin is a tumour/invasion suppressor gene mutated in human lobular breast cancers.* The EMBO Journal, 1995. **14**(24): p. 6107-6115.
36. Berx, G., et al., *E-cadherin is inactivated in a majority of invasive human lobular breast cancers by truncation mutations throughout its extracellular domain.* Oncogene, 1996. **13**(9): p. 1919-1925.
37. Becker, K.F., et al., *E-cadherin gene mutations provide clues to diffuse type gastric carcinomas.* Cancer Res, 1994. **54**(14): p. 3845-52.
38. Muta, H., et al., *E-cadherin gene mutations in signet ring cell carcinoma of the stomach.* Jpn J Cancer Res, 1996. **87**(8): p. 843-8.
39. Tamura, G., et al., *Inactivation of the E-cadherin gene in primary gastric carcinomas and gastric carcinoma cell lines.* Jpn J Cancer Res, 1996. **87**(11): p. 1153-9.
40. Risinger, J.I., et al., *Mutations of the E-cadherin gene in human gynecologic cancers.* Nat Genet, 1994. **7**(1): p. 98-102.
41. Guilford, P., B. Humar, and V. Blair, *Hereditary diffuse gastric cancer: translation of CDH1 germline mutations into clinical practice.* Gastric Cancer, 2010. **13**(1): p. 1-10.

42. Acloque, H., et al., *Epithelial-mesenchymal transitions: the importance of changing cell state in development and disease.* J Clin Invest, 2009. **119**(6): p. 1438-49.
43. Thiery, J.P. and J.P. Sleeman, *Complex networks orchestrate epithelial-mesenchymal transitions.* Nat Rev Mol Cell Biol, 2006. **7**(2): p. 131-42.
44. Kalluri, R. and R.A. Weinberg, *The basics of epithelial-mesenchymal transition.* J Clin Invest, 2009. **119**(6): p. 1420-8.
45. Chiang, A.C. and J. Massague, *Molecular basis of metastasis.* N Engl J Med, 2008. **359**(26): p. 2814-23.
46. Klein, C.A., *Cancer. The metastasis cascade.* Science, 2008. **321**(5897): p. 1785-7.
47. Chaffer, C.L. and R.A. Weinberg, *A perspective on cancer cell metastasis.* Science, 2011. **331**(6024): p. 1559-64.
48. Peinado, H., D. Olmeda, and A. Cano, *Snail, Zeb and bHLH factors in tumour progression: an alliance against the epithelial phenotype?* Nat Rev Cancer, 2007. **7**(6): p. 415-28.
49. Yang, J. and R.A. Weinberg, *Epithelial-Mesenchymal Transition: At the Crossroads of Development and Tumor Metastasis.* Developmental Cell, 2008. **14**(6): p. 818-829.
50. Adamson PC, B.R., Balis FM, et al., *Principles and Practices of Pediatric Oncology (ed 6) Chapter 10: General principles of chemotherapy*, ed. P. PA. 2011, Philadelphia, PA: Lippincott, Williams & Wilkins.
51. Smoll, N.R., *Relative survival of childhood and adult medulloblastomas and primitive neuroectodermal tumors (PNETs).* Cancer, 2012. **118**(5): p. 1313-22.
52. Gajjar, A.J. and G.W. Robinson, *Medulloblastoma - translating discoveries from the bench to the bedside.* Nat Rev Clin Oncol, 2014. **11**(12): p. 714-722.
53. Gajjar, A., *Physical performance limitations and participation restrictions among cancer survivors: a population-based study.* J Clin Oncol, 2006. **16**(3): p. 197-205.
54. Gurney, J.G., *Late neurocognitive sequelae in survivors of brain tumours in childhood.* Ann Epidemiol, 2004. **5**(7): p. 399-408.
55. Kana, R.K., *Endocrine outcomes for children with embryonal brain tumors after risk-adapted craniospinal and conformal primary-site irradiation and high-dose chemotherapy with stem-cell rescue on the SJMB-96 trial.* J Pediatr Hematol Oncol, 2008. **26**(7): p. 1112-8.
56. Kun, L.E., *Whole-brain irradiation and decline in intelligence: the influence of dose and age on IQ score.* Lancet Oncol, 1992. **10**(9): p. 1390-6.
57. Meadows, A.T., *Medulloblastoma in childhood: progressive intellectual deterioration.* J Clin Oncol, 1990. **6**(2): p. 60-5.
58. Packer, R.J., et al., *Treatment of children with medulloblastomas with reduced-dose craniospinal radiation therapy and adjuvant chemotherapy: A Children's Cancer Group Study.* J Clin Oncol, 1999. **17**(7): p. 2127-36.
59. Wolfe, K.R., *Cardiorespiratory fitness in survivors of pediatric posterior fossa tumor.* 2012. **34**(6): p. e222-7.
60. Mulhern, R.K., et al., *Neurocognitive consequences of risk-adapted therapy for childhood medulloblastoma.* J Clin Oncol, 2005. **23**(24): p. 5511-9.
61. Dietrich, J., et al., *Clinical patterns and biological correlates of cognitive dysfunction associated with cancer therapy.* Oncologist, 2008. **13**(12): p. 1285-95.
62. Monje, M., *Cranial radiation therapy and damage to hippocampal neurogenesis.* Dev Disabil Res Rev, 2008. **14**(3): p. 238-42.

63. Monje, M. and J. Dietrich, *Cognitive side effects of cancer therapy demonstrate a functional role for adult neurogenesis.* Behav Brain Res, 2012. **227**(2): p. 376-9.
64. Cameron, H.A. and E. Gould, *Adult neurogenesis is regulated by adrenal steroids in the dentate gyrus.* Neuroscience, 1994. **61**(2): p. 203-9.
65. Lemaire, V., et al., *Prenatal stress produces learning deficits associated with an inhibition of neurogenesis in the hippocampus.* Proc Natl Acad Sci U S A, 2000. **97**(20): p. 11032-7.
66. Madsen, T.M., et al., *Arrested neuronal proliferation and impaired hippocampal function following fractionated brain irradiation in the adult rat.* Neuroscience, 2003. **119**(3): p. 635-42.
67. Raber, J., et al., *Radiation-induced cognitive impairments are associated with changes in indicators of hippocampal neurogenesis.* Radiat Res, 2004. **162**(1): p. 39-47.
68. Rola, R., et al., *Radiation-induced impairment of hippocampal neurogenesis is associated with cognitive deficits in young mice.* Exp Neurol, 2004. **188**(2): p. 316-30.
69. Shors, T.J., et al., *Neurogenesis in the adult is involved in the formation of trace memories.* Nature, 2001. **410**(6826): p. 372-6.
70. Garthe, A., J. Behr, and G. Kempermann, *Adult-generated hippocampal neurons allow the flexible use of spatially precise learning strategies.* PLoS One, 2009. **4**(5): p. e5464.
71. Winocur, G., et al., *The effects of the anti-cancer drugs, methotrexate and 5-fluorouracil, on cognitive function in mice.* Pharmacol Biochem Behav, 2006. **85**(1): p. 66-75.
72. Mizumatsu, S., et al., *Extreme sensitivity of adult neurogenesis to low doses of X-irradiation.* Cancer Res, 2003. **63**(14): p. 4021-7.
73. Monje, M.L., H. Toda, and T.D. Palmer, *Inflammatory blockade restores adult hippocampal neurogenesis.* Science, 2003. **302**(5651): p. 1760-5.
74. Parent JM, T.E., Fike JR, Lowenstein DH, *Inhibition of dentate granule cell neurogenesis with brain irradiation does not prevent seizure-induced mossy fiber synaptic reorganization in the rat.* J Neurosci, 1999(19): p. 4508-4519.
75. Monje, M.L., et al., *Irradiation induces neural precursor-cell dysfunction.* Nat Med, 2002. **8**(9): p. 955-62.
76. Seigers, R., et al., *Long-lasting suppression of hippocampal cell proliferation and impaired cognitive performance by methotrexate in the rat.* Behav Brain Res, 2008. **186**(2): p. 168-75.
77. Monje, M.L., et al., *Impaired human hippocampal neurogenesis after treatment for central nervous system malignancies.* Ann Neurol, 2007. **62**(5): p. 515-20.
78. Louis, D.N., *The 2007 WHO classification of tumours of the central nervous system.* 2007. **114**(2): p. 97-109.
79. US National Library of Medicine. *Comparison of radiation therapy regimens in combination with chemotherapy in treating young patients with newly diagnosed standard-risk medulloblastoma*. 2014; Available from: http://www.clinicaltrials.gov/ct2/show/NCT00085735?term=NCT00085735&rank=1.
80. US National Library of Medicine. *Chemotherapy and radiation therapy in treating young patients with newly diagnosed, previously untreated, high-risk medulloblastoma*. 2014; Available from: http://www.clinicaltrials.gov/ct2/show/NCT00392327?term=NCT00392327&rank=1.

81. Thompson, M.C., et al., *Genomics identifies medulloblastoma subgroups that are enriched for specific genetic alterations.* J Clin Oncol, 2006. **24**(12): p. 1924-31.
82. Taylor, M.D., et al., *Molecular subgroups of medulloblastoma: the current consensus.* Acta Neuropathol, 2012. **123**(4): p. 465-72.
83. Gibson, P., et al., *Subtypes of medulloblastoma have distinct developmental origins.* Nature, 2010. **468**(7327): p. 1095-1099.
84. Kawauchi, D., et al., *A Mouse Model of the Most Aggressive Subgroup of Human Medulloblastoma.* Cancer Cell, 2012. **21**(2): p. 168-180.
85. Schüller, U., et al., *Acquisition of Granule Neuron Precursor Identity Is a Critical Determinant of Progenitor Cell Competence to Form Shh-Induced Medulloblastoma.* Cancer Cell, 2008. **14**(2): p. 123-134.
86. Yang, Z.-J., et al., *Medulloblastoma Can Be Initiated by Deletion of Patched in Lineage-Restricted Progenitors or Stem Cells.* Cancer Cell, 2008. **14**(2): p. 135-145.
87. Schwechheimer, K., L. Zhou, and W. Birchmeier, *E-Cadherin in human brain tumours: loss of immunoreactivity in malignant meningiomas.* Virchows Arch, 1998. **432**(2): p. 163-7.
88. Utsuki, S., et al., *Invasive meningioma is associated with a low expression of E-cadherin and beta-catenin.* Clinical neuropathology, 2005. **24**(1): p. 8-12.
89. Jones, P.A. and S.B. Baylin, *The fundamental role of epigenetic events in cancer.* Nat Rev Genet, 2002. **3**(6): p. 415-428.
90. Ebinger, M., et al., *Promoter methylation pattern of caspase-8, P16INK4A, MGMT, TIMP-3, and E-cadherin in medulloblastoma.* Pathol Oncol Res, 2004. **10**(1): p. 17-21.
91. Yokota, N., et al., *Role of Wnt pathway in medulloblastoma oncogenesis.* Int J Cancer, 2002. **101**(2): p. 198-201.
92. Robinson, G., et al., *Novel mutations target distinct subgroups of medulloblastoma.* Nature, 2012. **488**(7409): p. 43-8.
93. Orsulic, S., et al., *E-cadherin binding prevents beta-catenin nuclear localization and beta-catenin/LEF-1-mediated transactivation.* J Cell Sci, 1999. **112 (Pt 8)**: p. 1237-45.
94. Carone, D. *Chiari Malformation*. 2001 [cited 2015 14/3/15]; Available from: http://www.medfriendly.com/about-medfriendly.html.
95. Botlagunta, M., et al., *Oncogenic role of DDX3 in breast cancer biogenesis.* Oncogene, 2008. **27**(28): p. 3912-22.
96. Alao, J.P., *The regulation of cyclin D1 degradation: roles in cancer development and the potential for therapeutic invention.* Mol Cancer, 2007. **6**: p. 24.
97. Dang, C.V., A. Le, and P. Gao, *MYC-induced cancer cell energy metabolism and therapeutic opportunities.* Clin Cancer Res, 2009. **15**(21): p. 6479-83.
98. He, T.-C., et al., *Identification of c-MYC as a Target of the APC Pathway.* Science, 1998. **281**(5382): p. 1509-1512.
99. Tetsu, O. and F. McCormick, *Beta-catenin regulates expression of cyclin D1 in colon carcinoma cells.* Nature, 1999. **398**(6726): p. 422-6.
100. Kool, M., et al., *Integrated genomics identifies five medulloblastoma subtypes with distinct genetic profiles, pathway signatures and clinicopathological features.* PLoS One, 2008. **3**(8): p. e3088.
101. Savola, S., et al., *High Expression of Complement Component 5 (C5) at Tumor Site Associates with Superior Survival in Ewing's Sarcoma Family of Tumour Patients.* ISRN Oncol, 2011. **2011**: p. 168712.

102. Missiaglia, E., et al., *Genomic imbalances in rhabdomyosarcoma cell lines affect expression of genes frequently altered in primary tumors: an approach to identify candidate genes involved in tumor development.* Genes Chromosomes Cancer, 2009. **48**(6): p. 455-67.
103. Soon, W.W., et al., *Combined genomic and phenotype screening reveals secretory factor SPINK1 as an invasion and survival factor associated with patient prognosis in breast cancer.* EMBO Mol Med, 2011. **3**(8): p. 451-64.
104. Gentleman, R.C., et al., *Bioconductor: open software development for computational biology and bioinformatics.* Genome Biol, 2004. **5**(10): p. R80.
105. Gautier, L., et al., *affy—analysis of Affymetrix GeneChip data at the probe level.* Bioinformatics, 2004. **20**(3): p. 307-315.
106. Smyth, G.K., *Limma: linear models for microarray data*, in *Bioinformatics and computational biology solutions using R and Bioconductor*. 2005, Springer-Verlag New York.
107. Parman, C., C. Halling, and R. Gentleman, *affyQCReport: QC Report Generation for affyBatch objects*.
108. Jacobsen, P.F., D.J. Jenkyn, and J.M. Papadimitriou, *Establishment of a human medulloblastoma cell line and its heterotransplantation into nude mice.* J Neuropathol Exp Neurol, 1985. **44**(5): p. 472-85.
109. Carlson, M., *hgu133plus2.db: Affymetrix Human Genome U133 Plus 2.0 Array annotation data (chip hgu133plus2)*. R Package Version 2.8.0
110. Benjamini, Y. and Y. Hochberg, *Controlling the False Discovery Rate: A Practical and Powerful Approach to Multiple Testing.*
111. Telford, B.J., et al., *Synthetic Lethal Screens Identify Vulnerabilities in GPCR Signaling and Cytoskeletal Organization in E-Cadherin-Deficient Cells.* Mol Cancer Ther, 2015. **14**(5): p. 1213-23.
112. Chen, A., et al., *E-cadherin loss alters cytoskeletal organization and adhesion in non-malignant breast cells but is insufficient to induce an epithelial-mesenchymal transition.* BMC Cancer, 2014. **14**: p. 552.
113. Oliveros, J.C. *VENNY. An interactive tool for comparing lists with Venn Diagrams.* 2007; Available from: http://bioinfogp.cnb.csic.es/tools/venny/index.html.
114. Chambon, P., *A decade of molecular biology of retinoic acid receptors.* Faseb j, 1996. **10**(9): p. 940-54.
115. Ghyselinck, N.B., et al., *Role of the retinoic acid receptor beta (RARbeta) during mouse development.* Int J Dev Biol, 1997. **41**(3): p. 425-47.
116. Lohnes, D., et al., *Developmental roles of the retinoic acid receptors.* J Steroid Biochem Mol Biol, 1995. **53**(1-6): p. 475-86.
117. Wendling, O., et al., *Roles of retinoic acid receptors in early embryonic morphogenesis and hindbrain patterning.* Development, 2001. **128**(11): p. 2031-8.
118. Glass, C.K., *Some new twists in the regulation of gene expression by thyroid hormone and retinoic acid receptors.* J Endocrinol, 1996. **150**(3): p. 349-57.
119. Weiss, F.U., et al., *Retinoic acid receptor antagonists inhibit miR-10a expression and block metastatic behavior of pancreatic cancer.* Gastroenterology, 2009. **137**(6): p. 2136-45.e1-7.
120. Tsai, S. and S.J. Collins, *A dominant negative retinoic acid receptor blocks neutrophil differentiation at the promyelocyte stage.* Proc Natl Acad Sci U S A, 1993. **90**(15): p. 7153-7.

121. Williams, J.A., et al., *Retinoic acid receptors are required for skeletal growth, matrix homeostasis and growth plate function in postnatal mouse.* Dev Biol, 2009. **328**(2): p. 315-27.
122. Breitkopf, K., et al., *Expression patterns of PDGF-A, -B, -C and -D and the PDGF-receptors alpha and beta in activated rat hepatic stellate cells (HSC).* Cytokine, 2005. **31**(5): p. 349-57.
123. Uutela, M., et al., *PDGF-D induces macrophage recruitment, increased interstitial pressure, and blood vessel maturation during angiogenesis.* Blood, 2004. **104**(10): p. 3198-204.
124. Gupta, R., et al., *Downregulation of uPA/uPAR inhibits intermittent hypoxia-induced epithelial-mesenchymal transition (EMT) in DAOY and D283 medulloblastoma cells.* Int J Oncol, 2011. **38**(3): p. 733-44.
125. Gupta, et al., *Downregulation of uPA/uPAR inhibits intermittent hypoxia-induced epithelial-mesenchymal transition (EMT) in DAOY and D283 medulloblastoma cells.* International Journal of Oncology, 2011. **38**(3): p. 733-744.
126. Akhmanova, A. and M.O. Steinmetz, *Tracking the ends: a dynamic protein network controls the fate of microtubule tips.* Nat Rev Mol Cell Biol, 2008. **9**(4): p. 309-22.
127. Alfos, S., et al., *A retinoic acid receptor antagonist suppresses brain retinoic acid receptor overexpression and reverses a working memory deficit induced by chronic ethanol consumption in mice.* Alcohol Clin Exp Res, 2001. **25**(10): p. 1506-14.
128. Soule, H.D., et al., *Isolation and characterization of a spontaneously immortalized human breast epithelial cell line, MCF-10.* Cancer Res, 1990. **50**(18): p. 6075-86.
129. Batlle, E., et al., *The transcription factor snail is a repressor of E-cadherin gene expression in epithelial tumour cells.* Nat Cell Biol, 2000. **2**(2): p. 84-9.
130. Cao, Y., R. Cao, and E.M. Hedlund, *R Regulation of tumor angiogenesis and metastasis by FGF and PDGF signaling pathways.* J Mol Med (Berl), 2008. **86**(7): p. 785-9.
131. Mori, S., et al., *Identification of two juxtamembrane autophosphorylation sites in the PDGF beta-receptor; involvement in the interaction with Src family tyrosine kinases.* Embo j, 1993. **12**(6): p. 2257-64.
132. Felsenfeld, D.P., et al., *Selective regulation of integrin--cytoskeleton interactions by the tyrosine kinase Src.* Nat Cell Biol, 1999. **1**(4): p. 200-6.
133. Chang, J.H., et al., *c-Src regulates the simultaneous rearrangement of actin cytoskeleton, p190RhoGAP, and p120RasGAP following epidermal growth factor stimulation.* J Cell Biol, 1995. **130**(2): p. 355-68.
134. Demoulin, J.B., et al., *Ligand-induced recruitment of Na+/H+-exchanger regulatory factor to the PDGF (platelet-derived growth factor) receptor regulates actin cytoskeleton reorganization by PDGF.* Biochem J, 2003. **376**(Pt 2): p. 505-10.
135. Lee, Y.M., et al., *Retinoic acid leads to cytoskeletal rearrangement through AMPK-Rac1 and stimulates glucose uptake through AMPK-p38 MAPK in skeletal muscle cells.* J Biol Chem, 2008. **283**(49): p. 33969-74.
136. Borden, P. and R.A. Heller, *Transcriptional control of matrix metalloproteinases and the tissue inhibitors of matrix metalloproteinases.* Crit Rev Eukaryot Gene Expr, 1997. **7**(1-2): p. 159-78.
137. Chambers, A.F. and L.M. Matrisian, *Changing views of the role of matrix metalloproteinases in metastasis.* J Natl Cancer Inst, 1997. **89**(17): p. 1260-70.

138. MacDougall, J.R. and L.M. Matrisian, *Contributions of tumor and stromal matrix metalloproteinases to tumor progression, invasion and metastasis.* Cancer Metastasis Rev, 1995. **14**(4): p. 351-62.
139. Vincenti, M.P., et al., *Regulating expression of the gene for matrix metalloproteinase-1 (collagenase): mechanisms that control enzyme activity, transcription, and mRNA stability.* Crit Rev Eukaryot Gene Expr, 1996. **6**(4): p. 391-411.
140. Schoenermark, M.P., et al., *Retinoid-mediated suppression of tumor invasion and matrix metalloproteinase synthesis.* Ann N Y Acad Sci, 1999. **878**: p. 466-86.
141. Adachi, Y., et al., *Retinoic acids reduce matrilysin (matrix metalloproteinase 7) and inhibit tumor cell invasion in human colon cancer.* Tumour Biol, 2001. **22**(4): p. 247-53.
142. Varani, J., et al., *All-trans retinoic acid stimulates growth and extracellular matrix production in growth-inhibited cultured human skin fibroblasts.* J Invest Dermatol, 1990. **94**(5): p. 717-23.
143. Mali, P., K.M. Esvelt, and G.M. Church, *Cas9 as a versatile tool for engineering biology.* Nat Methods, 2013. **10**(10): p. 957-63.
144. Boch, J., *TALEs of genome targeting.* Nat Biotechnol, 2011. **29**(2): p. 135-6.
145. Jones, D.T., et al., *Dissecting the genomic complexity underlying medulloblastoma.* Nature, 2012. **488**(7409): p. 100-5.
146. Pugh, T.J., et al., *Medulloblastoma exome sequencing uncovers subtype-specific somatic mutations.* Nature, 2012. **488**(7409): p. 106-10.
147. Northcott, P.A., et al., *Medulloblastomics: the end of the beginning.* Nat Rev Cancer, 2012. **12**(12): p. 818-34.
148. Poschl, J., et al., *Genomic and transcriptomic analyses match medulloblastoma mouse models to their human counterparts.* Acta Neuropathol, 2014. **128**(1): p. 123-36.
149. Gibson, P., et al., *Subtypes of medulloblastoma have distinct developmental origins.* Nature, 2010. **468**(7327): p. 1095-9.